약학박사학위논문

Enantioselective Total Synthesis of (-)-Deguelin and Structure-activity Relationship (SAR) of Novel Hypoxia Inducible Factor-1α (HIF-1α) Inhibitors Targeting Retinal Neovascularization Disease

(-)-Deguelin의 입체선택적인 전합성 및 망막 신생혈관 질환을 표적 하는 새로운 HIF-1α 저해제의 구조활성관계 연구

2017년 2월

서울대학교 대학원
약학과 약품제조화학전공
이 승 범

Abstract

Seungbeom Lee

College of Pharmacy

Seoul National University

(-)-Deguelin is a natural rotenoid isolated from several botanical sources and has attracted much attention from biologists and chemists due to its promising anticancer and chemopreventive properties. Recently, we reported that deguelin interfered with ATP binding to Heat Shock Protein 90 (Hsp90), a protein associated with the stabilization and translocation of hypoxia inducible factor-1α (HIF-1α). First of all, we herein presented the enantioselective synthesis of (-)-deguelin accomplished through 12 steps from commercially available starting material, 3,4-dimethoxyphenol. The key features of our synthesis include the efficient preparation of the precursor for iterative cyclization via highly convergent assembly of two aromatic systems and facile construction of the cis-fused bisbenzopyran skeleton. Construction of the double cyclization precursor involves carbonylative epoxide ring opening catalyzed by cobalt and anionic aryl addition of two aromatic systems. The cis-fused bisbenzopyran skeleton was achieved by sequential Pd-catalyzed *O*- and *C*-arylation. The Pd-catalyzed *O*- and *C*-arylation were greatly improved in terms of yield and stereoselectivity compared to previous studies of asymmetric total synthesis of (-)-deguelin.

Another our effort was explanation of SAR for **SH-42** and development of novel HIF-1α inhibitors targeting the retinal neovascularization disease. Ocular diseases featuring pathologic neovascularization are the leading cause of blindness. Anti-VEGF agents have been conventionally used for the diseases, however the treatment is reconsidered recently in the aspect that VEGF acts as a trophic factor. Accordingly regulating upstream of VEGF, such as HIF-1α has emerged as a desirable therapeutic target. We already identified a series of ring-truncated deguelin analogs that induce destabilization of HIF-1α on retina cell as

well as cancer cell. Especially, the potent analog **SH-42** exhibited suppressing effects in hypoxia-mediated retinal neovascularization and vascular leakage. We herein report a complete structure-activity relationship study of ring-truncated deguelin analogs, **SH-42** on HIF-1α nano-luciferase activity inhibition. The analog **SH-199** which contained 2-fluorobenzene ring in place of 3,4-dimethoxybenzene ring of **SH-42** exhibited excellent in vitro HIF-1α inhibitory activity with an IC_{50} of 100 nM. Meanwhile, the analog **SH-173** which has greatly improved water solubility showed significant HIF-1α inhibitory activity and anti-angiogenic effect comparable to the analog **SH-42**. Importantly, as **SH-173** which has heteroatome-substituted benzene ring replacing the privileged chromene ring manifested the equipotent anti-angiogenic inhibitory activity on oxygen-induced retinopathy (OIR) model, a structural feature of the analog **SH-173** was identified as a novel scaffold of HIF-1α inhibitors in lieu of the chromene ring.

Keywords : Asymmetric total synthesis, Deguelin, Pd-catalyzed α-arylation, HIF-1α, retinal neovascularization disease, large scale synthesis, tandem claisen condensation-decarboxylation-alkylation sequence

Student Number : 2012-21609

Table of Contents

Abstract i

Table of Contents iii

List of Tables v

List of Figures vi

List of Schemes vii

Abbreviations viii

I. Introduction 1

1. Deguelin 1

1-1. Previous synthetic studies toward racemic deguelin 1

1-2. Previous asymmetric syntheses of (-)-deguelin 2

2. Heat Shock Protein 90 and Hypoxia-Inducible Factor-1 alpha 5

2-1. Hsp90 in cancer 6

2-2. HIF-1α regulation 7

3. Retinal Neovascularization Disease 10

3-1. Disease and therapies 10

3-2. Previous studies 15

II. Results and Discussion 17

1. Enantioselective total synthesis of (-)-deguelin 17

1-1. Retrosynthetic analysis 18

1-2. Preparation of first Pd-catalyzed cyclization precursor 19

1-3. First Pd-catalyzed cyclization and late-stage regioselective iodination 21

1-4. Endgame of asymmetric total synthesis of (-)-deguelin 22

2. Identification and application of representative Hsp90 inhibitor, **SH-42** into cancer 24

2-1. Large scale synthesis of **SH-42** 24

2-2. Mechanism study of **SH-42** 26

2-3. Applications of **SH-42** into cancer 27

2-3-1. Cytotoxicity of **SH-42** for drug-naïve cell lines 27

2-3-2. Xenograft model for **SH-42** 28

2-3-3. Reduced neuro toxicities induced by **SH-42** 29

3. Full SAR of novel HIF-1 inhibitors and application of the representative analog into retinal neovascularization disease 30

3-1. Modification of A-part analogs 32

3-2. Modification of B-part analogs 38

3-3. Modification of C-part analogs 40

3-4. Kinetic solubility of representative analogs 44

3-5. Anti-angiogenesis of representative chromene ring-truncated analog 45

3-6. Oxygen-inducible retinopathy model for representative analogs 46

III. Conclusion 48

IV. Experimental 49

V. References 75

VI. Appendix 84

VII. 국문초록 105

List of Tables

Table 1.	Optimization of late-stage regioselective iodination	22
Table 2.	Pd-catalyzed intramolecular *C*-arylation	23
Table 3.	Inhibition of HIF-1α nano-luciferase activity by A-part modified analogs	37
Table 4.	Inhibition of HIF-1α nano-luciferase activity by B-part modified analogs	39
Table 5.	Inhibition of HIF-1α nano-luciferase activity by chromene ring-truncated analogs	44

List of Figures

Figure 1.	Structures of (-)-deguelin (**1**), SH1280 (**2**) and rotenone (**3**)	1
Figure 2.	HSP90 domain structure and chaperone cycle	7
Figure 3.	Tumor hypoxia and expression of HIF-1α	8
Figure 4	HIF-1α regulation of Hsp90	10
Figure 5.	Common indications for intraocular anti-VEGF injections	11
Figure 6.	Diabetic retinopathy	12
Figure 7.	Anti-VEGF agents, Lucentis and Avastin	13
Figure 8.	Strategy toward previous representative analogs of deguelin, **SH-42** and **SH-80**	15
Figure 9.	Strategy for SAR of representative alanogs and initial synthetic procedures	16
Figure 10.	proposed mechanism of two type of α-arylation	18
Figure 11.	Fluorescence-based analysis of **SH-42** and Hsp90 binding	27
Figure 12.	Inhibitory activity of **SH-42** on colony formation of drug resistant cancer cells	28
Figure 13.	Anti-tumor formation activity of **SH-42** on mutant KRAS-driven Kras transgenic mice	29
Figure 14.	Inhibitory activity of **SH-42** on xenograft models	29
Figure 15.	Reduced toxicities of **SH-42** compared to deguelin	30
Figure 16.	Strategy for SAR of **SH-42** and **SH-80**	32
Figure 17.	Kinetic solubility of the representative analogs	45
Figure 18.	Anti-angiogenesis of the chromene ring-truncated analog, **SH-173**	46
Figure 19.	In vivo test for the chromene ring-truncated analog, **SH-173**	47

List of Schemes

Scheme 1.	Previous reported asymmetric total synthesis of (-)-deguelin	2
Scheme 2.	The synthetic strategy for analogs of deguelin	3
Scheme 3.	Previous synthetic approach to (-)-deguelin	4
Scheme 4.	Challenges in previous study	5
Scheme 5.	Previous Pd-catalyzed α-C-arylation	17
Scheme 6.	Retrosynthetic analysis of (-)-deguelin	19
Scheme 7.	Preparation of first Pd-catalyzed cyclization precursor	20
Scheme 8.	Excellent improvement of first Pd-catalyzed cyclization	21
Scheme 9.	Preparation of second Pd-catalyzed cyclization precursor	22
Scheme 10.	Synthetic history of **SH-42**	25
Scheme 11.	One step green chemistry method for scale-up of **SH-42**	26
Scheme 12.	Methods of synthesis of A-part modified analogs	33
Scheme 13.	Synthesis of A-part modified analog via method A	34
Scheme 14.	Synthesis of A-part modified analogs via method C	35
Scheme 15.	Preparation of chromene ring-truncated analogs via tandem reaction	42

Abbreviations

AD: Asymmetric Dihydroxylation

AII: Acute Intraocular Inflammation

Akt: Protein kinase B

AMD: Age-related Macular Degeneration

AP-1: Activator Protein 1

ARNT: ARyl hydrocarbon Nuclear receptor Translocator

ATP: Adenosine Triphosphate

AV: Axial Vein

bHLH: Basic-Helix-Loop-Helix

BINAP: 2,2'-bis(diphenylphosphino)-1,1'-binaphthyl

Boc: t-butyloxycarbonyl

CM: Cross-Metathesis

CNV: Choroidal Neovascularization

C-TAD: C-Terminal transactivation domain

DA: Dorsal Aorta

DBU: 1,8-diazabicyclo[5.4.0]undec-7-ene

DEAD: diethyl azodicarboxylate

DIBAL: diisobutylaluminum hydride

DMAP: N,N-dimethylaminopyridine

DME: Diabetic Macular Edema

DMF: N,N-dimethylformamide

DMP: Dess-Martin periodinane

DNA: Deoxyribonucleic acid

DPPF: 1,1´-bis(diphenylphosphino)ferrocene

DR: Diabetic Retinopathy

dr: Diastereomeric Ratio

EDCI: 1-Ethyl-3-(3-dimethylaminopropyl)carbodiimide

ee: Enantiomeric Excess

er: Enantiomeric Ratio

FDA: US Food and Drug Administration

FIH: factor inhibiting HIF

FITC: Fluorescein isothiocyanate

Fmoc: fluorenylmethyloxycarbonyl

GAA: geldanamycin

H&E: Hematoxylin & Eosin

HIF-1a: Hypoxia-Inducible Factor 1-alpha

HOBt: hydroxybenzotriazole

hpf: hours post fertilization

HPLC: High-Performance Liquid Chromatography

HRE: Hypoxia-Response Element

HRMECs: Human Retinal Microvascular Endothelial Cells

Hsp90: Heat Shock Protein 90

IBX: Iodobenzoic acid

JohnPhos: 2-(Di-*tert*-butylphosphino)biphenyl

LC/MS: Liquid chromatography-mass spectrometry

MOM: methyloxy methyl

mRNA: Messenger ribonucleic acid

MTS: 3-(4,5-dimethylthiazol-2-yl)-5-(3-carboxymethoxyphenyl)-2-(4-sulfophenyl)-2H-tetrazolium

NADH : Nicotinamide adenine dinucleotide

NaHMDS: sodium bis(trimethylsilyl)amide

NBS: N-Bromosuccinimide

NF-kB: Nuclear Factor kB

NIS: N-Iodosuccinimide

NMO: N-Methylmorpholine N-oxide

NMR: Nuclear Magnetic Resonance

NPDR: Non-Proliferative Diabetic Retinopathy

NSCLC: Non-Small-Cell Lung Cancer

N-TAD: N-Terminal transactivation domain

ODDD: Oxygen-Dependent Degradation Domain

OIR: Oxygen-Induced Retinopathy

PBS: Phosphate Buffered Saline

PDR: Proliferative Diabetic Retinopathy

PDX: Patient-derived xenograft

PHD: Prolyl Hydroxylase Domain

PI3K: Phosphatidylinositol-3-Kinase

RPE: Retinal Pigment Epithelium

Sphos: 2-Dicyclohexylphosphino-2´,6´-dimethoxybiphenyl

STZ: streptozotocin

TBS: tert-butyldimethylsilyl

TES: triethylsilyl

TFA: trifluoroacetic acid

THF: tetrahydrofuran

TPAP: Tetrapropylammonium perruthenate

VEGF: Vascular Endothelial Growth Factor

VHL: Von Hippel Lindau

VPF: Vascular Permeability Factor

I. Introduction

1. Deguelin

Deguelin (**1**) is a natural rotenoid isolated from several botanical sources[1] and has been known as one of the most active natural pesticides and insecticides.[2] Deguelin has attracted much attention from biologists and chemists due to its promising anticancer and chemopreventive properties. It inhibits induction of ornithine decarboxylase, an enzyme related with tumor progression.[3,4] The fluorescently-labeled deguelin conjugates showed a strong cellular co-localization with mitochondria, the site of the electron-transport chain in human cells.[5] Recently, we reported that deguelin interfered with ATP binding to Heat Shock Protein 90 (HSP90), a protein related with stabilization and translocation of hypoxia inducible factor-1α (HIF-1α).[6-9] In addition, we identified a key skeleton (**SH1280** = **SH-80**, **2**) responsible for HSP90 inhibition and developed a number of pharmacologically and toxicologically improved deguelin analogs.[10-12] More recently we have disclosed their significant suppressing effects in hypoxia-mediated retinal neovascularization and vascular leakage in diabetic retina.[11]

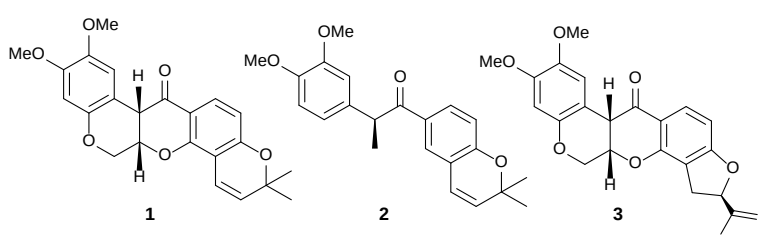

Figure 1. Structures of (-)-deguelin (1), SH1280 (2) and rotenone (3)

1-1. Previous synthetic studies toward racemic deguelin

According to numerous biological activities and unique structural features, many organic chemistry groups have desired achievement of synthesis of key skeleton and total synthesis of deguelin.

1-2. Previous asymmetric syntheses of (-)-deguelin

While racemic syntheses of deguelin and a formal synthesis from rotenone were reported earlier,[11-15] first enantioselective total synthesis of (-)-deguelin was reported in 2010 by Winssinger and coworkers.[16] In 2013, Scheidt and coworker reported the first catalytic, enantioselective total synthesis of (-)-deguelin and its enantiomer (Scheme 1).[17]

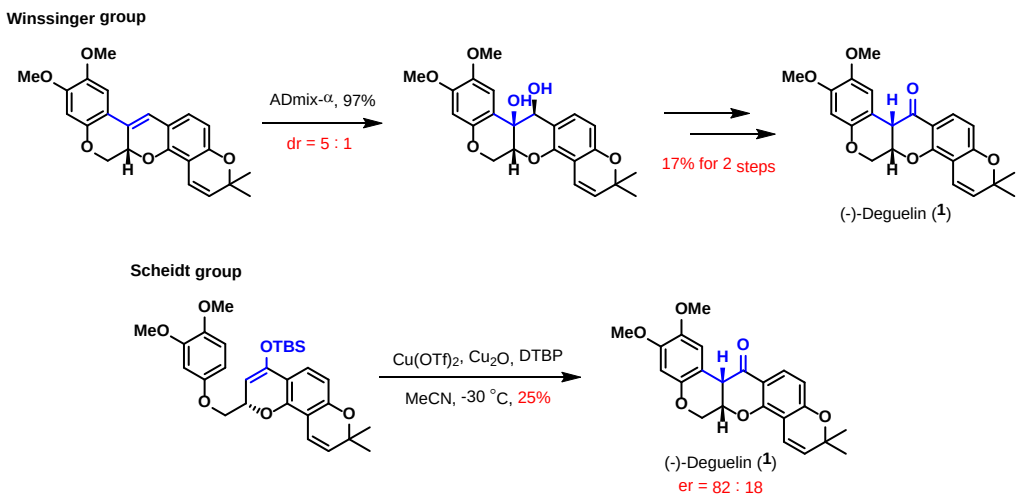

Scheme 1. Previous reported asymmetric total synthesis of (-)-deguelin

In the scheme of asymmetric total synthesis of (-)-deguelin by Winssinger group, nucleophilic epoxide opening of vinyloxirane, Heck cyclization, regioselective ring cyclization and Wittig reaction afforded chromene containing fragment. Two key fragment were condensed by Mitsunobu reaction and ring-closing metathesis afforded the desired internal olefin. Diastereomeric ratio in Sharpless asymmetric dihydroxylation with AD mix-α and yield of completion of total synthesis through 2 steps were only 5 : 1 and 17% respectively.

Recently, Scheidt and coworker reported the first catalytic, enantioselective total synthesis of (-)-deguelin via Cu-catalyzed oxidative α-arylation by final key step. However, 82 : 18

as enantiomeric ratio and 25% as key step yield were still low. To conclude, the enantioselective synthesis of cis-fused iterative pyran ring formation has been big challenge.

On the other hand, our research group previously tried the enantioselective total synthesis of (-)-degulelin and established the unified convergent synthetic strategy which has been also used for pyran ring-truncated bioactive derivatives of (-)-deguelin.(Scheme 2)

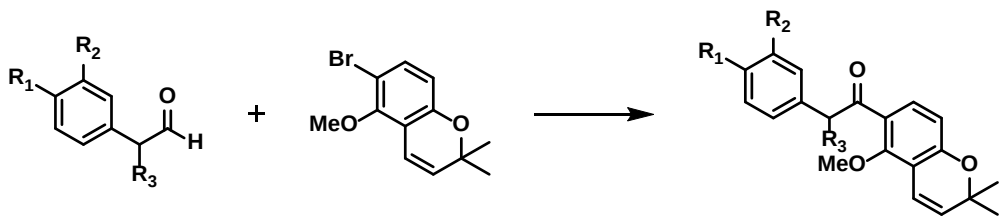

Scheme 2. The synthetic strategy for analogs of deguelin

Our initial synthetic approach to (-)-deguelin is shown in below. We envisioned that double Pd-catalyzed arylation of β-hydroxy ketone **5** would give the desired *cis*-fused bisbenzopyran system of **1** through transferring a chirality of the β-hydroxy moiety to the α-position of ketone. The final diastereoselective pyran ring formation was anticipated based on Pd-catalyzed α-arylation of ketone **4**. The first pyran ring formation would be possible via Pd-catalyzed *O*-arylation of β-hydroxy ketone **5**, which can be prepared from aldehyde **7** via convergent procedure. Anionic addition of chromene **6** to aldehyde **7**, which is derived by a carbonylative epoxide opening of **8**, provides **5**. Chromene **6**, which was reported by us, is conveniently prepared via a sequence of chemoselective propargylation of 6-nitro-resorcinol, regioselective Claisen rearrangement of the resulting alkylaryl ether, and Lewis acid-promoted etherification. [10]

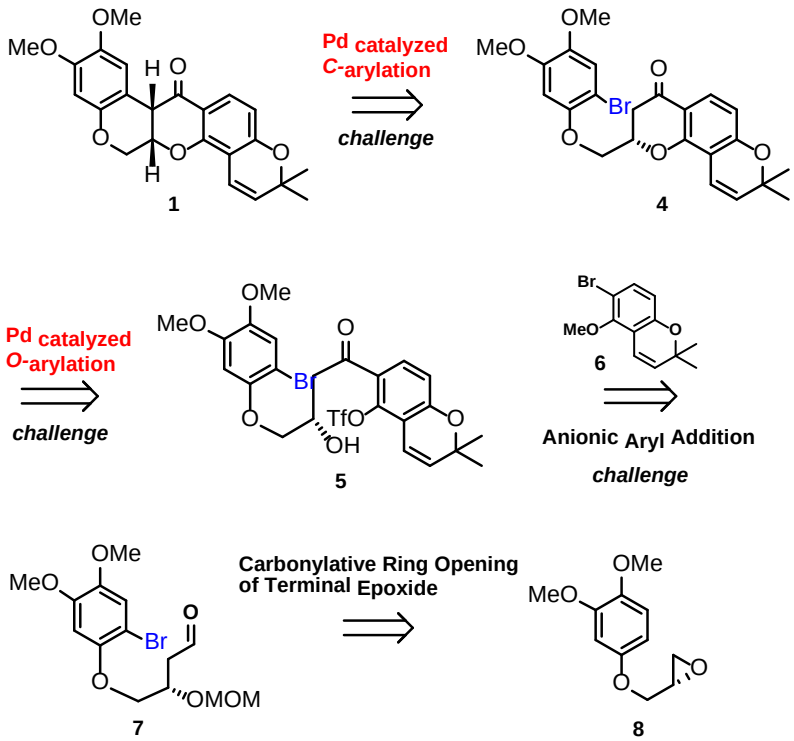

Scheme 3. Previous synthetic approach to (-)-deguelin

Despite extensive research, there were some challenges in our initial paln toward asymmetric total synthesis of (-)-deguelin.(Scheme 4) First of all, on account of early stage bromination, yield of anionic aryl addition of common intermediate aryl bromide **6** to bromoaryl aldehyde which was first key step was not satisfactory. It resulted from side reaction of bromoaryl aldehyde with *n*-butyllithium. In addition, Pd-catalyzed O- and C-arylation were also hard to be optimized. Byproduct which was coupled between secondary alcohol and arylbromide instead of aryltriflate and low yield were observed in first Pd-catalyzed O-arylation. The enantiomeric ratio and yield of second Pd-catalyzed C-arylation, final key step were low although we performed multitudinous conditions of Pd-catalyzed α–arylation.

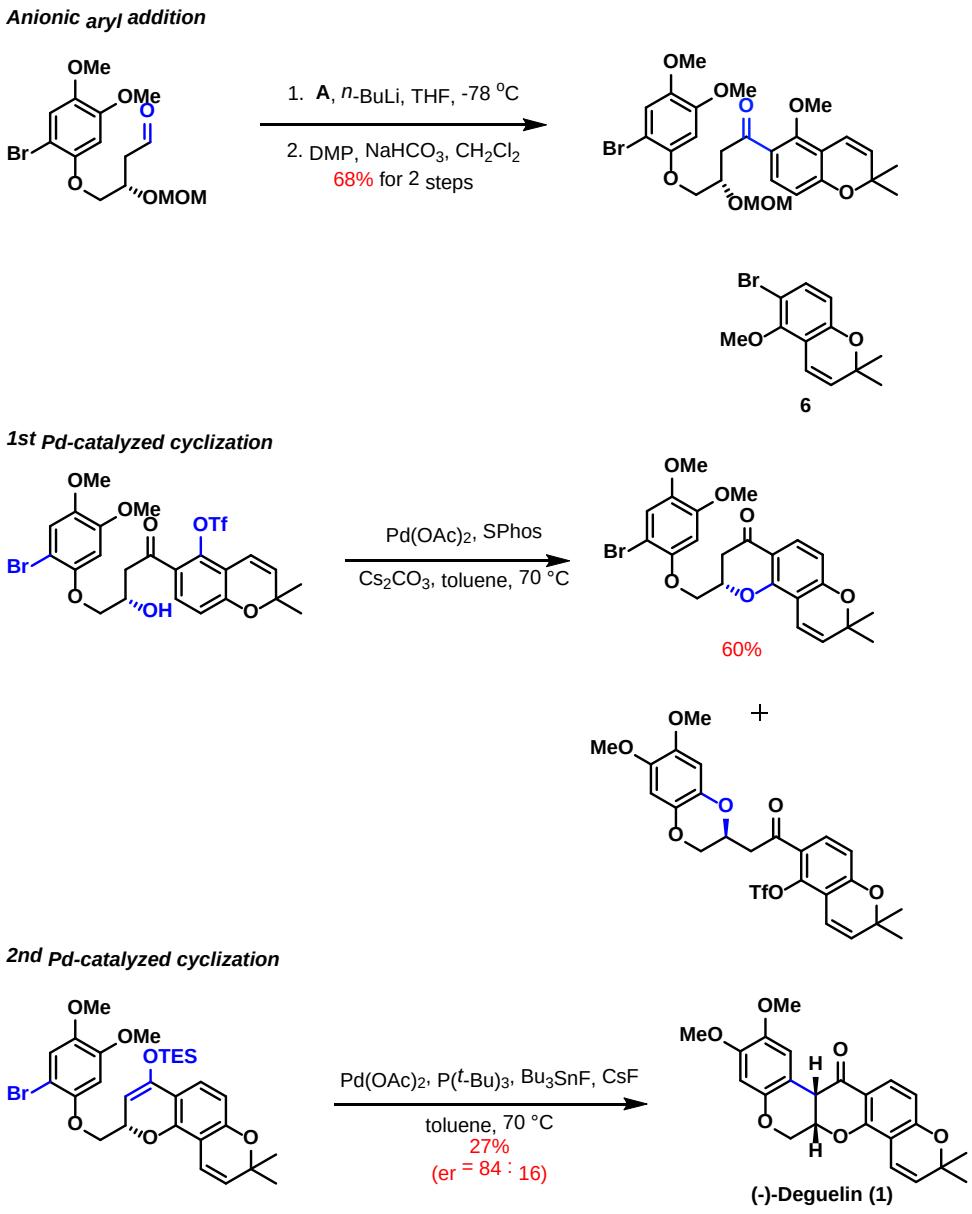

Scheme 4. Challenges in previous study

2. Heat Shock Protein 90 and Hypoxia-Inducible Factor-1 alpha

Heat shock protein 90 (Hsp90) is a protein concerned with maintaining normal folding, function and stability of client proteins such as Hypoxia-inducible factor 1 alpha. In normal conditions, Hsp90 has a influence on the signaling pathways regulating cellular phenotype

including cell growth, division, differentiation, migration and death.[17] Usually, when Hsp90 plays a role in cellular signaling pathways, dimer of Hsp90 is formed. Hsp90 has two ATP-binding sites, N-terminal and C-terminal ATP-binding site. The C-terminal domain possessing ATP-binding site is responsible for Hsp90 dimerization and contains binding site for co-chaperones.[18-20] Natural products, geldanamycin and radicicol are known as Hsp90 inhibitors binding to N-terminal ATP-binging site. While geldanamycin binds towards the front of the ATP-binding pocket, radicicol binds at the back of the ATP-binding pocket. The molecular machinery in which ATP/TDP binding status dictates the nature of the co-chaperones or client proteins binding to and released form Hsp90 is called 'chaperone cycle'. In chaperone cycle, ATP-dependent dimerization of the N-terminal domain is crucial. Thus, inhibition of ATP binding and hydrolysis gives rise to the recruitment of an ubiquitin ligase bring about the proteasomal degradation of client proteins.(Figure 2)[21] Owing to this well-known structure, function and operating machinery of Hsp90, it has developed over the last decade as one of most attractive drug targets for anti-cancer. [22-25]

2-1. Hsp90 in cancer

Hsp90 particularly participates in the development, maintenance and progression of tumor.[22,23,26] Higher expression level of Hsp90 in cells cause oncogene-transformed and malignant condition of cells.[27] Many oncogene products or proteins taking part in oncogenic process are client proteins of Hsp90. ErbB2, Raf-1 and Akt are client proteins of Hsp90 and hallmark trait proteins as self-sufficiency in growth signals. Plk, Wee1 and Myt1 play a role in hallmark trait as insensitivity to growth suppression signals. PIP and Akt are concerned with evasion of apoptosis. Acquisition of limitless replicative potential with hTERT is known. Met inducing invasion and metastasis of tumor is also a client protein of Hsp90. Importantly, HIF-1, FAK and Akt are responsible for sustained angiogenesis and relevant Hsp90 client protein.

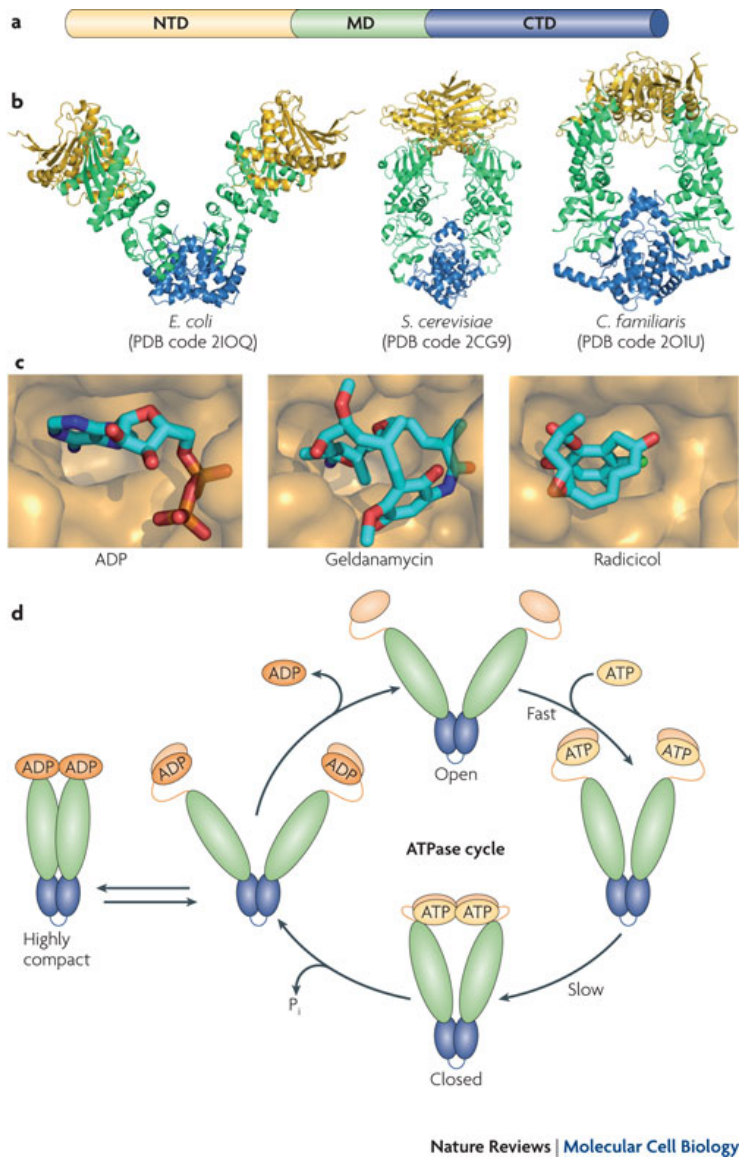

Figure 2. HSP90 domain structure and chaperone cycle

2-2. HIF-1α regulation

Hypoxia-inducible factor 1 alpha (HIF-1α) is one of the most powerful pro-angiogenic proteins regulated by Hsp90. A lot of solid tumors suffer from hypoxic condition as they

grow far away from blood vessel. Under the hypoxic condition, tumor has to develop new blood vessel to survive. It is known as ‘angiogenesis’ or ‘neovascularization’. HIF-1 which upregulates the expression of genes and proteins promoting angiogenesis, anaerobic metabolism and other survival cellular signaling pathways is a crucial mediator of the hypoxia-response of tumor cells.

In solid tumor, their rapid expansion rate cause surpassing the vascular supply resulting in lacking oxygen delivery. Tumor hypoxic responses are promoted by a variety of hypoxia-inducible transcription factors including nuclear factor κB (NF-κB), activator protein 1 (AP-1) and p53. Yet, HIF is the major regulator of hypoxic responses. Particularly, vascular endothelial growth factor (VEGF) which is the most potent angiogenic signal protein is upregulated by activation of HIF-1 expression.(Figure 3)[28-30]

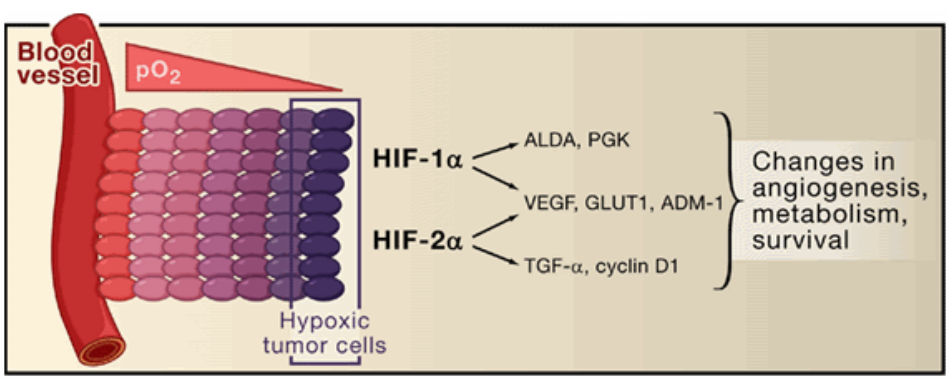

Figure 3. Tumor hypoxia and expression of HIF-1

Under normal oxygen concentrations called as normoxia, HIF-1α protein undergoes hydroxylation with oxygen by Prolyl Hydroxylase Domain (PHD) proteins in the presence of Fe^{2+}, 2-oxoglutarate and ascorbate. The von Hippel Lindau protein (VHL) recognizes the Hydroxylated HIF-1α and binds to become a complex which is the substrate of the recognition module of the E3 ubiquitin ligase complex. This complex induces the ubiquitylation of hydroxylated HIF-1α and allows recognition by the proteasome.

Subsequently, HIF-1α rapidly degraded via proteolytic degradation of proteasome.[31-33] Another normoxic regulation of HIF activity as a transcriptional factor is commenced with hydroxylation of an aspargine residue (Asn803) of HIF sequence. The transcriptional activity of this hydroxylated HIF is suppressed by interfering the intheraction with the co-activators, p300-CBP binding protein complex.[34]

In contrast, under oxygen deficient condition, hydroxylation via Proline Hydroxylase is limited by low oxygen concentration. Absence of hydroxyl group of HIF-1α proline residues(Pro402 and Pro564) prevents VHL from recognizing and binding HIF-1α. This molecular signaling pathway results in accumulation of HIF-1α and dimerization with HIF-1β. Heterodimerization between HIF-1α and HIF-1β is promoted by direct interaction with HIF-1α which cause changing and stabilization of HIF-1α conformation. The HIF-1α and HIF-1β complex binds to HRE within the promoters of hypoxia-inducible genes and recruits p300-CBP binding proteins which are transcriptional co-activators to promote full transcriptional activity.[35]

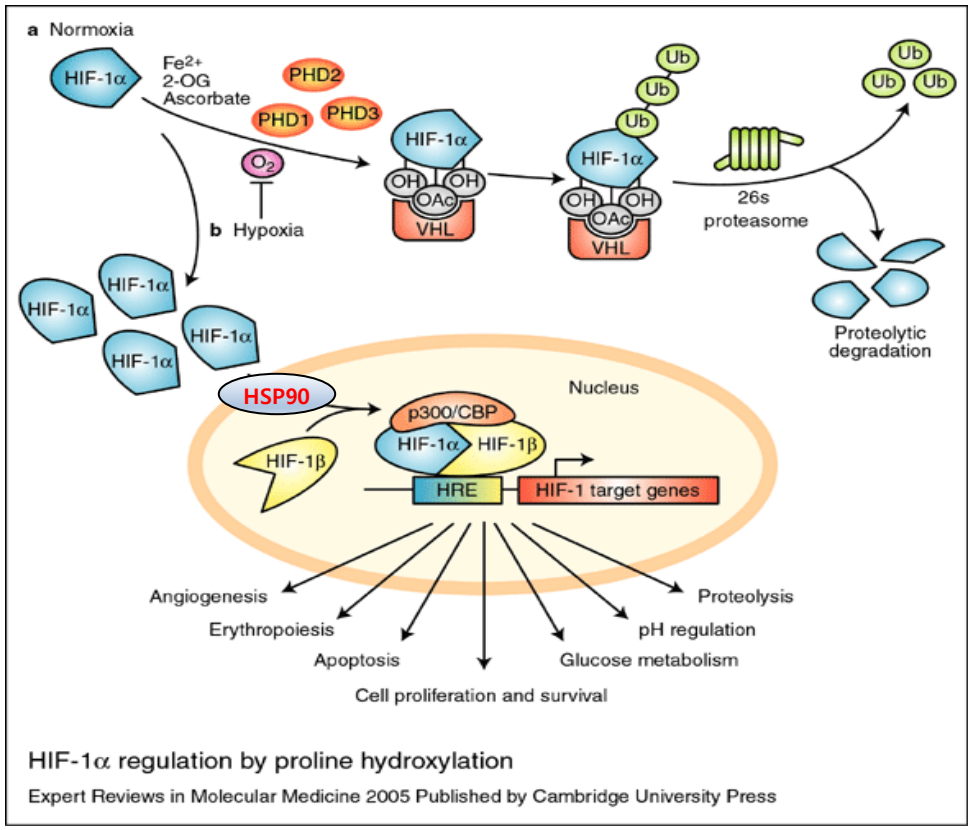

Figure 4. HIF-1α regulation of Hsp90

3. Retinal Neovascularization Disease

3-1. Disease and therapies

Angiogenesis on retinal or ocular region causes several ocular diseases called as retinal neovascularization disease. Major indications are age-related macular degeneration (AMD), diabetic retinopathy (DR), retinopathy of prematurity and central retinal vein occlusion. (Figure 5)[36] Market size of age-related macular degeneration and diabetic retinopathy is so much bigger than the others. The only one therapy is available for these retinal neovascularization diseases and that is using anti-VEGF biodrugs which have limitations as high-price and genetic toxicity.

AMD is a progressive chronic disease, major reason of vision loss among patients over the

age of 65. Factors of AMD are diverse as genetic and environmental influences including hyper-sunlight, oxidative stress, aging, smoking, obesity and hypertension.[37] Groups of AMD are two, dry and wet macular degeneration.[38] The dry-type AMD is defined by the presence of non-cellular polymorphous debris, 'drusen' between the basal lamina of RPE and Bruch's membrane.[39] Leading cause of the blindness is wet AMD although, Only 20% of people with AMD have the wet-type.[40] The wet-type AMD is defined by the growth of a choroidal neovascularization (CNV), which is growth of blood vessels of the choriocapillaris grow into the Bruch's membrane.[41] To conclude, vision loss may result from CNV formation in ocular regions.

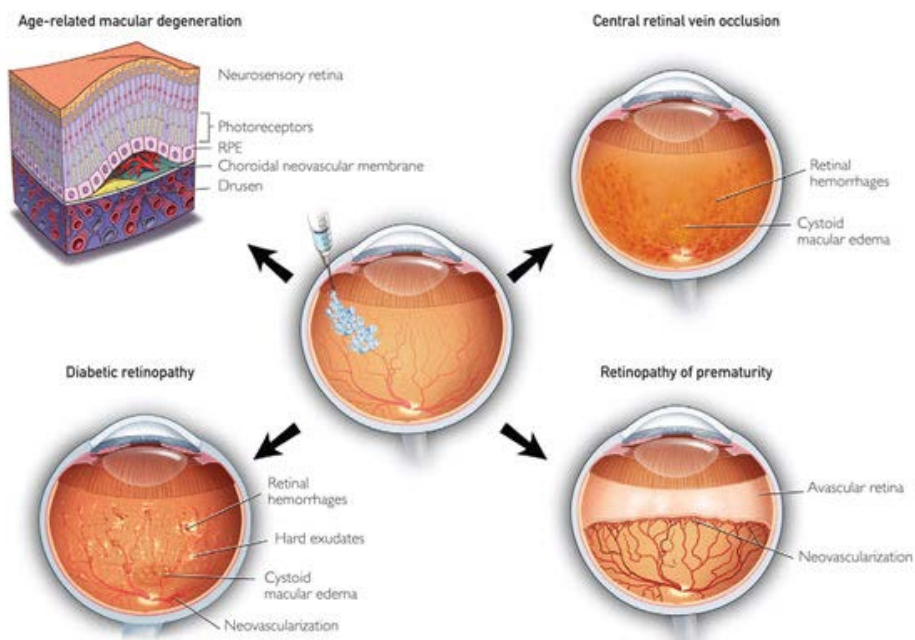

Figure 5. Common indications for intraocular anti-VEGF injections

Mechanism of AMD is known as the following sequences starting with hypoxia, chronic oxidative stress and inflammation.[39,42,43] Increased metabolic activity of the inflamed retina

and decreased circulation in retina cause higher consumption of oxygen, followed by hypoxia.[44,45] While, thickening of Bruch's membrane and formation of drusen cause stabilization of HIF.[71] In addition, it was reported that higher expression of HIF-1α and HIF-2α in CNV concerned with AMD.[46]

DR occurs in almost every patient exhibiting retinopathy symptoms among the diabetic patents. DR is a major reason of the four leading causes of vision loss.[47,48] DR is defined by biphasic progression with an initial non-proliferative diabetic retinopathy (NPDR) followed by a proliferative diabetic retinopathy (PDR) (Figure 6).[49]

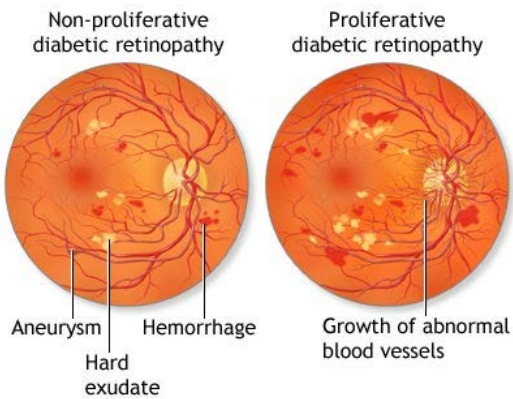

Figure 6. Diabetic retinopathy

Since blood glucose concentration gradually increases during the period of initial non-proliferative stages in diabetic patient, the blood vessels in the retina are weakened. The small saccular capillary outpouchings may occur and leak fluid into the retina.[50] The fluid result in swelling of the macula which cause blurred vision. The resulting hypoxia promotes the expression of angiogenic factors followed by neovascularization and make the disease into the proliferative stages.[51] The neovascular blood vessels in the retina and into the vitreous make the vision cloudy.[52,53]

By means of extensive research on VEGF over several decades, VEGF is known to play

an important role in both physiologic and pathologic angiogenesis. Also, the contribution on increased permeability across both the blood-retinal and blood-brain barriers has been revealed. Based on the preceding results, anti-VEGF agents started to be used in the management of ocular diseases.

The only one therapy is available for these retinal neovascularization diseases and that is using anti-VEGF biodrugs which have limitations as high-price and genetic toxicity.

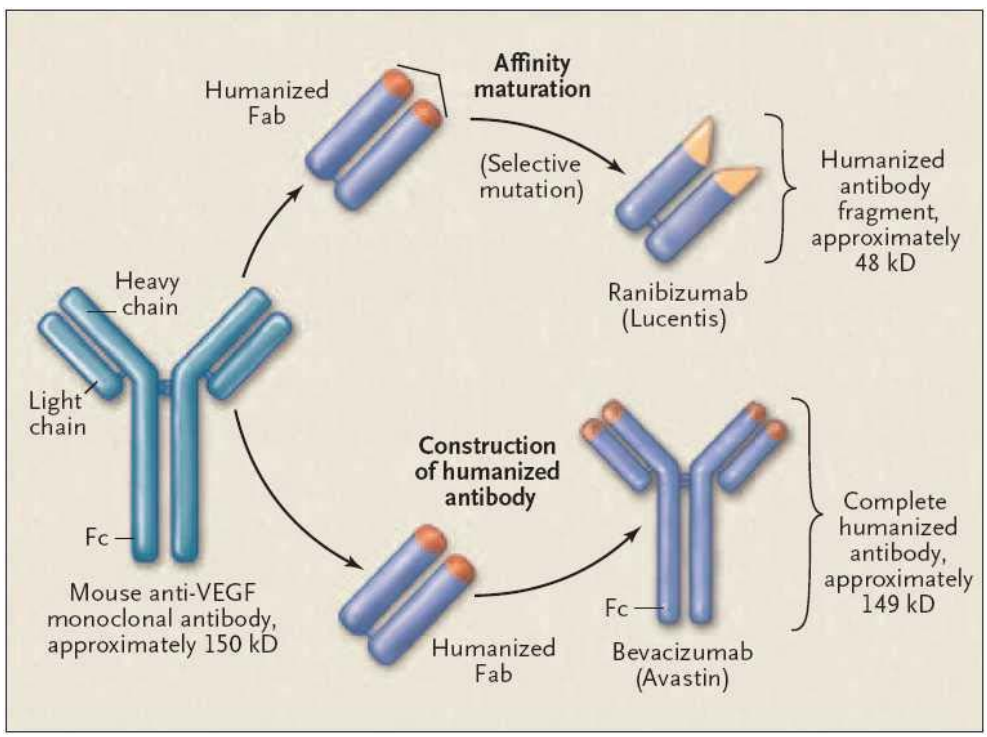

Figure 7. Anti-VEGF agents, Lucentis and Avastin

First administration via intravenous injection for wet AMD initiated with Bevacizumab (Avastin®) after approval for an off-labeled anti-cancer agent. According to uncontrolled open-label clinical studies of Avastin® over 12 weeks and 24 weeks, wet AMD patients showed significant improvement in visual function, retinal thickness and angiographic outcomes. Direct intravitreal injection of Avastin® which is a ful length of antibody derived

from mouse anti-VEGF monoclonal antibody (149 kD) also achieved improvement of the wet AMD with minimizing the systemic adverse effects supported by low diffusion rate through the retina into the choroid.(Figure 7)[54-56]

Modification of the complementary domain region of Avastin®, followed by affinity selection produced ranibizumab (Lucents®).[57] Lucents® showed the improvement in visual outcomes during the phase 3 clinical trial studies and was approved by the FDA for the treatment of wet AMD.[58,59] While, anti-VEGF agents have been used as treatment of DR because VEGF also plays important role in DR with diabetic macular edema. Recently, Lucents® is the drug of choice and only FDA-approved medicine for diabetic macular edema.

A number of adverse effects of Avastin® was reported. First, acute intraocular inflammation involving sterile endophthalmitis, pseudoendophthalmitis, posterior uveitis was reported by the comparison of AMD treatments trial in 2008. In addition, the number of patients complaining of systemic adverse effects was higher. On the contrary, both adverse effects occurred in lower rate with Lucents®.[60-66] The major problem in case of Lucents® is higher cost more than $2,000 per a sing dose of administration. It is contrast from a single dose of bevacizumab cost, $50.

Most importantly, neurotoxicity of anti-VEGF condition was well researched and reported. VEGF neutralization causes apoptosis of neuroretinal cell and malfunction of retina. Endo genous VEGF plays a significant role in development of choriocapillaris, maintaining of cone photoreceptor function and regulation of the multiple angiogenesis related genes. While direct inhibition of VEGF has been controversial, normal expression level of the multiple angiogenesis genes is observed when HIFs are deleted by mutations. Therefore, targeting HIFs which are the upstream target of VEGF may maintain physiological vasculature and function of neuroretinal cell.[67-70]

3-2. Previous studies

After the development of novel HIF-1α inhibitors based on natural product deguelin, we focused on elucidation of structure-activity relationship for representative compounds, **SH-42** and **SH-80** discovered as new HIF-1α inhibitors with a novel scaffold, avoiding the structural complexity of deguelin.(Figure 8) **SH-42** and **SH-80** exhibited excellent anti-proliferative activities in the H1299 cell line and suppressed HIF-1α expression and tested significant activity for in vivo model such as mouse choroidal neovascularization (CNV) and oxygen-induced retinopathy (OIR) model. The initial synthetic procedure for preparation of ring-truncated analogs and chromene ring-truncated analogs has been achieved.[71,72]

Despite we had synthesized diverse compound derived from representative compounds, **SH-42** and **SH-80**, the evaluation and full structure-activity relationship (SAR) for HIF-1α inhibition of derivatives have been remaining tasks. It is impossible to select representative derivatives of **SH-42** or **SH-80** before evaluation for anti-angiogenesis and in vivo ocular disease model since western blotting of HIF-1α which was primary screening assay is not reproducible and has big standard deviations. Thus, we attempt to confirm the activity for anti-angiogenesis and in vivo model after completion of full SAR of parent compounds through additional synthesis of novel HIF-1α analogs.(Figure 9)

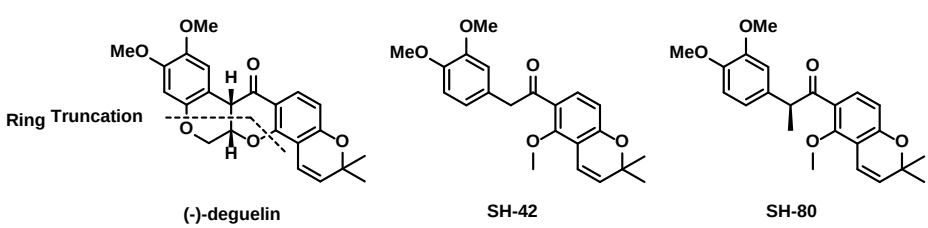

Figure 8. Strategy toward previous representative analogs of deguelin, SH-42 and SH-80

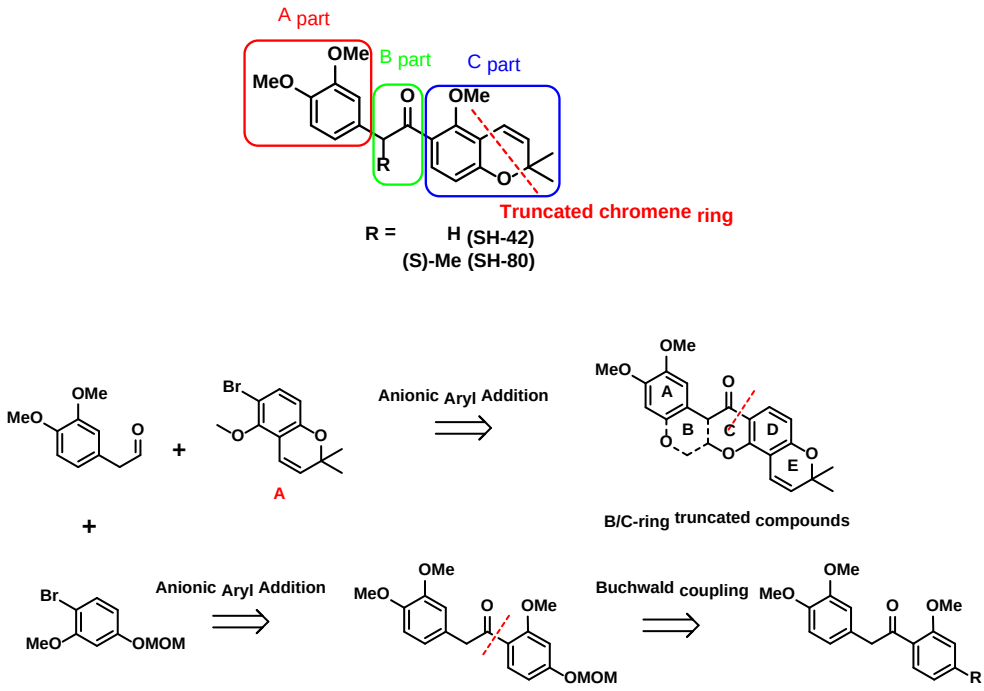

Figure 9. Strategy for SAR of representative alanogs and initial synthetic procedures

II. Results and Discussion

1. Enantioselective total synthesis of (-)-deguelin

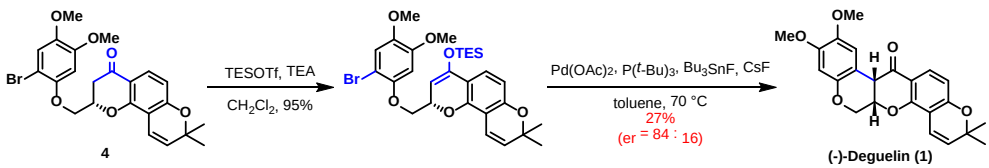

Scheme 5. Previous Pd-catalyzed α-C-arylation

After further attempts for successful cyclization of **4**, we decided to replace aryl bromide **4** with aryl iodide **9**, which was anticipated to undergo more facile oxidative addition with Pd-catalyst. We ultimately expected that more reactive oxidative addition would result in higher conversion yield and lower racemization during the *C*-arylation. As shown in Scheme 6, iodide substitution at the late stage was designed because we concerned that the labile aryl iodide moiety would not be tolerable during the *O*-arylation and preparation of the other arylation precursor **10**.

The most challengeable step in previous enantioselective synthesis of (-)-deguelin is the last step, Pd-catalyzed α-C-arylation. Mechanism of α-arylation begins with oxidative addition of Pd-ligand complex to arylhalide. In the presence of Pd-aryl complex, α-metalated ketone undergoes transmetalation toward Pd-aryl-ketone complex generating the desired product after reductive elimination of Pd-ligand complex.(Figure 10) The epimerization of β–phenoxy group may occur via elimination and oxa-michael addition during the presence of the enolether or α-metalated ketone formed from ketone with base since already generated (-)-deguelin did not undergo the epimerization in same Pd-catalyzed α-C-arylation reaction conditions. Thus, we attempted to decrease the existence

time of α-metalated ketone by escalation of oxidative addition rate to form excess Pd-aryl complex.

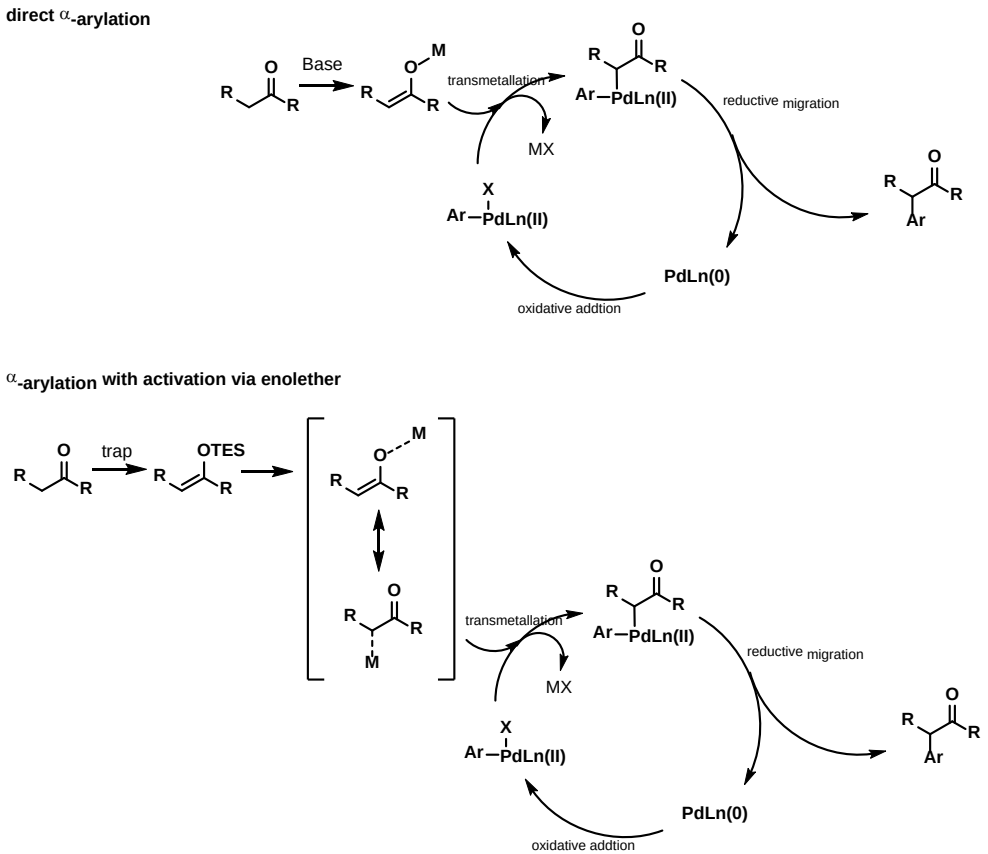

Figure 10. proposed mechanism of two type of α-arylation

1-1. Retrosynthetic analysis

Our synthetic approach to (-)-deguelin is shown in Scheme 6. We envisioned that double Pd-catalyzed arylation of β-hydroxy ketone **11** would give the desired *cis*-fused bisbenzopyran system of **1** through transferring a chirality of the β-hydroxy moiety to the α-position of ketone. The final diastereoselective pyran ring formation was anticipated based on Pd-catalyzed α-arylation of ketone **9**. The first pyran ring formation would be possible via Pd-catalyzed *O*-arylation of β-hydroxy ketone **11**, which can be prepared from

aldehyde **12** via convergent procedure. Anionic addition of chromene **6** to aldehyde **12**, which is derived by a carbonylative epoxide opening of **8**, provides **11**. Chromene **6**, which was reported by us, is conveniently prepared via a sequence of chemoselective propargylation of 6-nitro-resorcinol, regioselective Claisen rearrangement of the resulting alkylaryl ether, and Lewis acid-promoted etherification.[10]

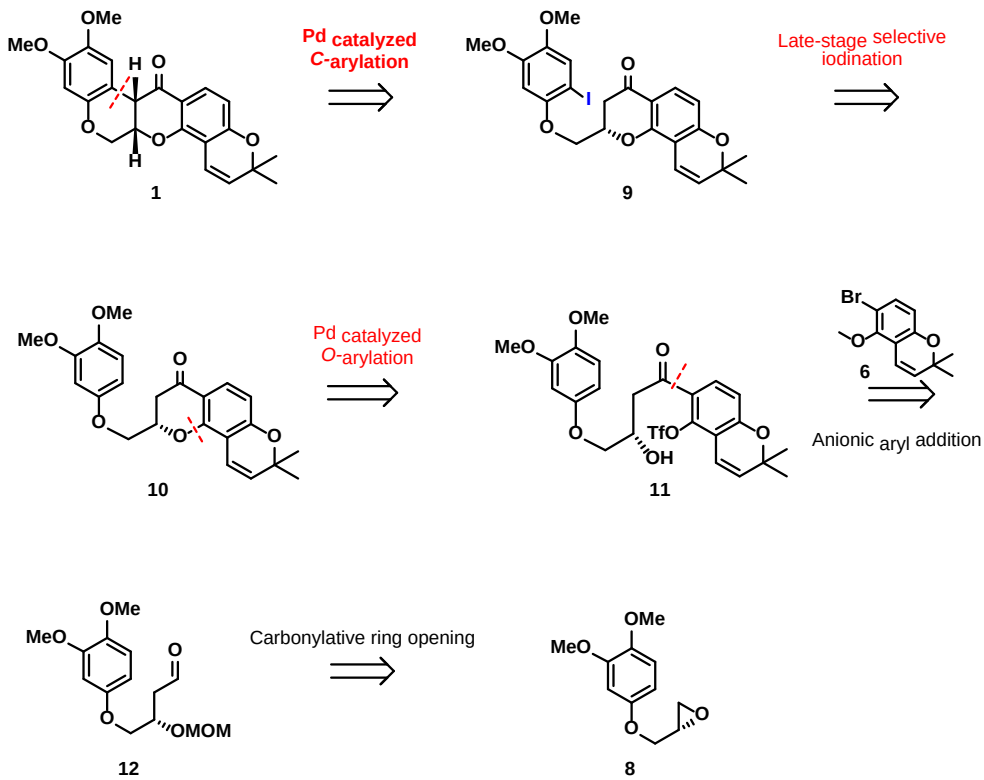

Scheme 6. Retrosynthetic analysis of (-)-deguelin

1-2. Preparation of first Pd-catalyzed cyclization precursor

As outlined in Scheme 7, the revised synthesis commenced with preparation of the advance intermediate **11**, which will be iodinated after the first arylation to give the second Pd-catalyzed arylation precursor **9**.

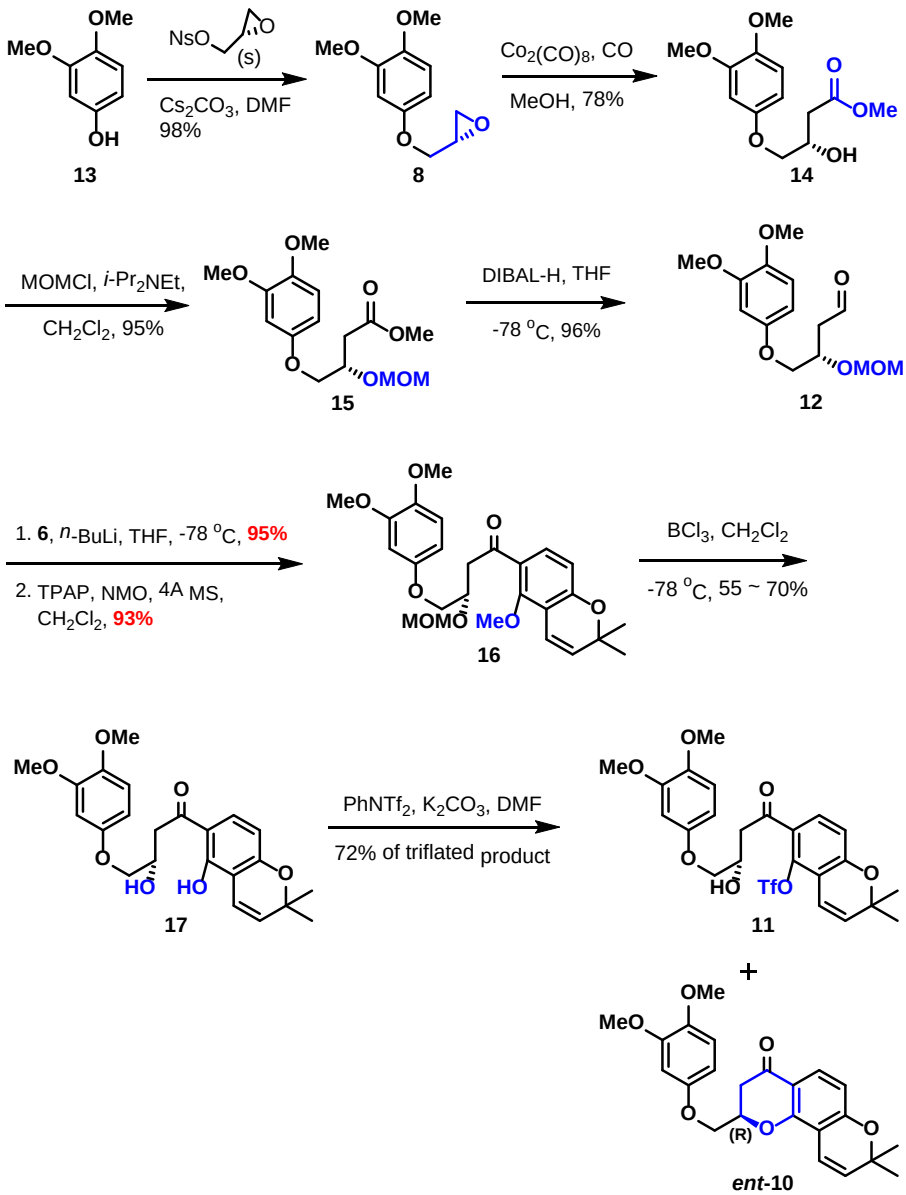

Scheme 7. Preparation of first Pd-catalyzed cyclization precursor

Treatment of 3,4-dimethoxyphenol **13** with (*S*)-glycidyl 3-nitrobenzenesulfonate produced epoxide **8** in 98% yield. Carbonylative ring opening of **8** with CO in the presence of $Co_2(CO)_8$ and MOM protection of the resulting β-hydroxy ester afforded **15** as a single product.

DIBAL reduction of ester **15** and coupling of the resulting aldehyde with the chromene unit **6** followed by DMP oxidation afforded ketone **16**. Global deprotection of **16** and chemoselective triflation of the resulting diol produced mono-triflate **11** as a first arylation precursor. Chemoselective triflation was again extensively examined under a variety reaction conditions. Finally, $PhN(Tf)_2$ treatment of diol dissolved by DMF in the presence of potassium carbonate provided the desired mono-triflate **11** in 72 % yield, which is higher than that for **5**.

1-3. First Pd-catalyzed cyclization and late-stage regioselective iodination

The Pd-catalyzed *O*-arylation of **11** toward tetrahydropyanone **10** was greatly improved as shown in Scheme 8 under the reaction conditions described for aryl bromide **4**. At this stage, preparation of intermediate **10** by a different strategy and its direct cyclization to (-)-deguelin was independently reported by Scheidt's group[73] although the conversion yield was still not satisfactory. Thus, we executed our own strategy to complete the synthesis of deguelin in expectation of improved results in terms of enatioselectivity and conversion yield.

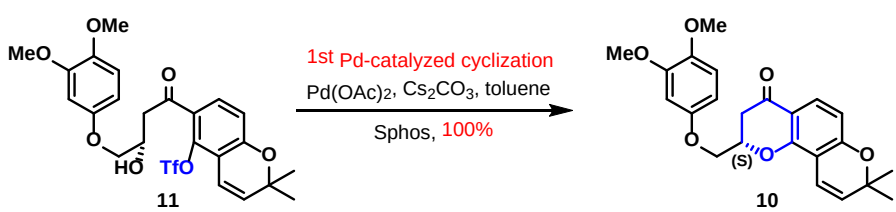

Scheme 8. Excellent improvement of first Pd-catalyzed cyclization

We exerted our effort for regioselective iodination of **10** without affecting another aromatic system, which was coupled before iodination compared to the halogenation substrate shown in **Scheme 3**. We optimized the iodination conditions to obtain the desired

iodination product **9** in a moderate yield.(Table 1)[74-76] The ketone **9** was quantitatively converted to silylenol ether **18**, which could be purified by chromatography.(Scheme 9)

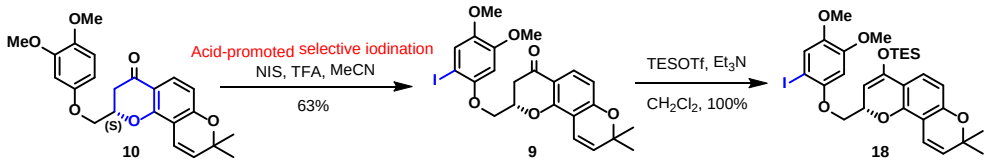

Scheme 9. Preparation of second Pd-catalyzed cyclization precursor

Table 1. Optimization of late-stage regioselective iodination

Entry	I-source	Additive	Solvent	Temperature	Time	Yield [a] of 9
1	I_2	-	MeCN	rt	60min	Decomposed
2		$AgNO_3$	MeOH	rt	O/N [b]	Byproduct
3		$AgNO_3$	MeCN	rt	O/N	43%
4				rt	10min	38%
5				-10℃	15min	40%
6				-10℃	3hrs	Decomposed
7	NIS	-	MeCN	rt	60min	51%
8		**TFA(cat.)**			15min	**63%**
9		Acetic acid(cat.)				27%
10		PPTS(cat.)				31%
11		PTSA(cat.)				34%
12		TFA(cat.)	THF	rt	30min	42%
13		I_2(0.3equiv.)	MeCN	rt	60min	54%
14		I_2(0.6equiv.)				56%
15		I_2(1.1equiv.)				36%

[a] Isolation yied of desired monoiodination product, [b] O/N = over night

1-4. Endgame of asymmetric total synthesis of (-)-deguelin

With the desired silylenol ether **18**, we investigated Pd-catalyzed *C*-arylation to obtain the enantiomerically enriched (-)-deguelin (**1**). Generally, $AsPh_3$ was superior over other ligands including P(*t*-Bu)$_3$ in terms of conversion yield and stereoselectivity. Presumably $AsPh_3$ stabilizes the Pd-substrate-stannane complex ultimately to increase yield and

stereoselectivity.[77] As shown in Table 2, CsF (1.4 equiv.) as a fluoride source was essential to produce the cyclization product. Interestingly, arylation in a co-solvent of toluene and THF (10 : 1) with gradual raise of temperature resulted in effective arylation although partly racemization was observed in the polar solvent, presumably via initial elimination of phenoxy group.[73] Noticeably, use of benzene considerably enhanced both enantioselectivity and conversion yield. In this particular case, the reaction was completed with minimal racemization. Consequently, the final cyclization was completed in 72% conversion yield with an 80 : 20 enantiomeric ratio. Reduced time for *C*-arylation increased enantioselectivity up to 90 : 10 although the conversion yield was decreased to 30%. Obviously, the significantly improved result is likely due to facile arylation of the iodinated precursor as well as optimized reaction conditions including solvent and ligand.

Table 2. Pd-catalyzed intramolecular *C*-arylation

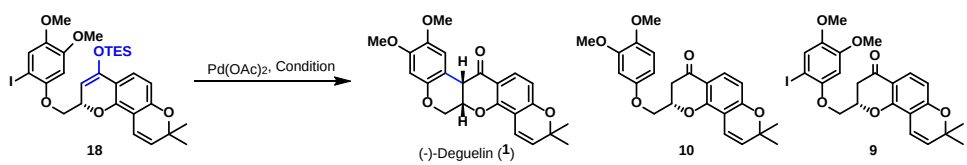

Entry	Ligand	Bu_3SnF (equiv.)	CsF (equiv.)	Solvent	Reaction time (h)	Temperature (°C)	Results	er
1	$P(t\text{-}Bu)_3$	1.4	1.4	toluene	O/N[a]	70	<10% of **1**	
2		3	3				Degradation	
3	$AsPh_3$	1.4	1.4	toluene	4	60	**1** (20~40%)	68 : 32
4		3	3				Degradation	
5		1.4	0		O/N		No reaction	
6		1.4	1.4	THF, DMF, MeCN or Et_2O	O/N	60	**9**	
7				Tol.:THF (10:1)			**1** (60%)	45 : 55
8				m-xylene			**1** (23%)	65 : 35
9				**benzene**			**1 (30%)**	**90 : 10**
10				**benzene**			**1 (72%)**	**80 : 20**
11				DCE			**10**	

[a] O/N = over night

In summary, total synthesis of (-)-deguelin was achieved through 12 steps with 8.4% overall yield. The key feature of our synthesis includes an efficient preparation of the double cyclization precursor via highly convergent assembly of two aromatic systems and facile construction of the *cis*-fused bisbenzopyran skeleton via Pd-catalyzed *O* and *C*-arylation. In addition, the key architecture of the intermediate involves carbonylative epoxide ring opening catalyzed by cobalt. Our iterative intramolecular arylation strategy seems quite widely applicable in the rotenoid synthesis.[78]

2. Identification and application of representative Hsp90 inhibitor, SH-42 into cancer

As we developed the representative ring-truncated analog **SH-42**, which showed excellent inhibitory activity on H1299 cell line and anti-angiogenic effect, the large amount of **SH-42** needed to be synthesized for examinations including cytotoxicity of multiple naïve cell lines, mechanism of direct binding to Hsp90, xenograft model derived from patient and neurotoxicity which was presented in case of natural product deguelin.

2-1. Large scale synthesis of SH-42

Previously, we had synthesized the representative analog, **SH-42** which was reported as **SH1242** in 2016, by the reaction sequence starting to anionic coupling between 3,4-dimethoxyphenylacetaldehyde and bromobenzopyran unit. Yet, bromobenzopyran unit, the common intermediate used to synthesis of various 3,4-dimethoxybenzene modified derivatives, has limitations of large scale synthesis due to their harsh synthetic reaction conditions and unsatisfactory total yield. Thus, we had designed reverse anionic coupling of previous method. 3,4-dimethoxyphenylmethylsulfonylide and corresponsive benzaldehyde

instead of 3,4-dimethoxyphenylacetaldehyde **19** and bromobenzopyran unit, respectively, were used. The yield was satisfactory and reaction conditions were much milder. However the scale up of **SH-42** was successful, the problems were generated such as lots of waste, environment-unfriendly reaction conditions and low step economy.(Scheme 10)

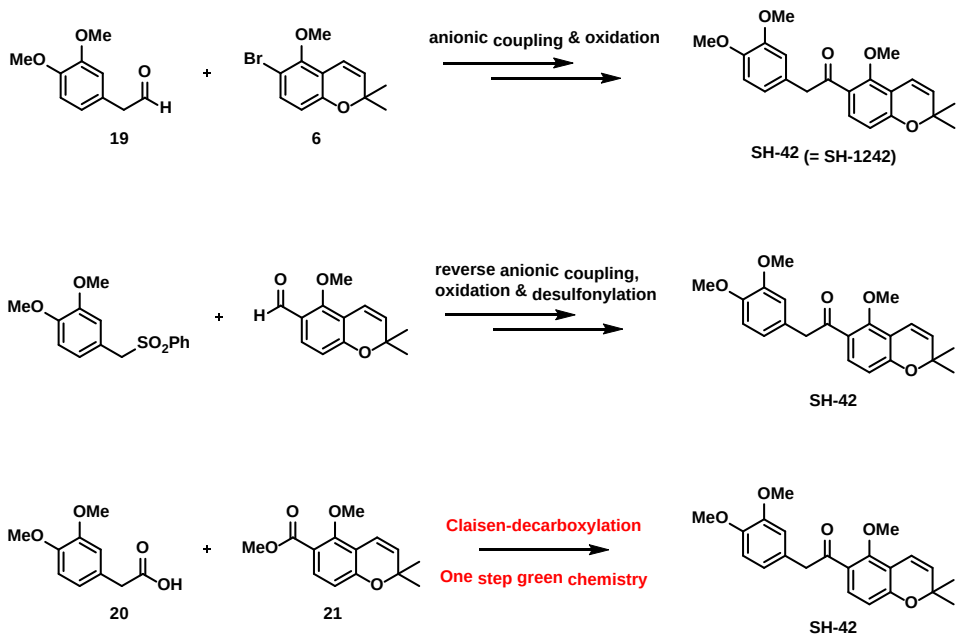

Scheme 10. Synthetic history of SH-42

Finally, we have achieved the efficient synthesis of **SH-42** via tandem claisen condensation-decarboxylation sequence in one pot reaction.(Scheme 11) From 3,4-dimethoxyphenylacetic acid **20**, the only one step is needed in this green chemistry method and the waste of the reaction is only carbondioxide and methanol which is relatively environment-friendly.

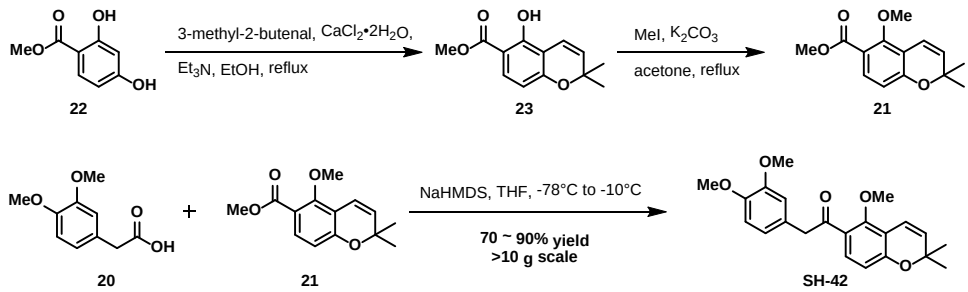

Scheme 11. One step green chemistry method for scale-up of SH-42

2-2. Mechanism study of SH-42

The C-terminal domain of Hsp90 plays a critical role in dimerization of Hsp90. Despite interaction between ATP and the C-terminal domain of Hsp90 was reported, 3D-structure and function of the Hsp90 C-terminal domain sequentially possessing a hydrophobic pocket has been unknown. The large scale synthesis of **SH-42** which is reported as the possible C-terminal ATP binding inhibitor of Hsp90 has afforded additional investigations to prove the biochemical aspects, function and pharmacophore of the Hsp90 C-terminal ATP binding site.[79-83]

We prepared and used the recombinant Hsp90 proteins including Full Length (FL), N-terminal (N), middle (M), and C-terminal (C) to perform the equilibrium binding examination based on fluorescence. We attempted to assess whether the binding site of **SH-42** are localized within the N- and/or C-terminal domains of Hsp90. In Fgure 11, the 340 nm fluorescence spectrum which was emitted from each part of Hsp90 with **SH-42** excited by 258 nm, was shown. The K_d values of **SH-42** for the fragmented Hsp90 N- and C-terminal domains were 27.3 μmol/L and 16.4 μmol/L, respectively. Titration of FL Hsp90 with **SH-42** showed a two-binding curve phase with K_d values of 13.95 μmol/L and 197.1 μmol/L. Under condition of blocked N-terminal ATP binding site of Hsp90 by preincubation with geldanamycin (GAA), the only one binding curve phase with K_d values of 15.7 μmol/L was observed.[84]

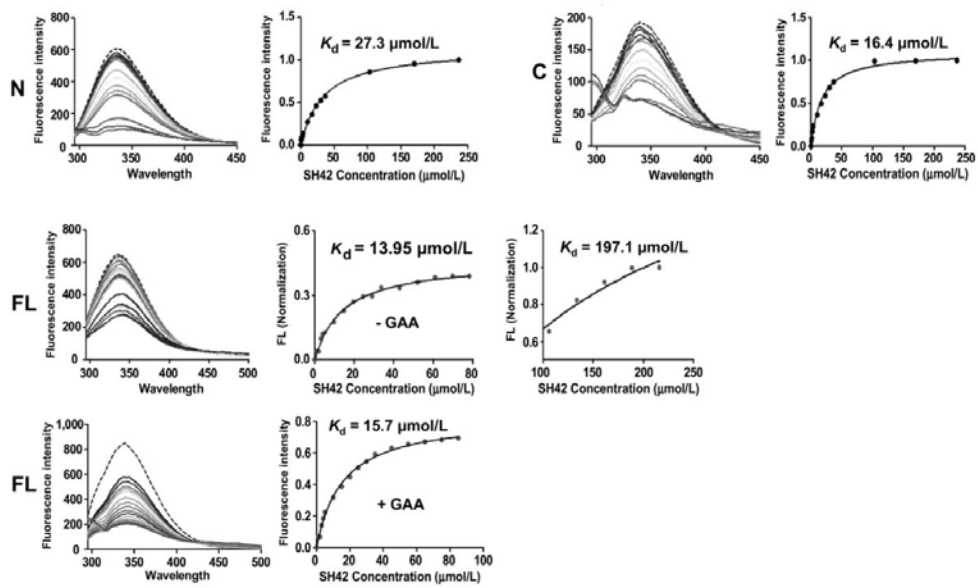

Figure 11. Fluorescence-based analysis of SH-42 and Hsp90 binding

2-3. Applications of SH-42 into cancer

With the help of large scale synthesis of the representative ring-truncated analog of deguelin, **SH-42**, various expeditions on anti-tumor activities and toxicities have become available.

2-3-1. Cytotoxicity of SH-42 for drug-naïve cell lines

As we concerned the development of the targeted anti-tumor agent toward a second-line therapy in the clinical uses, inhibitory activity for colony formation of **SH-42** on acquired resistant cancer cell lines to anti-tumor drugs such as paclitaxel resistant cancer cell lines (H226B/R and H460/R), EGFR TKI gefitinib resistant cancer cell line (PC9/GR), and IGF1R TKI linsitinib resistant cancer cell line (H292/R) were assessed.

SH-42 decreased the cell viability of the naïve cell lines as well as the drug-resistant cell lines. Significant inhibition on anchorage-dependent colony formation of both naïve and drug-resistant cell lines was observed by **SH-42**.(Figure 12)[84]

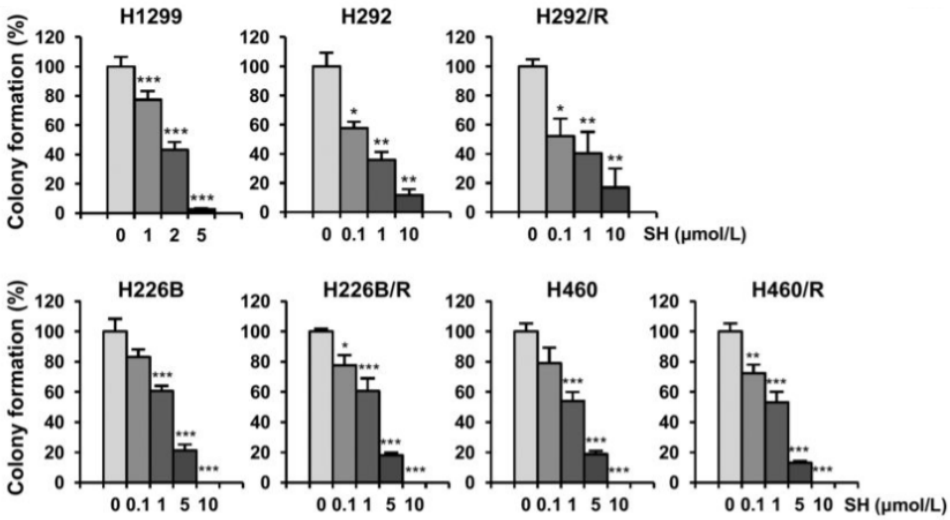

Figure 12. Inhibitory activity of SH-42 on colony formation of drug resistant cancer cells

2-3-2. Xenograft model for SH-42

Concerning with adaptation to artificial in vitro assay conditions of cancer cell lines[85], we examined inhibitory effect of **SH-42** on lung cancer growth in Kras-transgenic mice which must occur lung cancers with a 100% incidence.[86]. **SH-42** which had synthesized as multi-gram scale afforded the dose of 20 mg/kg that had excellent antitumor activities without visible toxicities on NSCLC xenograft model. Intraperitoneal administration with the dose of 20 mg/kg **SH-42** showed remarkable inhibition of lung cancer progression on mutant KRAS-driven Kras-transgenic mice in terms of tumor volume and weight.(Figure 13)[84]

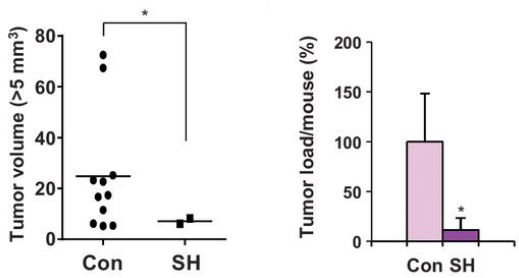

Figure 13. Anti-tumor formation activity of SH-42 on mutant KRAS-driven Kras transgenic mice

As we assured the clinical utility of **SH-42**, human NSCLC cell-derived xenograft model with **SH-42** was performed. First of all, **SH-42** reduced the tumor growth on H1299 xenograft model compared with a control group and also inhibited the tumor growth in case of patient-derived xenograft (PDX) model. At the dose of 4 mg/kg via oral gavage treatment which is the maximum tolerated dose of deguelin, **SH-42** showed significant inhibitory effect on H292 xenograft tumors comparable with geldanamycin and deguelin.(Figure 14)[84]

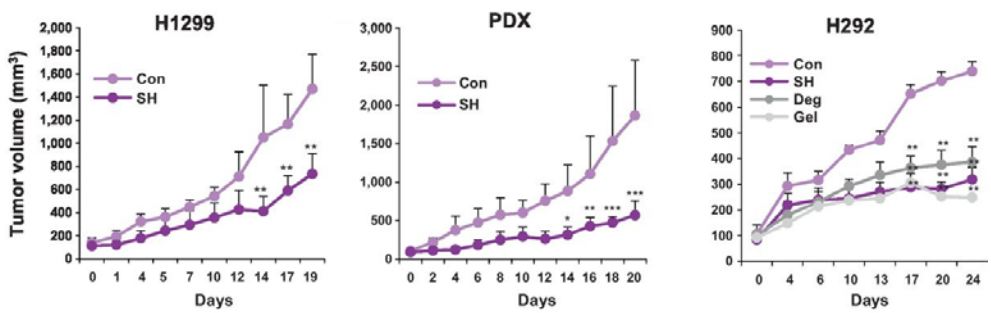

Figure 14. Inhibitory activity of SH-42 on xenograft models

2-3-3. Reduced neuro toxicities induced by SH-42

In the previous studies and clinical trials, deguelin (**1**) showed potential toxicities such as parkinsonism-like syndrome by decreasing the tyrosine hydroxylase immunoreactivity at the rat brain, ocular and liver toxicities.[87,88] Hence, we assessed toxicities of **SH-42** in vivo,

including neurotoxicity by measurement of tyrosine hydroxylase expression level and body weight of rats. Comparison with the effect of **SH-42** and deguelin on tyrosine hydroxylase immunoreactivity in the substantial nigra in rats manifested that the treatment of deguelin decreased the immunoreactivity much more than the treatment of **SH-42**. This result revealed that the potential neurotoxicity is reduced in case of **SH-42** compared with deguelin. Variation of body weight in rats also showed reduced toxicity of **SH-42** compared with deguelin.

On the viability of normal cells and on the neuropathologic lesions in rat brains treated with **SH-42** were tested. The reduced neuropathologic lesions in rat brains treated with SH-1242, was determined by immunofluorescence analysis of tyrosine hydroxyase. Body weight changes of vehicle- or drug-treated rats were manifested in below.(Con, control; SH, SH-1242; Deg, deguelin. *, $P < 0.05$; **, $P < 0.01$; ***, $P < 0.001$, compared with vehicle-treated control.) (Figure 15)[84]

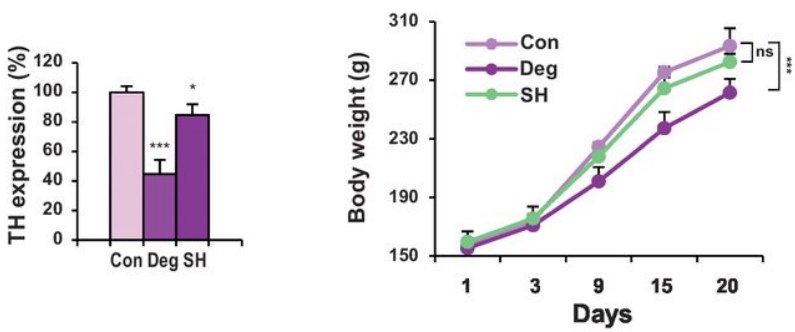

Figure 15. Reduced toxicities of SH-42 compared to deguelin

3. Full SAR of novel HIF-1α inhibitors and application of the representative analog into retinal neovascularization disease

Despite therapeutic potential of the ring-truncated deguelin derivatives, structure-activity relationship (SAR) studies of the compounds has been limited in terms of structural diversity.[10,89] In this article, we describe the design, synthesis, and biological evaluation of

the ring-truncated deguelin derivatives to establish a complete SAR study between the derivatives and HIF-1α. First, we analyzed the structure of the compounds **SH-42** and **SH-80** into three parts for structural modification.(Figure 16) We investigated a role of dimethoxy benzene ring at the A part as introducing diverse substituents on the benzene ring. The ketone moiety at the B part was transformed into alcohol, ester and amides. The role of substituents at the benzylic position was further studied, following up our earlier work.[10] C part-modified derivatives were designed on the basis of chromene-truncation strategy, which implying the possibility of discovering a novel scaffold for HIF-1α inhibition. The synthesized compounds were evaluated by HIF-1α inhibitory activities performing luciferase-reporter assay of HRE-A549 cell to establish SAR of the compounds. Considering drug-like properties of the compounds as well as results of primary in vitro assay, we selected an analog for further biological evaluation. Antiangiogenic activity of the selected compound was confirmed by in vitro angiogenesis assays including proliferation assay, migration assay, and tube formation assay. Finally, suppressing effect on hypoxia-mediated retinal neovascularization of the compound was assessed by utilizing the mouse oxygen-induced retinopathy (OIR) model.[90]

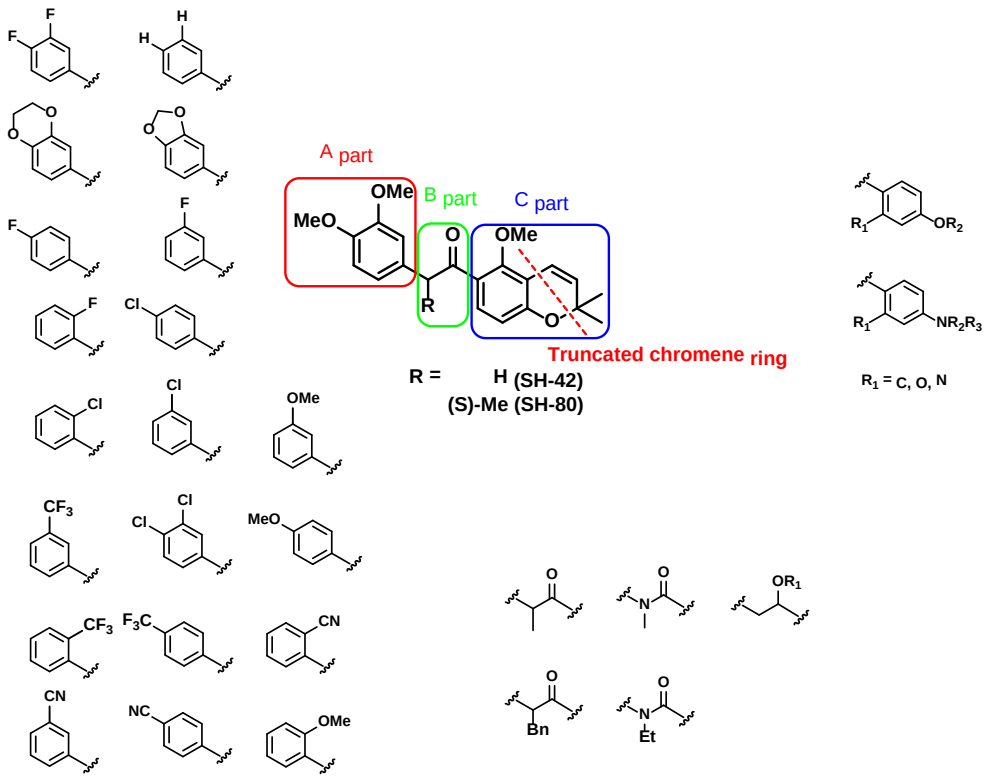

Figure 16. Strategy for SAR of SH-42 and SH-80

3-1. Modification of A-part analogs

The analogs were mostly prepared by linking a benzylic carbon and a carbonyl carbon. The synthetic methods of the carbon-carbon bond formation are outlined in Scheme 12. We previously reported addition of aryl anion to an aldehyde to afford secondary alcohol which was transformed into the corresponding ketone by oxidation reaction.(Scheme 12, Method A)[10,78] The method is well established, however, the chromene-containing aryl bromide **6** was prepared by relatively long six steps from resorcinol. To compensate the weak point of method A, we also utilized reverse anionic coupling between the phenyl sulfonyl intermediates and the chromene-containing aldehyde.(Scheme 12, Method B)[89,91] The preparation of the chromene unit was simplified into two steps from 2,4-dihydroxybenzaldehyde, but we need additional steps for introduction and removal of the

phenyl sulfonyl moiety. More importantly, both two methods used *n*-butyllithium to generate anion, which need to be optimized or replaced for a large-scale synthesis. We successfully established the synthetic method using Claisen-decarboxylation[92] to afford several A part-modified analogs and the key intermediate for chromene-truncated analogs.(Scheme 12, Method C).

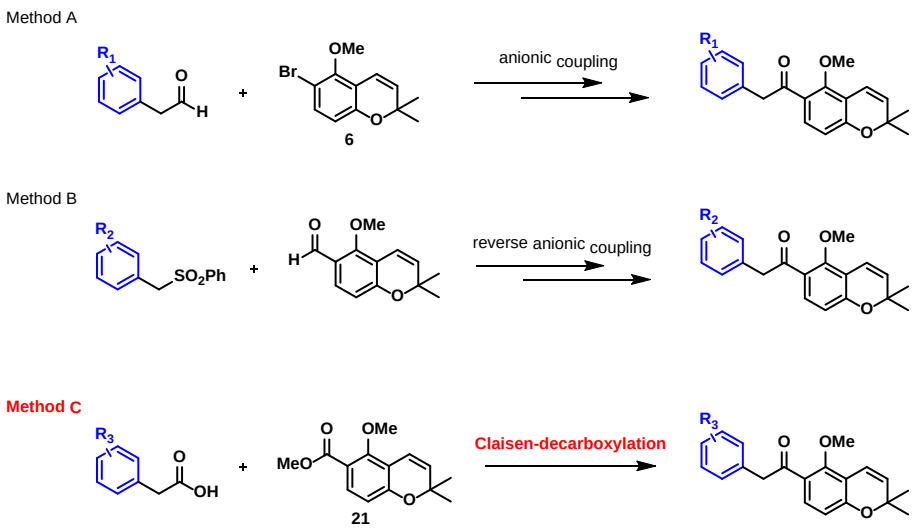

Scheme 12. Methods of synthesis of A-part modified analogs

Syntheses of the A-part modified analogs through the method A are outlined in Scheme 1. Phenethyl alcohols **24** were oxidized to afford the aldehydes. Secondary alcohols **25** were prepared by addition of aryl anion generated by treatment of *n*-butyllithium on aryl bromide **6**[10] to the aldehydes from **24**. Oxidation reactions using Dess-Martin periodinane or pyridinium chlorochromate gave the ketone analogs **26**.

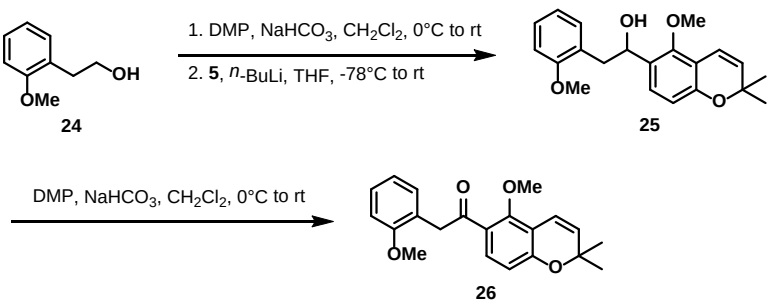

Scheme 13. Synthesis of A-part modified analog via method A

Recently, Wu and coworkers reported Claisen-decarboxylative reaction between carboxylic acids and benzoates as a preparative method for aryl ketones.[92] The method was preferable to two preceding methods in that most phenyl acetic acids were commercially available with reasonable prices, whereas phenyl acetaldehyde or phenyl sulfonyl intermediates were synthesized through several steps. Furthermore, as already shown in Scheme 14, the preparation of the counterpart required only two steps due to electron-withdrawing nature of ester moiety. Several A-part modified analogs were synthesized via the method C as described in Scheme 14. Phenyl acetic acids were treated with NaHMDS to generate dianions, which condensed with methyl benzoate **21** yielded final compounds **28**. It is noteworthy that dichloro compound **28f** was efficiently prepared by the method C (64% from phenyl acetic acid **27f** and an extra process for methyl benzoate **21** with 65% yield for 2 steps) compared to the method A (9% from 3,4-dichloridephenethyl alcohol and an extra process for aryl bromide **6** with 11% yield for 6 steps).

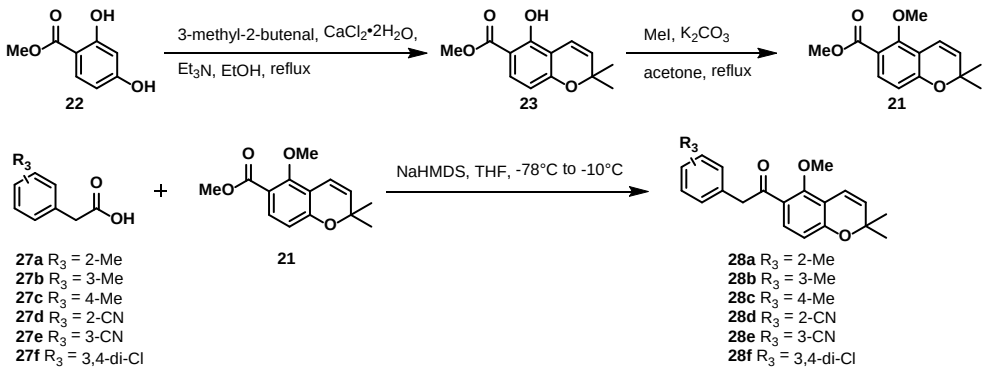

Scheme 14. Synthesis of A-part modified analogs via method C

We started from A-part modified analogs with diverse substituents. Two methoxy groups on A-part was initially thought to be significant moiety as we observed loss of antiproliferative activity with demethylated (monohydroxyl or dihydroxyl) deguelin analogs. Van Meir and coworkers also reported that dimethoxybezene played a crucial role in HIF-1α inhibitory activities of the sulfonamide analogs based on natural product-like chemical library.[93,94] The SAR of Analog **SH-42** is presented in Table 3. The parent compound **SH-42** with two methoxy groups exhibited HIF-1α inhibitory activity with IC_{50} value of 2.15 μM. We first prepared the analogs possessing no subsituent (**entry 2**) or substituent at both of 3- and 4- position (**entry 3-6**) in line with the analog **SH-42**. The analog in **entry 3** which has a dioxolane ring as a tethered form of two dimethoxy substituents showed lower activity compared to the analog **SH-42**, while the analog in **entry 4** with dioxane ring exhibited enhanced activity. We replaced electron-donating methoxy substituent with electron-withdrawing fluorine at 3- and 4- position, as both methoxy moiety and fluorine atom were considered to be hydrogen bond acceptors, even though there had been controversy over ability of fluorine atom to act as a hydrogen bond acceptor.[95,96] Difluoro analog in **entry 5** showed improved activity to the analog **SH-42**, whereas dichloro analog in **entry 6** showed lower activity. Interestingly, analog in **entry 2** with no substituent on benzene ring possessed submicromolar inhibition with IC_{50} of 880

nM, which showed the necessity of investigating the role of diverse substituents considering hydrogen bond, electronic effect and steric effect deviating from initial SAR study of deguelin. As difluoro analog in **entry 5** exhibited the enhanced activity, halogen atoms were firstly introduced to the benzene ring. Fluoro analogs **entry 7-9** and chloro analogs **entry 10-12** showed same tendency as HIF-1α inhibitory activities were in the order of 2- > 3- > 4- position. In addition, fluoro-analogs showed higher activities than chloro-analogs in comparison with the same position. The most potent 2-fluoro analog **SH-199** exhibited 20-fold higher activity than the analog **SH-42** with an IC_{50} value of 100 nM. Analogs with bigger electron-withdrawing trifluoromethyl group (**entry 13-15**) and cyanide group (**entry 16-18**) did not show the same tendency as 4-CF_3 analog in **entry 15** and 4-CN analog in **entry 18** possessed the most potent activity among the series. Analogs with electron-withdrawing group at 4- position showed little change on the activity regardless of types of substituents, while analogs at 2- position exhibited decreased activity as the size of substituent get bigger, which implies that binding site interacting with 2- position is sensitive to the size of substituent. Investigations on role of electron-donating substituents started from methoxy group what the analog **SH-42** possess. The 3-OMe analog in **entry 20** showed improved activity than the analog **SH-42**, however methoxy containing analogs in **entry 19-21** possessed lower activity compared to fluorine (**entry 7-9**) and chlorine (**entry 10-12**) containing analogs with the same position. Phenol analogs **9a** – **9c** were prepared to draw a comparison between methoxy group and hydroxyl group, which could act as a hydrogen bond donor. Interestingly, 2-OH analog in **entry 22** and 4-OH analog in **entry 24** showed significantly increased activity compared to their methoxy analogs, which contradicted the previous SAR study of deguelin using antiproliferative assay.[10] Analogs containing methyl substituent, which still has electron donating character but no hydrogen bond ability showed decreased activity in case the substituent placed at 3- and 4- position (**entry 26 and 27**). 2-Methyl analog **28a** only possessed submicromolar IC_{50} value among

methyl substituted analogs, and even superior to 2-OH analog in **entry 22**. Noticeably, analogs containing relatively small substituents (F, Cl, OH, Me) at 2-position exhibited excellent HIF-1α inhibitory activities with an IC_{50} of submicromolar level, while analogs with substituents over a certain size (CF_3, CN, OMe) showed lower activity. This fact supported the possibility again that there exists size-limited binding pocket at 2-position of benzene ring, without much regard to the electronic character or hydrogen bond ability of the substituents.

Table 3. Inhibition of HIF-1α nano-luciferase activity by A-part modified analogs

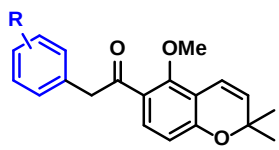

Entry	A-part or R	IC_{50}[a] (μM)	S.E.[b]
1 (**SH-42**)	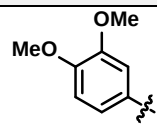	2.15	0.52
2		0.88	0.32
3	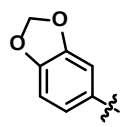	3.41	0.71
4	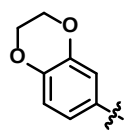	1.33	0.34
5	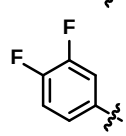	1.27	0.40
6 (**28f**)	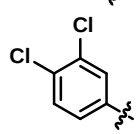	2.88	0.54

7 (**SH-199**)	2-F	0.10	0.01
8	3-F	0.36	0.15
9	4-F	1.02	0.29
10	2-Cl	0.33	0.07
11	3-Cl	0.61	0.20
12	4-Cl	1.27	0.12
13	2-CF_3	2.13	0.75
14	3-CF_3	2.37	0.74
15	4-CF_3	0.60	0.45
16 (**28d**)	2-CN	6.33	1.29
17 (**28e**)	3-CN	4.59	2.98
18	4-CN	1.24	0.52
19	2-OMe	3.21	0.74
20	3-OMe	0.82	0.20
21	4-OMe	6.21	2.39
22	2-OH	0.94	0.41
23	3-OH	1.44	0.88
24	4-OH	0.79	0.49
25 (**28a**)	2-Me	0.61	0.27
26 (**28b**)	3-Me	5.25	2.34
27 (**28c**)	4-Me	3.24	3.03

[a]Data are mean values of three independent experiments. [b]standard error.

3-2. Modification of B-part analogs

We previously synthesized and analyzed the substituent effect on cytotoxicity test at the benzylic position of the analog **SH-42** that dimethyl substituted analog showed decreased antiproliferative activity compared to nonsubstituted analog **SH-42** and monomethyl substituted analog **rac-SH-80**. We further incorporated diverse substituents including

fluorine, allyl group and benzyl group at the benzylic position. In accord with previous study, bulkier substituents resulted in lower HIF-1α inhibitory activities with the exception of methyl substituent (**rac-SH-80**), which seemed to produce appropriate constraint. We prepared the alcohol analog since deguelol, a reduced form of deguelin, exhibited 10-fold higher antiproliferative activity than deguelin. We also examined HIF-1α inhibitory activity of acetate analog, however both of alcohol and acetate analogs were inferior to the analog **SH-42**. Amide analog with no-substitution group at amide bond was equipotent to the ketone analog **SH-42** and the analogs with substituted amide showed similar tendency to the ketone series in the respect that as the size of alkyl group increased, HIF-1α inhibitory activity decreased.(Table 4)

Table 4. Inhibition of HIF-1α nano-luciferase activity by B-part modified analogs

Structure	IC_{50} [a] (μM)	S.E. [b]
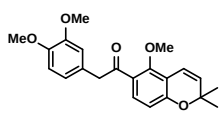	2.15	0.52
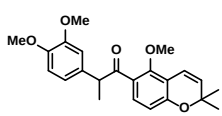	1.36	0.50
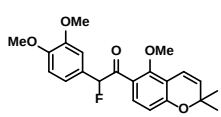	6.35	6.49
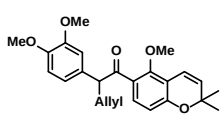	8.45	5.58
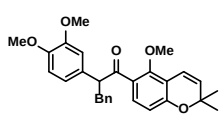	12.03	6.91

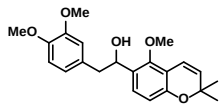	8.88	2.75
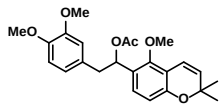	3.04	0.96
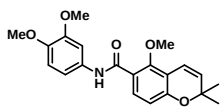	2.04	0.78
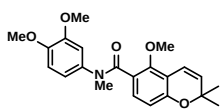	3.15	2.75
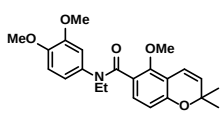	5.25	2.53
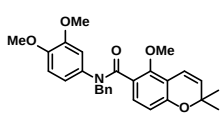	10.78	2.35

[a]Data are mean values of three independent experiments. [b]standard error.

3-3. Modification of chromene ring-truncated C-part analogs

A series of chromene-truncated analogs were synthesized via Claisen-decarboxylation as shown in Scheme 15. MOM protection on 4-hydroxyl group of methyl 2,4-dihydroxybenzoate and following methylation gave the methyl benzoate **29**. Treatment of NaHMDS to a mixture of commercially available 3,4-dimethoxyphenylacetic acid **20** and the methyl benzoate **29** at low temperature produced a ketone enolate, which could be trapped with iodomethane to give the common intermediate **30**. MOM deprotection using hydrochloric acid afforded the previously reported phenol intermediate, which could be transformed into both oxygen-substituted chromene-truncated analogs and a precursor for nitrogen-substituted chromene-truncated analogs. Finally, methyl and ethyl ether

compounds were synthesized from alkylation of phenol intermediate using iodomethane and iodoethane, respectively. Cyclohexyl ether was prepared from Mitsunobu reaction with cyclohexanol. While, in order to prepare nitrogen-containing chromene-truncated analogs, phenyl triflimide was treated to the phenol intermediate to yield the precursor of Buchwald reaction. Final previously reported amine compounds were successfully synthesized from palladium-catalyzed Buchwald-Hartwig reaction using palladium acetate as a base and corresponding amines.

The C-part of the analog **SH-42** included terminal chromene unit, a key structural feature of deguelin. The chromene unit was traditionally known as 'privileged structure' with versatile binding properties[97] and a large number of natural products containing chromene unit were reported with a variety of biological activities.[98] For this reason, various attempts had been made to incorporate chromene unit into therapeutic agents. Nicolaou and coworkers constructed natural product-like chemical libraries by the solid-phase synthesis of chromene units.[99-101] Recently, Van Meir and coworkers investigated on the development of HIF-1α inhibitors possessing chromene unit based on the hit compound from Nicolaou's library.[102,103]

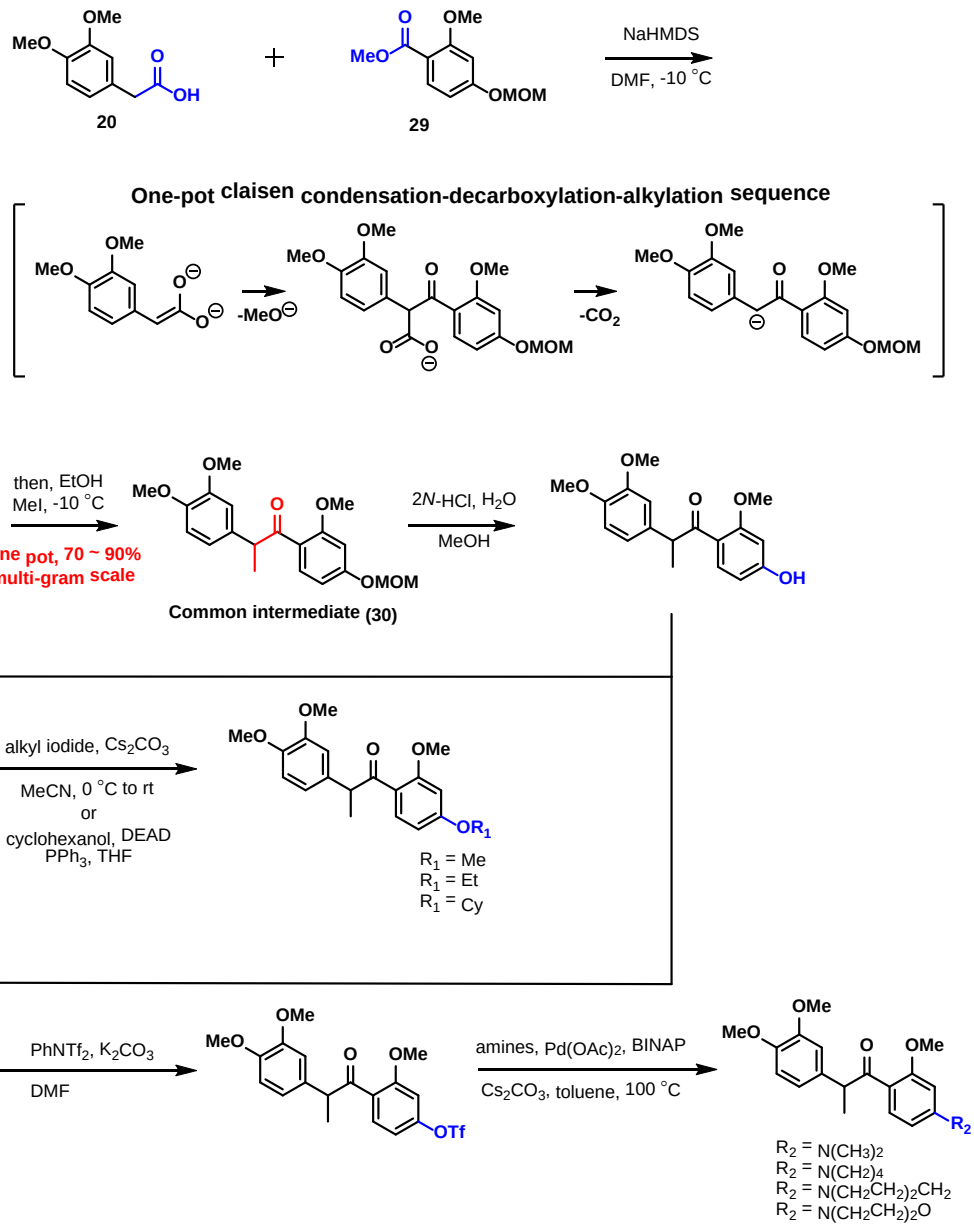

Scheme 15. Preparation of chromene ring-truncated analogs via tandem reaction

We examined the cell growth inhibitory activities of the early deguelin derivatives modified on the terminal chromene unit and the result implied that the chromene unit was crucial for appropriate interaction with Hsp90. However, the derivatives had two dihydropyran rings in the middle of the compounds and there were no attempts of

modification on the chromene unit to the ring-truncated deguelin analogs. In order to establish a complete SAR study of ring-truncated analog **SH-42**, a series of C-part modified analogs were prepared on the basis of chromene-truncation strategy. It also might enable to identify a novel scaffold for HIF-1α inhibition which meet novelty requirement escaping from well-qualified but not ingenious chromene unit. Especially, truncation of chromene ring mediated the introduction of additional polar moiety for improving physicochemical properties, which could be beneficial for intravitreal injection, a common administration route for ocular diseases.

The C-part modified analogs possessed methyl substituent at benzylic position since the analog **rac-SH-80** exhibited slightly higher activity than the analog **SH-42**. In addition, methyl substituent might be advantageous to have conformational rigidity as chromene-truncated analogs became floppier than chromene containing ones. HIF-1α inhibitory activities of the chromene-truncated analogs were presented in Table 5. In the beginning, we maintained the methoxy substituent at 2- position to carbonyl moiety as the methoxy group in chromene unit was considered to be beneficial in antiproliferative activity. The position of oxygen atom (**entry 1-4**) or nitrogen atom (**entry 5-10**) was fixed at 4- position, following the original position of oxygen in chromene ring. HIF-1α inhibitory activities of ether analogs were increased as the size of substituent get bigger. This tendency also continued in case of amine analogs, except for the analog containing morpholine substituent, which implied that the binding pocket accommodated terminal of the C-part required hydrophobic interaction, as shown in previous report.[10] Especially, the analog in **entry 7**, **SH-173** showed slightly higher activity than the analog **SH-42** with IC_{50} of 2.15 μM, suggesting heteroatom-substituted benzene ring as a novel scaffold for HIF-1α inhibitors replacing chromene unit. Next, we investigated the importance of methoxy substituent at 2-position by comparing analogs in **entry 6, 8, 9, 10**. And the result showed little differences according to the presence of methoxy subunit, unlike the case of chromene ring.

Table 5. Inhibition of HIF-1α nano-luciferase activity by chromene ring-truncated analogs

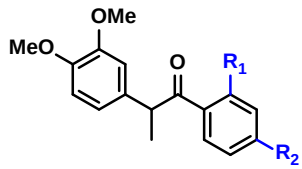

Entry	R_1	R_2	IC_{50}[a] (μM)	S.E.[b]
1	OMe	OH	N.A.[c]	-
2		OMe	N.A.	-
3		OEt	11.68	9.45
4		OCy	2.59	2.45
5		$N(CH_3)_2$	N.A.	-
6		$N(CH_2)_4$	2.82	1.66
7 (**SH-173**)		$N(CH_2CH_2)_2CH_2$	1.85	0.57
8		$N(CH_2CH_2)_2O$	8.74	8.00
9	H	$N(CH_2)_4$	2.61	1.27
10		$N(CH_2CH_2)_2O$	6.85	2.74

[a]Data are mean values of three independent experiments. [b]standard error. [c]No activity (N.A.) indicates that the analog exhibit activity with an IC_{50} higher than 15μM

3-4. Kinetic solubility of representative analogs

Through the SAR study of ring-truncated deguelin analogs, we successfully discovered some potent HIF-1α inhibitors with an IC_{50} of submicromolar level. We also found that the analog **SH-173**, which was modified to possess piperidine substituted benzene ring instead of the chromene ring, had higher HIF-1α inhibitory activity than the analog **SH-42**. With a number of possible analogs in hand for additional biological evaluation, we significantly considered physicochemical properties of the analogs in determining the candidate to

proceed further. As previously mentioned, it was due to the common administration route for ocular diseases, intravitreal injection.

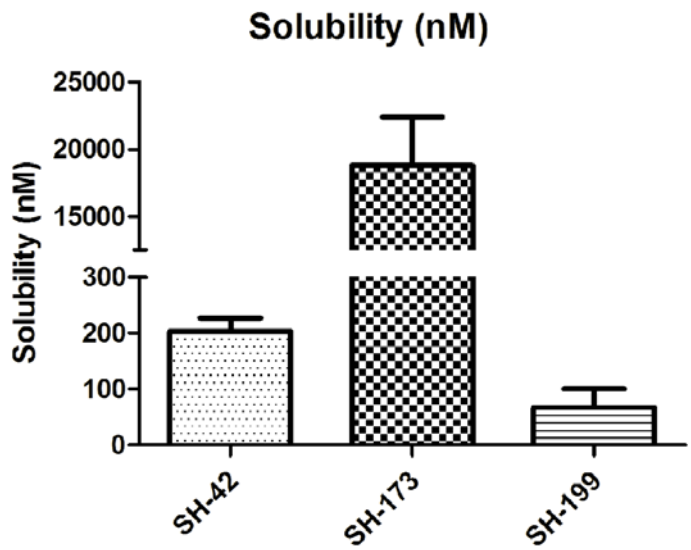

Figure 17. Kinetic solubility of the representative analogs

Kinetic solubility is a one of most popular methods to examine water solubility of drugs. High throughput screening for water solubility is possible by this method which directly uses DMSO stock solution of bioactive compound to measure water solubility in short time.[104] We tested the most potent in vitro HIF-1 nano-luciferase inhibitor **SH-199** and the chromene ring-truncated analog **SH-173** compared to **SH-42**. The solubility of representative chromene ring-truncated analog was 93-fold greater than the solubility of parent compound **SH-42**. The result is explained as increasing of polarity by tertiary amine moiety and flexibility by truncation of fused ring system, chromene ring. Interestingly, the most potent HIF-1 nano-luciferase inhibitor, **SH-199** was less water soluble than parent compound **SH-42** by 3 times.

3-5. Anti-angiogenesis of representative chromene ring-truncated analog

We examined the effect of the analog **SH-173** on hypoxia-mediated angiogenic processes. Angiogenesis is a complex process involving extensive interaction between cells, soluble factors and extracellular matrix components. The construction of a vascular network needs consecutive steps including cell proliferation, migration and tube formation.[105] We utilized conditioned media (CM) extracted from human colon cancer HCT116 cells treated with/without the analog **SH-42** and the analog **SH-173** under hypoxia. The antiangiogenic effects of the compounds were evaluated by observing changes in angiogenic processes mentioned above, with the treatment of CM to human umbilical vein endothelial cells (HUVECs). The analog **SH-173** effectively suppressed hypoxia-induced proliferation, migration and tube formation of HUVECs, nearly equipotent to the analog **SH-42**.(Figure 18) [11]

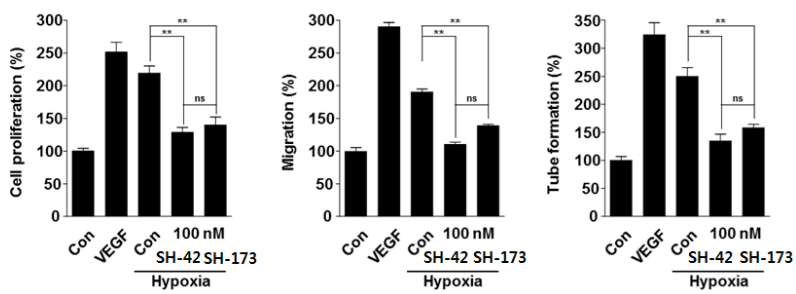

Figure 18. Anti-angiogenesis of the chromene ring-truncated analog, SH-173

3-6. Oxygen-inducible retinopathy model for representative analogs

Followed by in vitro antiangiogenic activity of **SH-173**, we investigated the efficacy of the compound in vivo using the mouse OIR model.[8,90] Analogs **SH-42** and **SH-173** were injected intravitreally with two concentrations of 100 nM and 1 μM. Staining of whole-mounted retinal tissues and its quantitative analysis showed that the analog **SH-173** effectively reduced retinal neovascular tufts at a comparable level to the analog **SH-42**.(Figure 19) The result confirmed the potential of heteroatom-substituted benzene ring as

a novel scaffold replacing chromene ring for the development of novel drugs targeting pathological angiogenesis in ocular diseases.

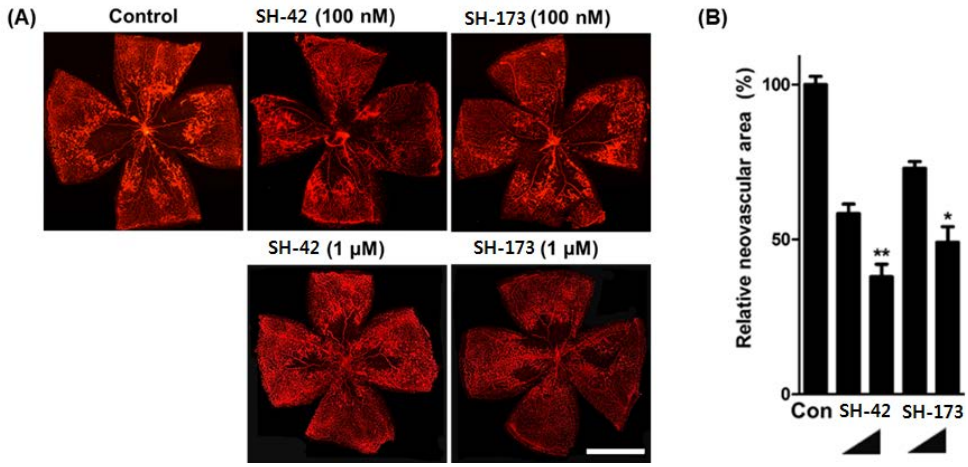

Figure 19. In vivo test for the chromene ring-truncated analog, SH-173

III. Conclusion

In summary, total synthesis of (-)-deguelin was achieved through 12 steps with 8.4% overall yield. The key feature of our synthesis includes an efficient preparation of the double cyclization precursor via highly convergent assembly of two aromatic systems and facile construction of the *cis*-fused bisbenzopyran skeleton via Pd-catalyzed *O* and *C*-arylation. In addition, the key architecture of the intermediate involves carbonylative epoxide ring opening catalyzed by cobalt. Our iterative intramolecular arylation strategy seems quite widely applicable in the rotenoid synthesis. In addition, we achieved the most efficient large scale synthetic process of the representative deguelin analog, **SH-42** and explored fine evidences of mechanism of action for Hsp90 inhibition, extensive anti-cancer effect and reduced toxicities by using multi-gram scale of **SH-42**. Moreover, we investigated the structural features of the representative B and C ring-truncated deguelin analog **SH-42** for HIF-1α inhibitory activity using HRE-luciferase reporter assay. We established the full SAR on the A-part by introducing benzene rings with diverse substituents at various positions instead of 3,4-dimethoxy benzene ring. The analog **SH-199**, which contained 2-fluorobenzene ring instead of 3,4-dimethoxy benzene ring showed the great inhibitory effect on HIF-1α nano-luciferase activity with an IC_{50} of 100 nM. Some of simple modifications at benzylic position and the ketone moiety reaffirmed the previously reported information regarding proper conformation of ring-truncated deguelin analogs. Noticeably, the C-part modified analog **SH-173** possessing piperidine substituted benzene ring in place of the chromene unit exhibited equipotent HIF-1α nano-luciferase inhibitory activity and anti-angiogenic effect in vitro assays compared with **SH-42**. The **SH-173** also manifested equipotent inhibitory activity in the OIR model in mice despite the privileged chromene ring is absence. These results strongly suggested heteroatom-substituted benzene ring as a novel scaffold for HIF-1α inhibitors replacing the chromene unit.

IV. Experimental

General experimental

Unless otherwise described, all commercial reagents and solvents were purchased from commercial suppliers and used without further purification. Tetrahydrofuran and diethyl ether were distilled from sodium benzophenone ketyl. Dichloromethane, triethylamine, acetonitrile, and pyridine were freshly distilled with calcium hydride. Flash column chromatography was carried out using silica-gel 60 (230-400 mesh, Merck) and preparative thin layer chromatography was used with glass-backed silica gel plates (1mm, Merck). Thin layer chromatography was performed to monitor reactions. All reactions were performed under dry argon atmosphere in flame-dried glassware. Optical rotations were measured using a JASCO DIP-1000 digital polarimeter at ambient temperature using 100 nm cells of 2 mL capacity. Infrared spectra were recorded on a Perkin-Elmer 1710 FT-IR spectrometer. Mass spectra were obtained using a VG Trio-2 GC-MS instrument, and high resolution mass spectra were obtained using a JEOL JMS-AX 505WA unit. ^{1}H and ^{13}C NMR spectra were recorded on either a JEOL JNM-LA 300 (300MHz), JEOL JNM-GCX (400MHz), BRUKERAMX-500 (500MHz) or JEOL (600MHz) spectrometers. Chemical shifts are provided in parts per million (ppm, δ) downfield from tetramethylsilane (internal standard) with coupling constant in hertz (Hz). Multiplicity is indicated by the following abbreviations: singlet (s), doublet (d), doublet of doublet (dd), triplet (t), quartet (q), quintet (quin) multiplet (m) and broad (br). The purity of the compounds was determined by normal phase high performance liquid chromatography (HPLC), (Gilson or Waters, CHIRALPAK® AD-H (4.6 × 250 mm) or CHIRALPAK® OD-H (4.6 × 250 mm))

1. Chemical Synthesis

1-1. Enantioselective total synthesis of (-)-deguelin

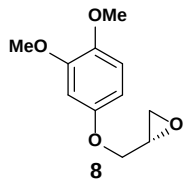

8

(*S*)-2-((3,4-Dimethoxyphenoxy)methyl)oxirane (8)

To a solution of (*S*)-(+)-glycidyl-3-nitrobenzenesulfonate (5.191 g, 19.6 mmol) and phenol **9** (2.016 g, 13.1 mmol) in dry DMF (39 mL) was added Cs_2CO_3 (21.528 g, 65.4 mmol) at ambient temperature. The reaction mixture was stirred for 4 h and quenched with water, and then extracted with EtOAc. The organic layer was washed with 1*N* NaOH aqueous solution and brine, dried over $MgSO_4$, and concentrated under reduced pressure. The residue was purified by flash column chromatography on silica gel (EtOAc : *n*-Hexane = 1 : 3) to afford 2.806 g (98%) of **8** as a white solid: $[\alpha]_D^{20}$ +4.4 (c 1.01, CH_2Cl_2); FT-IR (thin film, neat) ν_{max} 2955, 2923, 2853, 1598, 1514, 1464 cm^{-1}; ^{1}H-NMR ($CDCl_3$, 500 MHz) δ 6.74 (d, 1H, *J* = 8.7 Hz), 6.54 (d, 1H, *J* = 2.8 Hz), 6.38 (dd, 1H *J* = 8.7, 2.8 Hz), 4.16 (dd, 1H, *J* = 11.0, 3.1 Hz), 3.89 (dd, 1H, *J* = 11.0, 5.7 Hz), 3.82 (d, 6H, *J* = 10.9 Hz), 3.32 (m, 1H), 2.87 (t, 1H, *J* = 4.8 Hz), 2.72 (dd, 1H, *J* = 4.9, 2.6 Hz); ^{13}C-NMR ($CDCl_3$, 125 MHz) δ 153.1, 149.9, 143.9, 111.7, 103.9, 101.1, 69.3, 56.4, 55.8, 50.2, 44.6; HR-MS (FAB+) calcd for $C_{11}H_{14}O_4$ (M^+) 210.0892; found 210.0884.

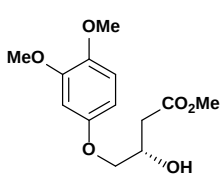

14

(*S*)-Methyl 4-(3,4-dimethoxyphenoxy)-3-hydroxybutanoate (14)

Cobalt carbonyl (2.346 g, 6.2 mmol) was added into a flame-dried 50mL round bottom flask. The flask was purged 5 times using CO balloon. Dry methanol (16 mL) was added and the mixture was stirred for 2 min. Epoxide **8** (6.490 g, 30.9 mmol) in dry methanol (16 mL) was added to the previous solution, and CO gas was bubbled into the mixture for 20 min. The resulting mixture was stirred until complete consumption of the starting material (monitored by TLC) at ambient temperature, diluted with ether, and filtered through a pad of celite. The filtrate was concentrated under reduced pressure and the residue was purified by flash column chromatography on silica gel (EtOAc : *n*-Hexane = 1 : 3) to afford 6.501 g (78%) of (*S*)-methyl 4-(3,4-dimethoxyphenoxy)-3-hydroxybutanoate **14** as a yellow liquid: $[\alpha]_D^{20}$ -46.8 (c 0.57, CH_2Cl_2); FT-IR (thin film, neat) ν_{max} 3502, 2998, 2952, 2834, 1736, 1611, 1597, 1513, 1440 cm^{-1}; ^{1}H-NMR ($CDCl_3$, 500 MHz) δ 6.75 (d, 1H, *J* = 8.7 Hz), 6.52 (d, 1H, *J* = 2.8 Hz), 6.39 (dd, 1H, *J* = 12.8, 2.8 Hz), 4.38 (m, 1H), 3.94 (d, 2H, *J* = 5.2 Hz), 3.83 (d, 6H, *J* = 10.9 Hz), 3.71 (s, 3H), 3.03 (s, 1H), 2.66 (d, 1H, *J* = 4.4 Hz), 2.65 (d, 1H, *J* = 7.3 Hz); ^{13}C-NMR ($CDCl_3$, 125 MHz) δ 172.5, 153.0, 149.9, 143.9, 111.8, 103.9, 100.9, 71.3, 66.8, 56.4, 55.8, 51.9, 37.8; HR-MS (FAB+) calcd for $C_{13}H_{18}O_6$ (M^+) 270.1103; found 270.1104

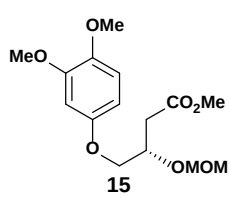

15

Methyl (*S*)-4-(3,4-dimethoxyphenoxy)-3-(methoxymethoxy)butanoate (15)

To a stirred solution of secondary alcohol **14** (2.086 g, 7.7 mmol) in DMF was added

diisopropylethylamine (6.8 mL, 38.6 mmol) at room temperature. The reaction mixture was stirred for 5 min and MOM chloride (2.7 mL, 33.2 mmol) was added at 0 °C. The reaction mixture was stirred at ambient temperature overnight, quenched with saturated NH_4Cl solution at 0 °C, and extracted with EtOAc. The organic layer was washed with saturated NH_4Cl solution and brine, dried over $MgSO_4$, and concentrated under reduced pressure. The residue was purified by flash column chromatography on silica gel (EtOAc : *n*-Hexane = 1 : 4) to afford 2.3195 g (96%) of **15** as a yellow liquid: $[\alpha]_D^{20}$ -4.8 (c 0.87, CH_2Cl_2); FT-IR (thin film, neat) ν_{max} 3057, 2994, 2953, 2834, 1737, 1612, 1597, 1512, 1465, 1452, 1439, 1373 cm^{-1}; ^{1}H-NMR ($CDCl_3$, 500 MHz) δ 6.75 (d, 1H, J = 8.7 Hz), 6.51 (d, 1H, J = 2.7 Hz), 6.38 (dd, 1H, J = 8.7, 2.7 Hz), 4.74 (m, 2H), 4.33 (m, 1H), 4.00 (dq, 2H, J = 12.8, 4.9 Hz), 3.82 (d, 6H, J = 11.1 Hz), 3.68 (s, 3H), 3.35 (s, 3H), 2.75-2.66 (m, 2H); ^{13}C-NMR ($CDCl_3$, 125 MHz) δ 171.5, 153.2, 149.9, 143.7, 111.8, 103.8, 100.9, 96.6, 72.8, 69.9, 56.4, 55.8, 55.6, 51.7, 37.4; HR-MS (FAB+) calcd for $C_{15}H_{22}O_7$ (M^+) 314.1366; found 314.1378

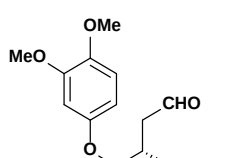

12

(*S*)-4-(3,4-Dimethoxyphenoxy)-3-(methoxymethoxy)butanal (12)

To a stirred solution of butanoate **15** (1.2 g, 3.9 mmol) in dry CH_2Cl_2 (20 mL) was dropwise added a solution of DIBAL-H (1.0 M solution in CH_2Cl_2, 4 mL) in toluene at -78 °C. The reaction mixture was stirred until complete consumption of starting material (monitored by TLC) and Rochelle solution was added dropwise at -78 °C. The reaction mixture was vigorously stirred at ambient temperature and extracted with EtOAc. The

organic layer was washed with brine, dried over $MgSO_4$, and concentrated under reduced pressure. The residue was purified by flash column chromatography on silica gel (EtOAc : *n*-Hexane = 1 : 3) to afford 1.05 g (96%) of **12** as white solid: $[\alpha]_D^{20}$ -187 (c 0.82, CH_2Cl_2); FT-IR (thin film, neat) ν_{max} 2998, 2938, 2833, 1725, 1597, 1513, 1452 cm^{-1}; ^{1}H-NMR ($CDCl_3$, 500 MHz) δ 9.83 (s, 1H), 6.74 (d, 1H, *J* = 8.8 Hz), 6.50 (d, 1H, *J* = 2.7 Hz), 6.36 (dd, 1H, *J* = 2.8, 8.8 Hz), 4.75 (q, 2H, *J* = 7.0 Hz), 4.45-4.40 (m, 1H), 4.04-3.97 (m, 2H), 3.83 (s, 3H), 3.81 (s, 3H), 3.36 (s, 3H), 2.83-2.78 (m, 2H); ^{13}C-NMR (C_6D_6, 100 MHz) δ 199.8, 152.7, 149.5, 143.4, 111.6, 103.5, 100.5, 96.0, 70.8, 69.7, 56.0, 55.4, 55.2, 46.0; HR-MS (FAB+) calcd for $C_{14}H_{20}O_6$ (M^+) 284.1260; found 284.1246

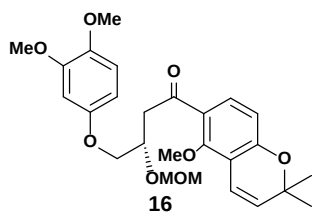

16

(*S*)-4-(3,4-Dimethoxyphenoxy)-1-(5-methoxy-2,2-dimethyl-2H-chromen-6-yl)-3-(methoxymethoxy)butan-1-one (16)

To a solution of aryl bromide **6** (1.7 g, 6.4 mmol) in dry THF (20 mL) was added *n*-BuLi (1.6 M solution in hexane, 3.6 mL) at -78 °C The reaction mixture was stirred for 15 min at the same temperature and a solution of **12** (1.0 g, 3.6 mmol) in dry THF (20 mL) was added at -78 °C. The mixture was stirred for 20 min at -78 °C and then warmed to ambient temperature. The resulting mixture was stirred for 5 min, quenched with water, and extracted with EtOAc. The organic layer was washed with brine, dried over $MgSO_4$, and concentrated under reduced pressure. The residue was filtered by short flash column chromatography on silica gel (EtOAc : *n*-Hexane = 1 : 2) to afford crude mixture of

diastereomers as a colorless liquid: $[\alpha]_D^{20}$ -26.6 (c 1.34, CH_2Cl_2); FT-IR (thin film, neat) ν_{max} 3504, 2936, 2830, 1599, 1512, 1465, 1370 cm^{-1};

To a solution of above product in dry CH_2Cl_2 (36 mL) was added sodium bicarbonate (852mg, 10.1 mmol). Dess-Martin periodinane (2.1 g, 5.1 mmol) was added. After complete consumption of secondary alcohol (monitored by TLC) , the reaction mixture was quenched with water and extracted with dichloromethane. The organic layer was washed with 5% sodium thiosulfate pentahydrate aqueous solution, dried over $MgSO_4$, and concentrated under reduced pressure. The residue was purified by flash column chromatography on silica gel (EtOAc : *n*-Hexane = 1 : 4) to afford 1.5 g (88% for 2steps) of **16** as a colorless liquid: $[\alpha]_D^{20}$ -7.8 (c 1.22, CH_2Cl_2); FT-IR (thin film, neat) ν_{max} 3080, 2969, 2937, 2830, 1671, 1634, 1590, 1567, 1512, 1463, 1419, 1371, 1315 cm^{-1}; ^{1}H-NMR ($CDCl_3$, 500 MHz) δ 7.56 (d, 1H, *J* = 8.7 Hz), 6.98 (s, 1H), 6.65 (s, 1H), 6.58 (d, 1H, *J* = 8.0 Hz), 6.55 (d, 1H, *J* = 9.3 Hz), 5.66 (d, 1H, *J* = 4.5 Hz), 4.79 (d, 1H, *J* = 13.6 Hz), 4.75 (d, 1H, *J* = 13.5 Hz), 4.55 (quint, 1H, *J* = 10.8 Hz), 4.13 (m, 1H), 3.86 (s, 3H), 3.79 (s, 3H), 3.78 (s, 3H), 3.49-3.31 (m, 2H), 3.34 (s, 3H), 1.42 (s, 6H); ^{13}C-NMR ($CDCl_3$, 125 MHz) δ 197.8, 158.0, 156.7, 149.4, 149.0, 144.0, 131.0, 130.4, 124.8, 116.5, 116.3, 114.8, 112.7, 101.7, 100.4, 96.9, 72.7, 72.3, 63.2, 56.6, 56.2, 55.6, 44.7, 27.9; HR-MS (FAB+) calcd for $C_{26}H_{33}O_8$ ($M + H^+$) 473.2175; found 473.2176

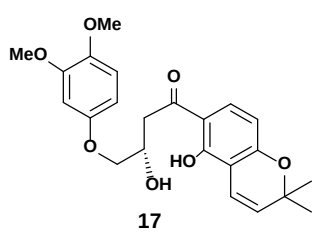

17

(*S*)-4-(3,4-Dimethoxyphenoxy)-3-hydroxy-1-(5-hydroxy-2,2-dimethyl-2H-chromen-6-

yl)butan-1-one (17)

To a solution of **16** (705mg, 1.5 mmol) in dry CH_2Cl_2 (15 mL) was added boron trichloride solution (1.0 M in CH_2Cl_2, 4.5 mL) at -78 °C. After complete consumption of substrate (monitored by TLC), the reaction mixture was quenched with water (15 mL) at -78 °C and extracted with dichloromethane. The organic layer was washed with brine, dried over $MgSO_4$, and concentrated under reduced pressure. The residue was purified by flash column chromatography on silica gel (EtOAc : *n*-Hexane = 1 : 4) to afford 365 mg (64%) of (*S*)-4-(3,4-dimethoxyphenoxy)-3-hydroxy-1-(5-hydroxy-2,2-dimethyl-2H-chromen-6-yl)butan-1-one **17** as a yellow liquid: $[\alpha]_D^{20}$ -15.2 (c 0.56, CH_2Cl_2); FT-IR (thin film, neat) ν_{max} 3491, 3087, 2969, 2931, 2837, 1734, 1641, 1614, 1512, 1486, 1463, 1426, 1376 cm^{-1}; ^{1}H-NMR ($CDCl_3$, 400 MHz) δ 12.74 (s, 1H), 7.53 (d, 1H, *J* = 6.6 Hz), 6.75 (d, 1H, *J* = 6.6 Hz), 6.68 (d, 1H, *J* = 7.5 Hz), 6.53 (d, 1H, *J* = 2.0 Hz), 6.39 (dd, 1H, *J* = 2.0, 6.5 Hz), 6.31 (d, 1H, *J* = 6.7 Hz), 5.56 (d, 1H, *J* = 7.6 Hz), 4.58-4.54 (m, 1H), 4.00 (d, 1H, *J* = 3.9 Hz), 3.83 (s, 3H), 3.81 (s, 3H), 3.24-3.19 (m, 3H), 1.43 (s, 6H); ^{13}C-NMR ($CDCl_3$, 100 MHz) δ 203.3, 160.1, 159.8, 153.0, 149.9, 143.8, 131.1, 128.3, 115.6, 113.6, 111.8, 109.3, 108.7, 103.9, 100.9, 77.9, 71.4, 66.7, 56.4, 55.8, 41.0, 28.3; HR-MS (FAB+) calcd for $C_{23}H_{26}O_7$ (M^+) 414.1679; found 414.1670

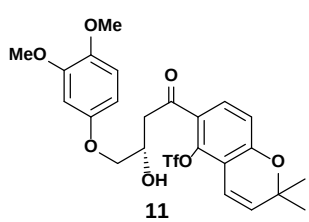

11

(*S*)-6-(4-(3,4-Dimethoxyphenoxy)-3-hydroxybutanoyl)-2,2-dimethyl-2H-chromen-5-yl trifluoromethanesulfonate (11)

To a solution of starting alochol **17** (974 mg, 2.4 mmol) in dry DMF (12 mL) were added K_2CO_3 (358 mg, 2.6 mmol) and $PhNTf_2$ (933 mg, 2.6 mmol) at ambient temperature. After complete consumption of substrate (monitored by TLC), the reaction mixture was quenched with water and extracted with ether. The organic layer was washed with brine, dried over $MgSO_4$, and concentrated under reduced pressure. The residue was purified by flash column chromatography on silica gel (EtOAc : *n*-Hexane = 1 : 4) to afford 1.141 g (72%) of triflate **11** as a yellow liquid: $[\alpha]_D^{20}$ -11.6 (c 0.97, CH_2Cl_2); FT-IR (thin film, neat) ν_{max} 3491, 3080, 2969, 2932, 2835, 1685, 1637, 1602, 1561, 1513, 1465, 1453, 1426, 1370, 1312 cm^{-1}; ^{1}H-NMR ($CDCl_3$, 500 MHz) δ 7.64 (d, 1H, *J* = 8.6 Hz), 6.98 (s, 1H), 6.84 (d, 1H, *J* = 8.6 Hz), 6.61 (s, 1H), 6.55 (d, 1H, *J* = 10.1 Hz), 5.84 (d, 1H, *J* = 10.1 Hz), 4.59 (m, 1H), 4.09 (dq, 1H, *J* = 17.0, 4.9 Hz), 3.84 (s, 3H), 3.80 (s, 3H), 3.36-3.23 (m, 2H), 3.17 (d, 1H, *J* = 4.5 Hz), 1.45 (d, 6H, *J* = 2.2 Hz); ^{13}C-NMR ($CDCl_3$, 125 MHz) δ 198.2, 157.8, 149.2, 149.1, 144.5, 142.6, 133.5, 130.6, 124.6, 119.7, 116.0, 115.9, 115.8, 114.9, 102.0, 100.9, 73.4, 66.7, 56.6, 56.2, 43.7, 27.9, 27.9; HR-MS (FAB+) calcd for $C_{24}H_{25}F_3O_9S$ (M^+) 546.1171; found 546.1162

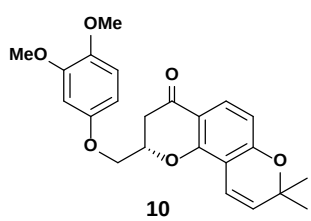

10

(*S*)-Ketone (10)

To triflate **11** (134mg, 0.2 mmol) in dry toluene (2 mL) were added $Pd(OAc)_2$ (8.9 mg, 0.04 mmol), SPhos (21 mg, 0.05 mmol), and Cs_2CO_3 (98 mg, 0.3 mmol). The reaction mixture was stirred at 70 °C for 3h. The reaction mixture was cooled down to ambient

temperature and filtered through a pad of celite. The solvent was removed under reduced pressure and the residue was purified by flash column chromatography on silica gel (EtOAc : *n*-Hexane = 1 : 4) to afford 79mg (100%) of **10** as a white solid: $[\alpha]_D^{20}$ -15.5 (c 0.66, CH_2Cl_2); FT-IR (thin film, neat) ν_{max} 3070, 2963, 2927, 2856, 1733, 1683, 1637, 1596, 1578, 1512, 1441, 1393, 1377, 1348, 1321 cm^{-1}; ^{1}H-NMR ($CDCl_3$, 500 MHz) δ 7.70 (d, 1H, *J* = 8.6 Hz), 7.00 (s, 1H), 6.61 (s, 1H), 6.60 (d, 1H, *J* = 9.6 Hz), 6.47 (d, 1H, *J* = 8.7 Hz), 5.56 (d, 1H, *J* = 10.0 Hz), 4.81 (m, 1H), 4.27 (d, 1H, *J* = 4.7 Hz), 3.85 (s, 3H), 3.82 (s, 3H), 2.99 (dd, 1H, *J* = 16.8, 12.7 Hz), 2.78 (dd, 1H, *J* = 16.8, 3.2 Hz), 1.44 (d, 6H, *J* = 16.6 Hz); ^{13}C-NMR ($CDCl_3$, 150 MHz) δ 190.1, 159.6, 157.2, 153.0, 150.0 144.1, 128.9, 127.9, 115.8, 114.7, 111.8, 111.2, 109.3, 104.1, 101.2, 77.5, 76.5, 69.9, 56.4, 55.9, 39.2, 28.4, 28.1 ; HR-MS (FAB+) calcd for $C_{23}H_{25}O_6$ (M + H^+) 397.1651; found 397.1659

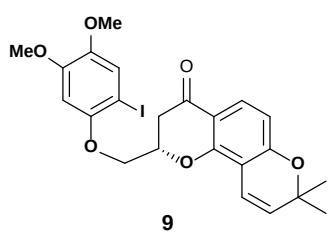

9

(*S*)-Iodoketone (9)

A solution of ketone **10** (46 mg, 0.1 mmol), NIS (29 mg, 0.12 mmol), and TFA (3 μL, 0.04 mmol) in acetonitrile (12 mL) was stirred for 4 h at ambient temperature. The solvent was evaporated reduced pressure and the residue was purified by flash column chromatography on silica gel (EtOAc : *n*-Hexane = 1 : 4) to afford 39 mg (64%) of **9** as a yellow solid: $[\alpha]_D^{20}$ -14.6 (c 1.19, CH_2Cl_2); FT-IR (thin film, neat) ν_{max} 3066, 2959, 2925, 2854, 1734, 1682, 1637, 1595, 1577, 1504, 1439, 1376, 1347 cm^{-1}; ^{1}H-NMR ($CDCl_3$, 400 MHz) δ 7.71 (d, 1H, *J* = 8.7 Hz), 7.18 (s, 1H), 6.64 (d, 1H, *J* = 10.2 Hz), 6.55 (s, 1H), 6.48 (d, 1H, *J* = 8.6 Hz),

5.56 (d, 1H, *J* = 10.0 Hz), 4.87-4.81 (m, 1H), 4.26 (d, 1H, *J* = 4.7 Hz), 3.86 (s, 3H), 3.82 (s, 3H), 3.01 (dd, 1H, *J* = 12.8, 16.9 Hz), 2.79 (dd, 1H, *J* = 3.1, 16.9 Hz), 1.45 (s, 3H), 1.41 (s, 3H); ^{13}C-NMR ($CDCl_3$, 100 MHz) δ 190.0, 159.6, 157.1, 151.9, 150.2, 145.1, 128.9, 127.9, 121.5, 115.8, 114.7, 111.2, 109.3, 100.1, 77.5, 76.4, 74.5, 72.0, 56.6, 56.2, 39.3, 28.4, 28.0; HR-MS (FAB+) calcd for $C_{23}H_{23}IO_6$ (M^+) 522.0539; found 522.0538

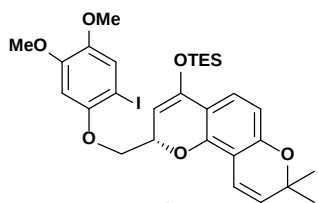

18

(*S*)-Iodosilylenolether ((-)-18)

To a solution of ketone **9** (22 mg, 0.05 mmol) in dry dichloromethane (0.5 mL) were added TESOTf (0.02 mL, 0.09 mmol) and triethylamine (0.02 mL, 0.14 mmol) in one portion at ambient temperature. The reaction mixture was stirred for 30 min, quenched with saturated sodium bicarbonate aqueous solution, and extracted with ethyl aceatate. The solvent was removed by reduced pressure and the residue was purified by short flash column chromatography on silica gel (EtOAc : *n*-Hexane/Et_3N = 1 : 10 : 0.2) to afford 26 mg (100%) of **18** as a colorless liquid: $[\alpha]_D^{20}$ +9.2 (c 0.37, CH_2Cl_2); FT-IR (thin film, neat) ν_{max} 2955, 2934, 2870, 1737, 1630, 1579, 1439, 1359, 1313 cm^{-1}; ^{1}H-NMR (C_6D_6, 300 MHz) δ 7.47 (d, 1H, *J* = 8.2 Hz), 6.98 (s, 1H), 6.92 (d, 1H, *J* = 15.0 Hz), 6.66 (d, 1H, *J* = 8.2 Hz), 6.32 (s, 1H), 5.34 (m, 1H), 5.24 (d, 1H, *J* = 10.0 Hz), 4.77 (d, 1H, *J* = 4.0 Hz), 4.12 (dd, 1H, *J* = 10.0, 7.2 Hz), 3.80 (dd, 1H, *J* = 10.2, 4.3 Hz), 3.24 (s, 3H), 3.22 (s, 3H), 3.22 (s, 3H), 1.24 (s, 6H), 0.99 (t, 9H, *J* = 8.2 Hz), 0.70 (q, 6H, *J* = 8.0 Hz); ^{13}C-NMR ($CDCl_3$, 100 MHz) δ 155.5, 152.3, 151.3, 150.6, 147.9, 146.0, 129.3, 123.2, 122.8, 117.1,

114.7, 110.4, 109.4, 100.9, 95.1, 76.3, 75.4, 74.6, 72.5, 56.2, 55.6, 30.2, 28.1, 27.9, 6.9, 5.3, 1.4, 0.0; HR-MS (FAB+) calcd for $C_{29}H_{38}IO_6Si$ (M + H^+) 637.1482; found 637.1475

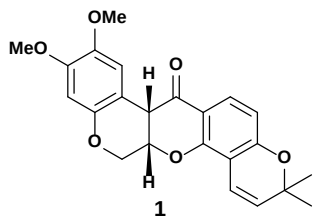

1

(-)-Deguelin (1) from Iodosilylenolether (-)-18

To a mixture of $Pd(OAc)_2$ (1.5 mg, 0.01 mmol), CsF (13.9 mg, 0.09 mmol), and Bu_3SnF (28 mg, 0.09 mmol), was added As(*t*-Bu)$_3$ (4.5 mg, 0.015 mmol) in dry toluene (0.15 mL). Silylenolether **18** (41.7 mg, 0.07 mmol) in dry benzene (0.50 mL) was added and the reaction mixture was stirred at 60°C for 3.5h. The reaction mixture was cooled down to ambient temperature and filtered through a pad of celite. The solvent was removed under reduced pressure and the residue was purified by flash column chromatography on silica gel (EtOAc : *n*-Hexane = 1 : 4) to afford 19 mg (72%) of **1** as a foaming white solid: $[\alpha]_D^{20}$ -25.1 (c 0.15, CH_2Cl_2); FT-IR (thin film, neat) ν_{max} 2952, 2925, 2853, 1674, 1635, 1598, 1578, 1513, 1443, 1393, 1378, 1346, 1274, 1235, 1215, 1199, 1148, 1113, 1095, 1079, 1061, 1011, 910, 893, 818, 771, 735, 704, 679, 635, 609 cm^{-1}; ^{1}H-NMR ($CDCl_3$, 500 MHz) δ 7.73 (d, 1H, *J* = 8.7 Hz), 6.77 (s, 1H), 6.63 (d, 1H, *J* = 10.1 Hz), 6.43 (d, 1H, *J* = 8.6 Hz), 6.43 (s, 1H), 5.54 (d, 1H, *J* = 10.1 Hz), 4.90 (m, 1H), 4.62 (dd, 1H, *J* = 3.1, 12.1 Hz), 4.17 (d, 1H, *J* = 12.1 Hz), 3.82 (d, 1H, *J* = 3.1 Hz), 3.79 (s, 3H), 3.75 (s, 3H), 1.43 (s, 3H), 1.35 (s, 3H); ^{13}C-NMR ($CDCl_3$, 125 MHz) δ 189.2, 160.1, 156.9, 149.5, 147.4, 143.9, 128.7, 128.6, 115.8, 112.8, 111.5, 110.4, 109.1, 104.7, 100.9, 77.7, 72.4, 66.3, 56.3, 55.8, 44.4, 28.5, 28.1; HR-MS (FAB+) calcd for $C_{23}H_{23}O_6$ (M + H^+) 395.1495; found 395.1485

2-2. General procedures

General Dess-Martin oxidation procedure

To a solution of alcohol (1 equiv) in CH_2Cl_2 were added $NaHCO_3$ (3 equiv), Dess-Martin periodinane (1.5 equiv) at 0 °C. Then, the reaction mixture was stirred for 1 h at ambient temperature and quenched with 10% sodium thiosulfate solution and extracted with CH_2Cl_2. The organic layer was washed with brine, dried over $MgSO_4$, and concentrated under reduced pressure. The residue was purified by flash column chromatography on silica gel to afford the desired product.

General anionic coupling procedure

To a solution of aryl bromide (1.8 equiv) in THF was added dropwise *n*-BuLi solution (1.6 M solution in *n*-hexane, 1.65 equiv) at -78 °C. The resulting solution was stirred for 30 min at -78 °C, and aldehyde (1 equiv) in THF was added. The reaction mixture was stirred for 1 h at -78 °C. The reaction mixture was washed with saturated NH_4Cl solution and extracted with EtOAc. The organic layer was washed with brine, dried over $MgSO_4$, and concentrated under reduced pressure. The residue was purified by flash column chromatography on silica gel to afford the desired product.

General MOM-protection procedure

To a suspension of sodium hydride (60%, dispersion in paraffin liquid, 1.75 equiv) in DMF was added phenol (1 equiv) dissolved in DMF. The reaction mixture was stirred for 30 min at 0 °C until the evolution of H_2 gas ceased. MOMCl (1.6 equiv) was then added at 0 °C, and the resulting suspension was warmed to ambient temperature and stirred for 2 h. The reaction mixture was cooled to 0 °C, diluted with iced water, extracted with Et_2O. The organic layer was washed with brine, dried over $MgSO_4$, and concentrated under reduced pressure. The residue was purified by flash column chromatography on silica gel to afford

the desired product.

General MOM-deprotection procedure

To a solution of ketone in methanol was added 3*N* HCl (4 mL / mmol). The resulting solution was heated to 60 °C and stirred for 4 h at the same temperature. The reaction mixture was cooled to ambient temperature and extracted with EtOAc. The organic layer was washed with brine, dried over $MgSO_4$, and concentrated under reduced pressure. The residue was purified by flash column chromatography on silica gel to afford the desired product.

General triflation procedure

To a solution of phenol (1 equiv) in DMF were added potassium carbonate (1.15 equiv) and $PhNTf_2$ (1.2 equiv) respectively. The reaction mixture was stirred for 4 h and extracted with Et_2O. The organic layer was washed with brine, dried over $MgSO_4$, and concentrated under reduced pressure. The residue was purified by flash column chromatography on silica gel to afford the desired product.

General Buchwald-Hartwig reaction procedure

To a flask charged with palladium acetate (0.1 equiv), BINAP (0.2 equiv) and cesium carbonate (1.4 equiv) were added triflate (1 equiv) and amine (1.2 equiv) in toluene and the reaction mixture was stirred for 30 min at ambient temperature. The resulting solution was heated to 100 °C and stirred overnight at the same temperature. The reaction mixture was cooled to ambient temperature, filtered through Celite pad. The residue was purified by flash column chromatography on silica gel to afford the desired product.

General alkylation procedure

To a solution of phenol (1 equiv) in acetonitrile were added cesium carbonate (1.5 equiv) and alkyl halide (2 equiv) at 0 °C. The resulting solution was stirred for 20 min at 0 °C, and warmed up to ambient temperature and stirred for 1 h. The reaction was quenched with water, extracted with EtOAc. The organic layer was washed with brine, dried over $MgSO_4$, and concentrated under reduced pressure. The residue was purified by flash column chromatography on silica gel to afford the desired product.

General tandem claisen condensation-decarboxylation procedure

To a stirred solution of phenyl acetic acid (1 equiv) and benzoate (1.1 equiv) in dry DMF (0.02 M) was dropwise added a 1 M solution of NaHMDS (4 equiv) in THF at -10 °C over 5 min. After completion of the reaction, the solvent was removed by evaporator. The residue was extracted with DCM and washed with brine. The extract was concentrated and purified by flash column chromatography on silica gel to afford the desired product.

2-3. Large scale synthesis of SH-42

Methyl 5-hydroxy-2,2-dimethyl-2H-chromene-6-carboxylate (23)

To a stirred solution of phenol **22** (2.56 g) and 3-methyl-2-butenal (2.97 mL) in absolute ethanol were added calcium chloride dehydrate (1.82 g) and trimethylamine (6.9 mL) at room temperature. The mixture was warmed to reflux. After completion of reaction, the result mixture was cooled down to ambient temperature. The solvent was removed under reduced pressure and extracted with ethyl acetate and brine. The extract was concentrated and the residue was purified by flash-column chromatography on silica gel (EtOAc : Hex = 1 : 30) to afford 4.76 (32%) g of **23** ^{1}H-NMR ($CDCl_3$, 300 MHz) δ 7.59 (d, 1H, , J = 8.7 Hz), 6.69 (d, 1H, J = 9.9 Hz), 6.31 (d, 1H, J = 8.7 Hz), 5.55 (d, 1H, J = 10.0 Hz), 3.88 (s, 3H), 1.42 (s, 6H).

Methyl 5-methoxy-2,2-dimethyl-2H-chromene-6-carboxylate (21)

Purification by flash column chromatography on silica gel (EtOAc : Hex = 1 : 30) after general alkylation protocol of phenol **23** with iodomethane afforded the 108.1 mg (99%) of ester **21**. ^{1}H-NMR ($CDCl_3$, 300 MHz) δ 7.66 (d, 1H, , *J* = 8.6 Hz), 6.62 (d, 1H, *J* = 10.6 Hz), 6.56 (d, 1H, *J* = 8.6 Hz), 5.63 (d, 1H, *J* = 10.0 Hz), 3.85 (s, 3H), 3.82 (s, 3H), 1.42 (s, 6H).

Large scale synthesis of SH-42 via tandem reaction

3,4-Dimethoxyphenylacetic acid with ester **21** afforded the **SH-42** as white solid (70 ~ 90%, multigram scale) purified by recrystallization (purity > 99% determined by HPLC) general tandem claisen condensation-decarboxylation procedure. Spectral data were same as previous repot.[10]

2-4. Synthesis of SH-42 and SH-80 analogs

1-(5-methoxy-2,2-dimethyl-2H-chromen-6-yl)-2-(2-methoxyphenyl)ethan-1-ol (25)

General oxidation procedure using 2-methoxyphenethylalcohol followed by general anionic coupling procedure between resulting aldehyde (39.0 mg) and aryl bromide **6** (104.7 mg) afforded secondary alcohol **25** (77.3 mg, 52% for 2 steps). : ^{1}H-NMR ($CDCl_3$, 300 MHz) δ 7.59 (d, 1H, , *J* = 8.7 Hz), 6.69 (d, 1H, *J* = 9.9 Hz), 6.31 (d, 1H, *J* = 8.7 Hz), 5.55 (d, 1H, *J* = 10.0 Hz), 3.88 (s, 3H), 1.42 (s, 6H).

1-(5-methoxy-2,2-dimethyl-2H-chromen-6-yl)-2-(2-methoxyphenyl)ethan-1-one (26)

General oxidation procedure of alcohol **25** (23.0 mg) afforded the 8.6 mg (36%) of final **26** as pale yellow solid. ^{1}H-NMR ($CDCl_3$, 600 MHz) *δ* 7.54 (d, *J* = 8.7 Hz, 1H), 7.22 (dd, *J* = 8.2, 7.4 Hz, 1H), 7.14 (d, *J* = 7.4 Hz, 1H), 6.90 (dd, *J* = 8.7, 7.3 Hz, 1H), 6.84 (d, *J* = 8.2

Hz, 1H), 6.60 (d, *J* = 10.1 Hz, 1H), 6.58 (d, *J* = 8.7 Hz, 1H), 5.65 (d, *J* = 9.6 Hz, 1H), 4.23 (s, 2H), 3.81 (s, 3H), 3.74 (s, 3H), 1.43 (s, 6H); ^{13}C-NMR ($CDCl_3$, 150 MHz) δ 198.3, 157.5, 157.4, 156.3, 131.3, 131.0, 130.4, 128.2, 125.3, 124.4, 120.5, 116.7, 114.8, 112.4, 110.4, 76.8, 63.1, 55.3, 43.6, 28.0; HR-MS (ESI) calcd for $C_{21}H_{23}O_4$ ($M+H^+$) 339.1591, found 339.1580.

1-(5-methoxy-2,2-dimethyl-2H-chromen-6-yl)-2-(o-tolyl)ethan-1-one (28a)

Secondary alcohol **27a** (81.4 mg, 0.54 mmol) afforded 125.5 mg (72%) of **28a** as a white solid via general tandem claisen condensation-decarboxylation reaction procedure. Purification via flash column chromatography on silica gel (EtOAc/*n*-Hexane = 1:10): ^{1}H-NMR ($CDCl_3$, 500 MHz) δ 7.52 (d, *J* = 8.6 Hz, 1H), 7.20 (m, 4H), 6.60 (d, *J* = 9.8 Hz, 1H), 6.60 (d, *J* = 8.7 Hz, 1H), 5.68 (d, *J* = 10.0 Hz, 1H), 4.27 (s, 2H), 3.79 (s, 3H), 2.23 (s, 3H), 1.44 (s, 6H); ^{13}C-NMR ($CDCl_3$, 125 MHz) δ 198.0, 157.7, 156.4, 137.0, 134.0, 130.9, 130.5, 130.2, 127.0, 126.0, 126.0, 125.2, 116.6, 114.8, 112.7, 76.8, 63.2, 46.9, 28.0, 19.8; HR-MS (ESI) calcd for $C_{21}H_{23}O_3$ ($M+H^+$) 323.1642, found 323.1648.

1-(5-methoxy-2,2-dimethyl-2H-chromen-6-yl)-2-(m-tolyl)ethan-1-one (28b)

Secondary alcohol **27b** (77.6 mg, 0.52 mmol) afforded 22.1 mg (13%) of **28b** as a white solid via general tandem claisen condensation-decarboxylation reaction procedure. Purification via flash column chromatography on silica gel (EtOAc/*n*-Hexane = 1:10): ^{1}H-NMR ($CDCl_3$, 400 MHz) δ 7.49 (d, *J* = 8.6 Hz, 1H), 7.17 (t, *J* = 7.5 Hz, 1H), 7.03 (dd, *J* = 7.5, 6.8 Hz, 3H), 6.58 (dd, *J* = 9.7, 8.4 Hz, 2H), 5.66 (d, *J* = 10.0 Hz, 1H), 4.21 (s, 2H), 3.74 (s, 3H), 2.30 (s, 3H), 1.43 (s, 6H); ^{13}C-NMR ($CDCl_3$, 100 MHz) δ 198.4, 157.7, 156.4, 137.9, 134.9, 131.2, 130.5, 130.3, 128.3, 127.4, 126.6, 124.9, 116.5, 114.8, 112.6, 76.8, 63.2, 48.5, 28.0, 21.3; HR-MS (ESI) calcd for $C_{21}H_{23}O_3$ ($M+H^+$) 323.1642, found 323.1653.

1-(5-methoxy-2,2-dimethyl-2H-chromen-6-yl)-2-(p-tolyl)ethan-1-one (28c)

Secondary alcohol **27c** (52.1 mg, 0.35 mmol) afforded 70.6 mg (63%) of **28c** as a pink solid via general tandem claisen condensation-decarboxylation reaction procedure. Purification via flash column chromatography on silica gel (EtOAc/*n*-Hexane = 1:6): ^{1}H-NMR ($CDCl_3$, 500 MHz) δ 7.48 (d, J = 8.6 Hz, 1H), 7.11 (dd, J = 15.4, 8.1 Hz, 4H), 6.59 (d, J = 10.3 Hz, 1H), 6.57 (d, J = 8.6 Hz, 1H), 5.66 (d, J = 10.0 Hz, 1H), 4.20 (s, 2H), 3.74 (s, 3H), 2.29 (s, 3H), 1.43 (s, 6H); ^{13}C-NMR ($CDCl_3$, 125 MHz) δ 198.5, 157.6, 156.4, 136.1, 131.9, 131.1, 130.4, 129.4, 129.1, 124.9, 116.5, 114.8, 112.6, 76.8, 63.2, 48.2, 28.0, 21.0; HR-MS (ESI) calcd for $C_{21}H_{23}O_3$ ($M+H^+$) 323.1642, found 323.1649.

2-(2-(2,2-dimethyl-2H-chromen-6-yl)-2-oxoethyl)benzonitrile (28d)

Secondary alcohol **27d** (31.8 mg, 0.20 mmol) afforded 6.6 mg (11%) of **28d** as a yellow oil via general tandem claisen condensation-decarboxylation reaction procedure. Purification via flash column chromatography on silica gel (EtOAc/*n*-Hexane = 1:4): ^{1}H-NMR ($CDCl_3$, 800 MHz) δ 7.77 (dd, J = 7.8, 1.0 Hz, 1H), 7.65 (dd, J = 7.8, 2.2 Hz, 1H), 7.63 (d, J = 8.6 Hz, 1H), 7.49 (d, J = 7.8 Hz, 1H), 7.48 (t, J = 7.7 Hz, 1H), 6.68 (d, J = 10.0 Hz, 1H), 6.66 (d, J = 8.6 Hz, 1H), 5.87 (d, J = 10.0 Hz, 1H), 4.61 (s, 2H), 3.92 (s, 3H), 1.43 (s, 6H); ^{13}C-NMR ($CDCl_3$, 200 MHz) δ 195.4, 150.0, 157.8, 140.7, 133.5, 133.2, 132.2, 131.8, 131.7, 128.2, 125.3, 118.6, 117.2, 115.7, 114.8, 113.4, 77.7, 63.7, 48.1, 28.1; HR-MS (ESI) calcd for $C_{20}H_{18}NO_2$ ($M+H^+$) 304.1332, found 304.1349.

3-(2-(2,2-dimethyl-2H-chromen-6-yl)-2-oxoethyl)benzonitrile (28e)

Secondary alcohol **27e** (30.5 mg, 0.19 mmol) afforded 30.1 mg (50%) of **28e** as a yellow oil via general tandem claisen condensation-decarboxylation reaction procedure. Purification via flash column chromatography on silica gel (EtOAc/*n*-Hexane = 1:4): ^{1}H-NMR ($CDCl_3$, 600 MHz) δ 7.53 (s, 1H), 7.51 (d, J = 7.8 Hz, 1H), 7.50 (d, J = 8.7 Hz, 1H),

7.47 (d, *J* = 7.8 Hz, 1H), 7.39 (t, *J* = 7.6 Hz, 1H), 6.59 (d, *J* = 9.2 Hz, 1H), 6.57 (d, *J* = 10.0 Hz, 1H), 5.68 (d, *J* = 9.7 Hz, 1H), 4.28 (s, 2H), 3.77 (s, 3H), 1.43 (s, 6H); ^{13}C-NMR ($CDCl_3$, 150 MHz) δ 196.6, 158.3, 156.6, 136.6, 134.3, 133.2, 131.1, 130.7, 130.4, 129.0, 124.1, 118.8, 116.3, 114.8, 112.9, 112.4, 77.0, 63.2, 47.8, 28.0; HR-MS (ESI) calcd for $C_{20}H_{18}NO_2$ ($M+H^+$) 304.1332, found 304.1339.

2-(3,4-dichlorophenyl)-1-(5-methoxy-2,2-dimethyl-2H-chromen-6-yl)ethan-1-one (28f)

Secondary alcohol **27f** (18.0 mg, 0.047 mmol) afforded 7.9 mg (45%) of **28f** as a yellow oil via general tandem claisen condensation-decarboxylation reaction procedure. Purification via flash column chromatography on silica gel (EtOAc/*n*-Hexane = 1:6): ^{1}H-NMR ($CDCl_3$, 300 MHz) δ 7.49 (d, *J* = 9.0 Hz, 1H), 7.35 (d, *J* = 6.9 Hz, 1H), 7.33 (s, 1H), 7.07 (dd, *J* = 8.4, 2.4 Hz, 1H), 6.60 – 6.56 (m, 2H), 5.68 (d, *J* = 9.9 Hz, 1H), 4.19 (s, 2H), 3.76 (s, 3H), 1.43 (s, 6H); ^{13}C-NMR ($CDCl_3$, 75 MHz) δ 196.9, 158.2, 156.6, 135.3, 132.3, 131.6, 131.2, 130.8, 130.6, 130.2, 129.1, 124.4, 116.4, 114.8, 112.9, 77.1, 63.3, 47.5, 28.0, 28.0; HR-MS (FAB) calcd for $C_{20}H_{19}Cl_2O_3$ ($M+H^+$) 377.0711, found 377.0709.

methyl 2-methoxy-4-(methoxymethoxy)benzoate (29)

To stirred solution of phenol **22** (10.24 g, 59.1 mmol) in dry DCM were added DIPEA (15.9 mL, 147.7 mmol) and MOMCl (7.16 mL, 88.6 mmol) at 0℃. After completion of reaction, the resulting mixture was quenched with water and extracted with DCM. The extract was concentrated and purified by flash column chromatography on silicagel (EtOAc : Hex = 1 : 15) to afford 13.3 g (100%) of methyl 2-hydroxy-4-(methoxymethoxy)benzoate. ^{1}H-NMR ($CDCl_3$, 300 MHz) δ 7.73 (d, 1H, *J* = 8.9 Hz), 6.60 (d, 1H, *J* = 2.4 Hz), 6.51 (dd, 1H, *J* = 8.9, 2.5 Hz), 5.17 (s, 2H), 3.89 (s, 3H), 3.45 (s, 3H).

methyl 2-hydroxy-4-(methoxymethoxy)benzoate (12.6 g, 59.6 mmol) with iodomethane

(18.6 mL, 298.0 mmol) afforded 13.4 g (99%) of benzoate **29** via general alkylation procedure and flash column chromatography on silica gel (EtOAc : Hex = 1 : 4). ^{1}H-NMR ($CDCl_3$, 300 MHz) δ 7.79 (d, 1H, *J* = 9.1 Hz), 6.62 – 6.59 (m, 2H), 5.18 (s, 2H), 3.86 (s, 3H), 3.82 (s, 3H), 3.45 (s, 3H).

2-(3,4-dimethoxyphenyl)-1-(2-methoxy-4-(methoxymethoxy)phenyl)ethan-1-one (30)

After general tandem claisen condensation-decarboxylation reaction between 3,4-dimethoxyphenylacetic acid and benzoate **29**, the resulting mixture was quenched with absolute ethanol (1 mL/1 mmol of NaHMDS) followed by dropwise addition of iodomethane (1.1 equiv) at -10℃ and monitored by thin layer chromatography. After completion of alkylation sequence, the solvent was removed by reduced pressure and dissolved by water followed by extraction with DCM. The organic layer was collected and evaporated. Purification of the residue via flash column chromatography on silica gel (EtOAc : Hex = 1 : 4) afforded the common intermediate **30** as a colorless oil (70 ~ 90%, multigram scale). ^{1}H-NMR ($CDCl_3$, 500 MHz) δ 7.56 (d, 1H, *J* = 8.6 Hz), 6.74 – 6.71 (m, 3H), 6.56 (dd, 1H, *J* = 8.6, 2.0 Hz), 6.49 (d, 1H, *J* = 1.9 Hz), 5.14 (s, 2H), 4.67 (q, 1H, *J* = 6.9 Hz), 3.82 (s, 3H), 3.80 (s, 3H), 3.79 (s, 3H), 3.43 (s, 3H), 1.44 (d, 3H, *J* = 6.9 Hz).

Other intermediates and final compounds

Other intermediates and final compounds were already synthesized and reported.[10,72,106,107]

Kinetic Solubility

Solubility of **SH-42**, **SH-173**, and **SH-199** was determined in DPBS (Welgene Inc., Daegu, Korea). For the determination of equilibrium solubility, the excess amount of each compound was dissolved in DPBS, and the mixture agitated for 24 hours in room temperature. The mixture was centrifuged at 13,200 rpm for 10 minutes (Eppendorf 5415R,

Hamburg, Germany), and filtered with a filter (0.2 μm pore size syringe filter, Minisart RC15, Sartorius Stedim Biotech, Goettingen, Germany). The supernatant of the sample was diluted with methanol (1:10 dilution for **SH-42** and **SH-199**; 1:100 dilution for **SH-173**) and the mixture analyzed by LC/MS/MS system (Applied Biosystems 3200 Qtrap MS/MS system with Alliance Waters e2695 LC system) for their concentration in the media.

2. Biological Evaluation

Binding titration experiments using fluorescence measurements

To examine the binding properties of **SH-42** to Hsp90, fluorescence-based-5-equilibrium binding experiments were performed. A full-length protein, truncated N- and Cterminal domain of Hsp90 were each equilibrated with various concentrations of ligands before measuring fluorescence emission. All titration experiments were conducted at 20°C using a Jasco FP 6500 spectrofluorometer (Easton, MD, USA). Ligand stock solutions were titrated into a protein sample dissolved in phosphate buffer (pH 7.4) containing 137 mM NaCl, 2.7 mM KCl, 10 mM Na_2HPO_4 and 2 mM KH_2PO_4. The total volume of DMSO used to solubilize the ligand was less than 2% in all cases. The proteins were excited at 285 nm, and the decrease of fluorescence emission at 340 nm after ligand binding was measured as a function of ligand concentration. All titration data were fit to a hyperbolic binding equation to obtain Kd values.

Cell culture for anti-cancer assay

HT-22 and RPE cells were cultured in DMEM supplemented with 10% fetal bovine serum (FBS) and antibiotics. Other cancer cells were cultured in RPMI 1640 medium supplemented with 10% FBS and antibiotics. BEAS-2B and HBE cells were maintained in KSFM (Invitrogen) supplemented with EGF and bovine pituitary extracts. HUVECs were

cultured in endothelial cell basal medium [EBM-2 (Lonza Inc., Allendale, NJ, USA)] supplemented with EGM-2 SingleQuots (Lonza). HUVECs between passages 3 and 8 were used. Cells were incubated at 37°C with 5% CO2 in a humidified atmosphere. Drug-resistant cells that have acquired resistance to paclitaxel (H226B/R and H460/R) and an IGF-1R TKI linsitinib (H292/R) were generated by continuous exposure to increasing concentrations of corresponding anticancer drugs for more than 6 months. H226B/K-Ras cells were generated by retroviral transduction of mutant K-Ras.

Anchorage-dependent colony formation

For the anchorage-dependent colony formation assay, cells were seeded onto 6-well plates at a density of 300 cells/well and then treated with increasing concentrations of **SH-42** for 2 weeks. The colonies were fixed with 100% methanol, stained with 0.005% crystal violet solution at room temperature, and then washed with deionized water 3-5 times. The colonies were photographed and counted. **SH-42**, diluted in complete medium, was added to the agar after the top agar solidified. The cells embedded in the top agar were incubated for 2 weeks at 37°C with 5% CO2. After incubation, the colonies were stained with MTT solution and then photographed and counted.

Animal studies of SH-42 as anti-cancer agent

All animal procedures were performed according to a protocol approved by the Seoul National University Institutional Animal Care and Use Committee (approval numbers SNU-121207-2 and SNU-130820-6). For xenograft and PDX experiments, the tumor-bearing mice were treated with treated with vehicle (10% DMSO in corn oil), **SH-42** (4 or 20 mg/kg), deguelin (4 mg/kg), or geldanamycin (4 mg/kg) by oral gavage (for H292 xenografts) or intraperitoneal injection (for H1299 xenografts and PDX) six times per week for 3 weeks. In the experiment using Kras transgenic mice, vehicle or **SH-42** was

administered by intraperitoneal injection (20 mg/kg) once a day for 8 weeks. To examine the parkinsonism-like neurotoxic effects of **SH-42** and deguelin, 8- to 10-week old Sprague–Dawley rats were treated with **SH-42** or deguelin (4 mg/kg, dissolved in corn oil) by oral gavage every day for 20 days.

For xenograft experiments, H1299 and H292 cells (5 x 106 cells/mouse) were subcutaneously injected into the right flank of 6-week old NOD/SCID or nude mice. For patientderived tumor xenograft (PDX) experiments, tumors that had been passed more than 3 times - 4 - in mice were minced into 2-mm3 pieces and subcutaneously inoculated into NOD/SCID mice. After the tumor volume reached 50-150 mm3 , the mice were randomly grouped and treated with vehicle and compounds as described in Materials and Methods. Tumor growth was determined by measuring the short and long diameters of the tumor with a caliper, and body weight was measured twice per week to monitor toxicity. The tumor volume was calculated using the following formula: tumor volume (mm3) = (short diameter)2 × (long diameter) × 0.5. To determine whether **SH-42** can inhibit K-Ras-driven spontaneous lung tumor formation, the K-Ras (G12D) transgenic mouse model [kindly provided by Dr. Guillermina Lozano (MD Anderson Cancer Center, Houston, TX, USA)] was used in experiments. To accelerate lung tumor formation, we backcrossed the K-ras transgenic mice in a C57BL6/129/sv background into the FVB/N background, which is known for its relatively high incidence of spontaneous lung tumors (3). Three-month-old mice were randomized into two groups (n=5) and treated with vehicle or **SH-42** for 8 weeks. Tumor growth was monitored using the IVIS-Spectrum microCT and Living Image (ver. 4.2) software (PerkinElmer, Alameda, CA, USA). To facilitate tumor monitoring, registered axial respiratory-gated CT image analysis and a fluorescence image analyses using an MMPSense 680 probe (PerkinElmer; 2 nmol/150 μl in PBS) were performed in mice treated with **SH-42** or vehicle at 5 months of age as previously described (4,5). The mice were euthanized, and tumor formation was evaluated and compared with that of the

vehicle-treated control group. Microscopic evaluations of lung tissue were also performed to measure mean tumor number (N) and volume (V) in a blinded fashion after hematoxylin and eosin (H&E) staining. The tumor volume was calculated using the following formula: V (mm3) = (long diameter x short diameter2)/2, and the tumor load was calculated using the following formula: mean tumor number (N) x mean tumor volume (V) in a blind fashion. The number and size of tumors were calculated in five sections uniformly distributed throughout each lung.

Cell culture and hypoxia treatment for HIF-1α inhibition assays

Culture conditions for cells were as follows: DMEM (Gibco, Carlsbad, CA) with 10% FBS (Gibco) and 1% penicillin-streptomycin (Gibco) for ARPE-19 cells (American Type Culture Collection, Manassas, VA); M199 medium (Gibco) with 20% FBS (Gibco), 1% penicillinstreptomycin (Gibco), 3 ng/ml bFGF (Millipore, Billerica, MA), and 5 IU/ml heparin (Sigma-Aldrich, St. Louis, MO) for human retinal microvascular endothelial cells (HRMECs;Applied Cell Biology Research Institute, Kirkland, WA); RPMI1640 (Gibco) with 10% FBS (Gibco) and 1% penicillin-streptomycin (Gibco) for SNUOT-Rb1 cells (Gibco) with 10% FBS (Gibco), N-2 Supplement (Gibco), and 1% penicillinstreptomycin (Gibco) for human brain astrocytes (Applied Cell Biology Research Institute). Cells were incubated at 37 °C in an atmosphere of 95% air and 5% CO_2. For hypoxia treatment, cells were incubated in the hypoxic chamber with 1% O_2 (Coy Laboratory, Grass Lake Charter Township, MI).

HIF-1α nano-luciferase assay

HRE-A549 cells stably transfected with hypoxia-response element-luciferase construct were incubated in Dulbecco's modified Eagle's medium. Following overnight serum deprivation, the cells were treated with or without Deguelin or its derivatives. After 1h

incubation, the cells were incubated in hypoxia-chamber for 24 h at 37 °C. Luciferase activity was measured by adding luciferase assay reagent (Promega, Madison, WI).

Measurement of kinetic water solubility

Solubility of SH042, SH173, and SH199 (revision required for compound names) was determined in DPBS (Welgene Inc., Daegu, Korea). For the determination of equilibrium solubility, the excess amount of each compound was dissolved in DPBS, and the mixture agitated for 24 hours in room temperature. The mixture was centrifuged at 13,200 rpm for 10 minutes (Eppendorf 5415R, Hamburg, Germany), and filtered with a filter (0.2 μm pore size syringe filter, Minisart RC15, Sartorius Stedim Biotech, Goettingen, Germany). The supernatant of the sample was diluted with methanol (1:10 dilution for SH042 and SH199; 1:100 dilution for SH173) and the mixture analyzed by LC/MS/MS system (Applied Biosystems 3200 Qtrap MS/MS system with Alliance Waters e2695 LC system) for their concentration in the media.

Preparation of conditioned media (CM)

H1299 cells were cultured with M199 containing 1% FBS and treated with hypoxia or each compound. The media were collected and centrifuged through a centrifugal filter device (3 kDa cut-off; Millipore). Because the molecular masses of both compounds (**SH-42** and **SH-173**) are less than 0.4 kDa and we collected the retentate, this centrifugation was regarded as effective to remove any trace of **SH-42** and **SH-173** from CM

Migration assay

Migration assay was performed as previously described using Transwell plates (8.0 μm pores). The lower wells were filled with fresh M199 (1% FBS) with VEGF or both compounds for the evaluation of VEGF-induced migration and CM based on M199 (1%

FBS) for the evaluation of hypoxia-mediated migration. HUVECs (1 x 10^5 cells) were loaded on the upper well. After the incubation for 4 hours, the cells were fixed and stained with H&E. Migration was quantified by counting the migratory cells using inverted phasecontrast microscope (Leica, Wetzlar, Germany).

Proliferation assay

HUVECs (5 x 10^3 cells) were seeded in gelatin-coated 96-well plates. After the incubation for 24 hours, the media were changed with CM based on M199 (1% FBS) and the cells were cultured for additional 24 hours. Cell proliferation was determined by [3H]-thymidine incorporation assays as previously described. Labeled DNA was solubilized in 0.2 N NaOH/0.1% SDS and quantitatively analyzed by a liquid scintillation counter (Beckman Coulter, Brea, CA).

Tube formation assay

Tube formation was evaluated as previously described. HUVECs (2 x 10^5 cells) were plated on Matrigel (BD, San Jose, CA)-coated 24-well plates in CM based on M199 (1% FBS) and incubated for 20 hours. Tube formation was quantitatively analyzed by measuring the length of tubes in 5 randomly selected fields (x100 magnification) from each well using the Image-Pro Plus (v 4.5; Media Cybernetics, San Diego, CA).

OIR

Animals : C57BL/6 mice were obtained from Central Lab. Animal (Seoul, Korea). The care, use, and treatment of all animals were in agreement with the ARVO statement for the use of animals in ophthalmic and vision research and the guidelines established by the Seoul National University Institutional Animal Care and Use Committee.

OIR was induced in newborn mice as previously described.[10] Briefly, newborn mice were placed in hyperoxia (75 ± 0.5% O_2) from postnatal day (P) 7 to P12 and returned to normoxia. At P14, we intravitreally injected 1 μl of PBS or each compound (100 nM) into the right eyes of mice (n = 6). At P17, the enucleated eyes were processed for further analyses. For qualitative analyses, FITC-dextran (500 kDa) was perfused intravenously 1 hour before the sacrifice. The retinal flatmounts were observed via the fluorescence microscope (Olympus, Tokyo, Japan). For quantitative analyses, the eyes were prepared for Hematoxylin and eosin (H&E) staining and the slides were observed via the light microscope (Carl Zeiss, Oberkochen, Germany).

Statistics.

Differences between control and treatment groups were assessed using the 2-tailed unpaired T-test. All statistical analyses were performed using Prism 5 (GraphPad Software, La Jolla, CA). The mean ± SEM was shown in figures.

V. References

1. Fukami, H.; Nakajima, M.; Jacobson, M.; Crosby, D., Naturally occurring insecticides. *Rotenone and Rotenoids* **1971**, 71.

2. Botta, B.; Menendez, P.; Zappia, G.; de Lima, R. A.; Torge, R.; Monache, G. D., Prenylated Isoflavonoids: Botanical Distribution, Structures, Biological Activities and Biotechnological Studies. An Update (1995-2006). *Curr. Med. Chem.* **2009,** *16* (26), 3414-3468.

3. Gerhäuser, C.; Lee, S. K.; Kosmeder, J. W.; Moriarty, R. M.; Hamel, E.; Mehta, R. G.; Moon, R. C.; Pezzuto, J. M., Regulation of ornithine decarboxylase induction by deguelin, a natural product cancer chemopreventive agent. *Cancer Res.* **1997,** *57* (16), 3429-3435.

4. Luo, J. K.; Luyengi, L.; Fong, H. H.; Kinghorn, A. D.; Moriarty, R. M.; Mehta14, R. G.; Constantinou, A.; Moon, R. C.; Pezzuto, J. M., Rotenoids mediate potent cancer chemopreventive activity through transcriptional regulation of ornithine decarboxylase. *Nat. Med.* **1995,** *1* (3), 260-266.

5. Garcia, J.; Barluenga, S.; Gorska, K.; Sasse, F.; Winssinger, N., Synthesis of deguelin–biotin conjugates and investigation into deguelin's interactions. *Biorg. Med. Chem.* **2012,** *20* (2), 672-680.

6. Oh, S. H.; Woo, J. K.; Yazici, Y. D.; Myers, J. N.; Kim, W.-Y.; Jin, Q.; Hong, S. S.; Park, H.-J.; Suh, Y.-G.; Kim, K.-W., Structural basis for depletion of heat shock protein 90 client proteins by deguelin. *J. Natl. Cancer Inst.* **2007,** *99* (12), 949-961.

7. Oh, S. H.; Woo, J. K.; Jin, Q.; Kang, H. J.; Jeong, J. W.; Kim, K. W.; Hong, W. K.; Lee, H. Y., Identification of novel antiangiogenic anticancer activities of deguelin targeting hypoxia-inducible factor-1 alpha. *Int. J. Cancer* **2008,** *122* (1), 5-14.

8. Kim, J.; Yu, Y.; Shin, J.; Lee, H. Y.; Kim, K. W., Deguelin inhibits retinal neovascularization by down-regulation of HIF-1α in oxygen-induced retinopathy. *J. Cell. Mol. Med.* **2008,** *12* (6a), 2407-2415.

9. Kim, J. H.; Kim, J. H.; Yu, Y. S.; Park, K. H.; Kang, H. J.; Lee, H.-Y.; Kim, K.-W., Antiangiogenic effect of deguelin on choroidal neovascularization. *J. Pharmacol. Exp. Ther.* **2008,** *324* (2), 643-647.

10. Chang, D.-J.; An, H.; Kim, K.-s.; Kim, H. H.; Jung, J.; Lee, J. M.; Kim, N.-J.; Han, Y. T.; Yun, H.; Lee, S.; Lee, G.; Lee, S.; Lee, J. S.; Cha, J.-H.; Park, J.-H.; Park, J. W.; Lee, S.-C.; Kim, S. G.; Kim, J. H.; Lee, H.-Y.; Kim, K.-W.; Suh, Y.-G., Design, synthesis,

and biological evaluation of novel deguelin-based heat shock protein 90 (HSP90) inhibitors targeting proliferation and angiogenesis. *J. Med. Chem.* **2012,** *55* (24), 10863-10884.

11. Jo, D. H.; An, H.; Chang, D.-J.; Baek, Y.-Y.; Cho, C. S.; Jun, H. O.; Park, S.-J.; Kim, J. H.; Lee, H.-Y.; Kim, K.-W.; Lee, J.; Park, H.-J.; Kim, Y.-M.; Suh, Y.-G.; Kim, J. H., Hypoxia-mediated retinal neovascularization and vascular leakage in diabetic retina is suppressed by HIF-1α destabilization by SH-1242 and SH-1280, novel hsp90 inhibitors. *J. Mol. Med.* **2014**, 1-10.

12. Anzeveno, P. B., Rotenoid Interconversion - Synthesis of Deguelin from Rotenone. *J. Org. Chem.* **1979,** *44* (14), 2578-2580.

13. Fukami, H.; Oda, J.; Sakata, G.; Nakajima, M., Total Synthesis of dl-Deguelin. *Bulletin of the Agricultural Chemical Society of Japan* **1960,** *24* (3), 327-328.

14. Fukami, H.; Oda, J.; Sakata, G.; Nakajima, M., Total Synthesis of dl-Deguelin: (Synthesis of Rotenoids V). *Agric. Biol. Chem.* **1961,** *25* (3), 252-256.

15. Omokawa, H.; Yamashita, K., Chemical studies on rotenoed. III. Synthesis of (+)-deguelin. *Agric. Biol. Chem.* **1974,** *38* (9), 1731-1734.

16. Pastine, S. J.; Sames, D., Concise synthesis of the chemopreventitive agent (±)-deguelin via a key 6-endo hydroarylation. *Org. Lett.* **2003,** *5* (22), 4053-4055.

17. Maloney, A.; Workman, P. HSP90 as a new therapeutic target for cancer therapy: the story unfolds. *Expert Opin. Biol. Ther.* **2002,** 2, 3-24.

18. Minami, Y.; Kimura, Y.; Kawasaki, H.; Suzuki, K.; Yahara, I. The carboxy-terminal region of mammalian HSP90 is required for its dimerization and function in vivo. *Mol. Cell. Biol.* **1994,** 14, 1459-1464.

19. Harris, S. F.; Shiau, A. K.; Agard, D. A. The crystal structure of the carboxy-terminal dimerization domain of htpG, the Escherichia coli Hsp90, reveals a potential substrate binding site. *Structure* **2004,** 12, 1087-1097.

20. Nemoto, T.; Ohara-Nemoto, Y.; Ota, M.; Takagi, T.; Yokoyama, K. Mechanism of dimer formation of the 90-kDa heat-shock protein. *Eur. J. Biochem.* **1995,** 233, 1-8.

21. Mikko T.; Daniel F. J.; Susan L. *Nature Reviews Molecular Cell Biology* **2010**, 11, 515-528

22. Maloney, A.; Workman, P. HSP90 as a new therapeutic target for cancer therapy: the story unfolds. *Expert Opin. Biol. Ther.* **2002,** 2, 3-24.

23. Isaacs, J. S.; Xu, W.; Neckers, L. Heat shock protein 90 as a molecular target for cancer therapeutics. *Cancer Cell* **2003,** 3, 213-217.

24. Scheibel, T.; Buchner, J. The Hsp90 complex--a super-chaperone machine as a novel drug target. *Biochem. Pharmacol.* **1998,** 56, 675-682.

25. Smith, D. F.; Whitesell, L.; Katsanis, E. Molecular chaperones: biology and prospects for pharmacological intervention. *Pharmacol. Rev.* **1998,** 50, 493-514.

26. Jolly, C.; Morimoto, R. I. Role of the heat shock response and molecular chaperones in oncogenesis and cell death. *J. Natl. Cancer Inst.* **2000,** 92, 1564-1572.

27. Ferrarini, M.; Heltai, S.; Zocchi, M. R.; Rugarli, C. Unusual expression and localization of heat-shock proteins in human tumor cells. *Int. J. Cancer* **1992,** 51, 613-619.

28. Carroll, V. A.; Ashcroft, M. Targeting the molecular basis for tumour hypoxia. *Expert Rev. Mol. Med.* **2005,** 7, 1-16.

29. Semenza, G. Signal transduction to hypoxia-inducible factor 1. *Biochem. Pharmacol.* **2002,** 64, 993-998.

30. Semenza, G. L. Regulation of mammalian O2 homeostasis by hypoxia-inducible factor 1. *Annu. Rev. Cell Dev. Biol.* **1999,** 15, 551-578.

31. Ivan, M.; Kondo, K.; Yang, H.; Kim, W.; Valiando, J.; Ohh, M.; Salic, A.; Asara, J. M.; Lane, W. S.; Kaelin, W. G., Jr. HIFalpha targeted for VHL-mediated destruction by proline hydroxylation: implications for O2 sensing. *Science* **2001,** 292, 464-468.

32. Yu, F.; White, S. B.; Zhao, Q.; Lee, F. S. HIF-1alpha binding to VHL is regulated by stimulus-sensitive proline hydroxylation. *Proc. Natl. Acad. Sci. U. S. A.* **2001,** 98, 9630-9635.

33. Ohh, M.; Park, C. W.; Ivan, M.; Hoffman, M. A.; Kim, T. Y.; Huang, L. E.; Pavletich, N.; Chau, V.; Kaelin, W. G. Ubiquitination of hypoxia-inducible factor requires direct binding to the beta-domain of the von Hippel-Lindau protein. *Nat. Cell Biol.* **2000,** 2, 423-427.

34. Mahon, P. C.; Hirota, K.; Semenza, G. L. FIH-1: a novel protein that interacts with HIF-1alpha and VHL to mediate repression of HIF-1 transcriptional activity. *Genes Dev.* **2001,** 15, 2675-2686.

35. Gradin, K.; McGuire, J.; Wenger, R. H.; Kvietikova, I.; fhitelaw, M. L.; Toftgard, R.; Tora, L.; Gassmann, M.; Poellinger, L. Functional interference between hypoxia and dioxin signal transduction pathways: competition for recruitment of the Arnt transcription factor. *Mol. Cell. Biol.* **1996,** 16, 5221-5231.

36. Mayo Clinic Hompage. http://www.mayoclinic.org/medical-professionals/clinical-updates/ophthalmology/aflibercept-shows-promise-game-changer-patients-age-related-macular%20degeneration (accessed Nov 25, 2016).

37. Klein, R.; Cruickshanks, K. J.; Nash, S. D.; Krantz, E. M.; Nieto, F. J.; Huang, G. H.; Pankow, J. S.; Klein, B. E. The prevalence of age-related macular degeneration and associated risk factors. *Arch. Ophthalmol.* **2010,** 128, 750-758.

38. Cook, H. L.; Patel, P. J.; Tufail, A. Age-related macular degeneration: diagnosis and management. *Br. Med. Bull.* **2008,** 85, 127-149.

39. Arjamaa, O.; Nikinmaa, M.; Salminen, A.; Kaarniranta, K. Regulatory role of HIF-1alpha in the pathogenesis of age-related macular degeneration (AMD). *Ageing research reviews* **2009,** 8, 349-358.

40. Grunwald, J. E.; Metelitsina, T. I.; Dupont, J. C.; Ying, G. S.; Maguire, M. G. Reduced foveolar choroidal blood flow in eyes with increasing AMD severity. *Invest. Ophthalmol. Vis. Sci.* **2005,** 46, 1033-1038.

41. Bird, A. C. Therapeutic targets in age-related macular disease. *J. Clin. Invest.* **2010,** 120, 3033-3041.

42. Beatty, S.; Koh, H.; Phil, M.; Henson, D.; Boulton, M. The role of oxidative stress in the pathogenesis of age-related macular degeneration. *Surv. Ophthalmol.* **2000,** 45, 115-134.

43. Donoso, L. A.; Kim, D.; Frost, A.; Callahan, A.; Hageman, G. The role of inflammation in the pathogenesis of age-related macular degeneration. *Surv. Ophthalmol.* **2006,** 51, 137-152.

44. Grunwald, J. E.; Metelitsina, T. I.; Dupont, J. C.; Ying, G. S.; Maguire, M. G. Reduced foveolar choroidal blood flow in eyes with increasing AMD severity. *Invest. Ophthalmol. Vis. Sci.* **2005,** 46, 1033-1038.

45. Taylor, C. T. Interdependent roles for hypoxia inducible factor and nuclear factor-kappaB in hypoxic inflammation. *J. Physiol.* **2008,** 586, 4055-4059.

46. Inoue, Y.; Yanagi, Y.; Matsuura, K.; Takahashi, H.; Tamaki, Y.; Araie, M. Expression of hypoxia-inducible factor 1alpha and 2alpha in choroidal neovascular membranes associated with age-related macular degeneration. *Br. J. Ophthalmol.* **2007,** 91, 1720-1721.

47. Kocur, I.; Resnikoff, S. Visual impairment and blindness in Europe and their prevention. *Br. J. Ophthalmol.* **2002,** 86, 716-722.

48. Ferris, F. L., 3rd; Davis, M. D.; Aiello, L. M. Treatment of diabetic retinopathy. *N. Engl. J. Med.* **1999,** 341, 667-678.

49. EyeRis Vision Center Homepage. http://www.eyerisvision.com/diabetic-retinopathy.html (accessed Nov 4, 2013).

50. Bhavsar, A. R. Diabetic retinopathy: the latest in current management. *Retina* **2006,** 26, S71-79.

51. Bursell, S. E.; Clermont, A. C.; Kinsley, B. T.; Simonson, D. C.; Aiello, L. M.; Wolpert, H. A. Retinal blood flow changes in patients with insulin-dependent diabetes

mellitus and no diabetic retinopathy. *Invest. Ophthalmol. Vis. Sci.* **1996,** 37, 886-897.

52. Josifova, T.; Plestina-Borjan, I.; Henrich, P. B. Proliferative diabetic retinopathy: predictive and preventive measures at hypoxia induced retinal changes. *The EPMA journal* **2010,** 1, 73-77.

53. Morello, C. M. Etiology and natural history of diabetic retinopathy: an overview. *Am. J. Health Syst. Pharm.* **2007,** 64, S3-7.

54. Rosenfeld, P. J.; Moshfeghi, A. A.; Puliafito, C. A. Optical coherence tomography findings after an intravitreal injection of bevacizumab (avastin) for neovascular age-related macular degeneration. *Ophthalmic Surg. Lasers Imaging* **2005,** 36, 331-335.

55. Michels, S.; Rosenfeld, P. J.; Puliafito, C. A.; Marcus, E. N.; Venkatraman, A. S. Systemic bevacizumab (Avastin) therapy for neovascular age-related macular degeneration twelve-week results of an uncontrolled open-label clinical study. *Ophthalmology* **2005,** 112, 1035-1047.

56. Moshfeghi, A. A.; Rosenfeld, P. J.; Puliafito, C. A.; Michels, S.; Marcus, E. N.; Lenchus, J. D.; Venkatraman, A. S. Systemic bevacizumab (Avastin) therapy for neovascular age-related macular degeneration: twenty-four-week results of an uncontrolled open-label clinical study. *Ophthalmology* **2006,** 113, 2002.e2001-2012.

57. Chen, Y.; Wiesmann, C.; Fuh, G.; Li, B.; Christinger, H. W.; McKay, P.; de Vos, A. M.; Lowman, H. B. Selection and analysis of an optimized anti-VEGF antibody: crystal structure of an affinity-matured Fab in complex with antigen. *J. Mol. Biol.* **1999,** 293, 865-881.

58. Brown, D. M.; Kaiser, P. K.; Michels, M.; Soubrane, G.; Heier, J. S.; Kim, R. Y.; Sy, J. P.; Schneider, S. Ranibizumab versus verteporfin for neovascular age-related macular degeneration. *N. Engl. J. Med.* **2006,** 355, 1432-1444.

59. Rosenfeld, P. J.; Brown, D. M.; Heier, J. S.; Boyer, D. S.; Kaiser, P. K.; Chung, C. Y.; Kim, R. Y. Ranibizumab for neovascular age-related macular degeneration. *N. Engl. J. Med.* **2006,** 355, 1419-1431.

60. Chong, D. Y.; Anand, R.; Williams, P. D.; Qureshi, J. A.; Callanan, D. G. Characterization of sterile intraocular inflammatory responses after intravitreal bevacizumab injection. *Retina* **2010,** 30, 1432-1440.

61. Fielden, M.; Nelson, B.; Kherani, A. Acute intraocular inflammation following intravitreal injection of bevacizumab--a large cluster of cases. *Acta Ophthalmol* **2011,** 89, e664-665.

62. Johnson, D.; Hollands, H.; Hollands, S.; Sharma, S. Incidence and characteristics of acute intraocular inflammation after intravitreal injection of bevacizumab: a

retrospective cohort study. *Can. J. Ophthalmol.* **2010,** 45, 239-242.

63. Sato, T.; Emi, K.; Ikeda, T.; Bando, H.; Sato, S.; Morita, S.; Oyagi, T.; Sawada, K. Severe intraocular inflammation after intravitreal injection of bevacizumab. *Ophthalmology* **2010,** 117, 512-516, 516.e511-512.

64. Yamashiro, K.; Tsujikawa, A.; Miyamoto, K.; Oh, H.; Otani, A.; Tamuara, H.; Ooto, S.; Sasahara, M.; Iwama, D.; Yoshimura, N. Sterile endophthalmitis after intravitreal injection of bevacizumab obtained from a single batch. *Retina* **2010,** 30, 485-490.

65. 92. Chong, D. Y.; Anand, R.; Williams, P. D.; Qureshi, J. A.; Callanan, D. G. Characterization of sterile intraocular inflammatory responses after intravitreal bevacizumab injection. *Retina* **2010,** 30, 1432-1440.

66. Fielden, M.; Nelson, B.; Kherani, A. Acute intraocular inflammation following intravitreal injection of bevacizumab--a large cluster of cases. *Acta Ophthalmol* **2011,** 89, e664-665.

67. Jin, K.; Zhu, Y.; Sun, Y.; Mao, X. O.; Xie, L.; Greenberg, D. A. Vascular endothelial growth factor (VEGF) stimulates neurogenesis in vitro and in vivo. *Proc. Natl. Acad. Sci. U. S. A.* **2002,** 99, 11946-11950.

68. Robinson, G. S.; Ju, M.; Shih, S. C.; Xu, X.; McMahon, G.; Caldwell, R. B.; Smith, L. E. Nonvascular role for VEGF: VEGFR-1, 2 activity is critical for neural retinal development. *FASEB J.* **2001,** 15, 1215-1217.

69. Saint-Geniez, M.; Maharaj, A. S.; Walshe, T. E.; Tucker, B. A.; Sekiyama, E.; Kurihara, T.; Darland, D. C.; Young, M. J.; D'Amore, P. A. Endogenous VEGF is required for visual function: evidence for a survival role on muller cells and photoreceptors. *PLoS One* **2008,** 3, e3554.

70. Kurihara, T.; Westenskow, P. D.; Bravo, S.; Aguilar, E.; Friedlander, M. Targeted deletion of Vegfa in adult mice induces vision loss. *J. Clin. Invest.* **2012,** 122, 4213-4217.

71. Chang, D. J. Structure-Activity Relationships of Deguelin as Hsp90 Inhibitor and Development of Novel Hsp90 inhibitor. Ph. D. Thesis, Seoul National University, 2009.

72. Lee, G. Design, synthesis and biological evaluation of novel HIF-1 alpha inhibitor. MS Thesis, Seoul National University, 2012.

73. Hu, B.; Ellingboe, J.; Gunawan, I.; Han, S.; Largis, E.; Li, Z.; Malamas, M.; Mulvey, R.; Oliphant, A.; Sum, F.-W., 2, 4-thiazolidinediones as potent and selective human β 3 agonists. *Bioorg. Med. Chem. Lett.* **2001,** *11* (6), 757-760.

74. Tajik, H.; Mohammadpoor-Baltork, I.; Rasht-Abadi, H. R., Selective Para-Iodination of Methoxyarenes, Phenols, and Anilines with Iodine in the Presence of Poly (4-Vinylpyridine)-Supported Peroxodisulfate. *Synth. Commun.* **2004,** *34* (19), 3579-

3585.

75. Castanet, A.-S.; Colobert, F.; Broutin, P.-E., Mild and regioselective iodination of electron-rich aromatics with N-iodosuccinimide and catalytic trifluoroacetic acid. *Tetrahedron Lett.* **2002,** *43* (29), 5047-5048.

76. Farina, V.; Krishnan, B., Large rate accelerations in the Stille reaction with tri-2-furylphosphine and triphenylarsine as palladium ligands: mechanistic and synthetic implications. *J. Am. Chem. Soc.* **1991,** *113* (25), 9585-9595.

77. Kitson, R. R.; Chang, C.-H.; Xiong, R.; Williams, H. E.; Davis, A. L.; Lewis, W.; Dehn, D. L.; Siegel, D.; Roe, S. M.; Prodromou, C.; Ross, D.; Moody, C. J., Synthesis of 19-substituted geldanamycins with altered conformations and their binding to heat shock protein Hsp90. *Nat. Chem.* **2013,** *5* (4), 307-314.

78. Lee S.; An H.; Chang DJ..; Jang J.; Kim Ky.; Sim J.; Lee JY.; Suh YG.; Total synthesis of (−)-deguelin via an iterative pyran-ring formation strategy. *Chem. Comm.* **2015**, 51, 9026-9029

79. Whitesell L, Lindquist SL. HSP90 and the chaperoning of cancer. *Nat. Rev. Cancer.* **2005**, 5, 761–772

80. Taipale M, Jarosz DF, Lindquist S. HSP90 at the hub of protein homeostasis: emerging mechanistic insights. *Nat. Rev. Mol. Cell. Biol*. **2010**, 11, 515–528

81. Soti C, Racz A, Csermely P. A Nucleotide-dependent molecular switch controls ATP binding at the C-terminal domain of Hsp90. N-terminal nucleotide binding unmasks a C-terminal binding pocket. *J. Biol. Chem.* **2002**, 277, 7066–7075

82. Marcu MG, Chadli A, Bouhouche I, Catelli M, Neckers LM. The heat shock protein 90 antagonist novobiocin interacts with a previously unrecognized ATP-binding domain in the carboxyl terminus of the chaperone. *J. Biol. Chem.* **2000**, 275, 37181–37186.

83. Garnier C, Lafitte D, Tsvetkov PO, Barbier P, Leclerc-Devin J, Millot JM, et al. Binding of ATP to heat shock protein 90: evidence for an ATP-binding site in the C-terminal domain. *J. Biol. Chem.* **2002**, 277, 12208–12214.

84. Lee SC.; Min HY.; Choi H.; Bae S.; Park K.;, Hyun S.; Lee H.; Moon J.; Park S.; Kim J.; An H.; Park SJ.; Seo J.; Lee S.; Kim YM.; Park HJ.; Lee SK.; Lee JW.; Lee JY. Kim KW. Suh YG.; Lee HY. Deguelin Analogue SH-1242 Inhibits Hsp90 Activity and Exerts Potent Anticancer Efficacy with Limited Neurotoxicity. *Cancer Res.* **2016**, 76, (3), 686-699

85. Zhang W, Huang P. Cancer-stromal interactions: role in cell survival, metabolism and drug sensitivity. *Cancer Biol. Ther.* **2011**, 11, 150–156.

86. Johnson L, Mercer K, Greenbaum D, Bronson RT, Crowley D, Tuveson DA, et al. Somatic activation of the K-ras oncogene causes early onset lung cancer in mice. *Nature*

2001, 410, 1111–1116.

87. Caboni P, Sherer TB, Zhang N, Taylor G, Na HM, Greenamyre JT, et al. Rotenone, deguelin, their metabolites, and the rat model of Parkinson's disease. *Che.m Res. Toxicol.* **2004**, 17, 1540–1548.

88. Jhaveri K, Taldone T, Modi S, Chiosis G. Advances in the clinical development of heat shock protein 90 (Hsp90) inhibitors in cancers. *Biochim. Biophys. Acta*. **2012**, 1823, 742–755.

89. Kim, H. S.; Hong, M.; Lee, S.-C.; Lee, H.-Y.; Suh, Y.-G.; Oh, D.-C.; Seo, J. H.; Choi, H.; Kim, J. Y.; Kim, K.-W.; Kim, J. H.; Kim, J.; Kim, Y.-M.; Park, S.-J.; Park, H.-J.; Lee, J. Ring-truncated deguelin derivatives as potent Hypoxia Inducible Factor-1alpha (HIF-1alpha) inhibitors. Eur. J. Med. Chem. 2015, 104, 157-164.

90. Smith, L. E.; Wesolowski, E.; McLellan, A.; Kostyk, S. K.; D'Amato, R.; Sullivan, R.; D'Amore, P. A. Oxygen-induced retinopathy in the mouse. Invest. Ophthalmol. Vis. Sci. 1994, 35, 101-111.

91. Suh, Y.-G.; Chang, D.-J.; An, H.; Kim, K.-W.; Kim, Y.-M.; Lee, H.-Y. Novel compound or pharmaceutically acceptable salt thereof, and pharmaceutical composition containing same as active ingredient. WO2014007412 A1, 2014.

92. Wu, G.; Yin, W.; Shen, H. C.; Huang, Y. One-pot synthesis of useful heterocycles in medicinal chemistry using a cascade strategy. Green Chem. 2012, 14, 580-585.

93. Mooring, S. R.; Jin, H.; Devi, N. S.; Jabbar, A. A.; Kaluz, S.; Liu, Y.; Van Meir, E. G.; Wang, B. Design and synthesis of novel small-molecule inhibitors of the hypoxia inducible factor pathway. J. Med. Chem. 2011, 54, 8471-8489.

94. Mun, J.; Jabbar, A. A.; Devi, N. S.; Liu, Y.; Van Meir, E. G.; Goodman, M. M. Structure-activity relationship of 2,2-dimethyl-2H-chromene based arylsulfonamide analogs of 3,4-dimethoxy-N-[(2,2-dimethyl-2H-chromen-6-yl)methyl]-N-phenylbenzenesulfonamide , a novel small molecule hypoxia inducible factor-1 (HIF-1) pathway inhibitor and anti-cancer agent. Bioorg. Med. Chem. 2012, 20, 4590-4597.

95. Bissantz, C.; Kuhn, B.; Stahl, M. A medicinal chemist’s guide to molecular interactions. J. Med. Chem. 2010, 53, 5061-5084.

96. Dunitz, J. D.; Taylor, R. Organic fluorine hardly ever accepts hydrogen bonds. Chemistry–A European Journal 1997, 3, 89-98.

97. Boldi, A. M. Combinatorial Synthesis of Natural Product-Based Libraries. Taylor & Francis: 2006.

98. Costa, M.; Dias, T. A.; Brito, A.; Proenca, F. Biological importance of structurally diversified chromenes. Eur. J. Med. Chem. 2016, 123, 487-507.

99. Nicolaou, K.; Pfefferkorn, J.; Roecker, A.; Cao, G.-Q.; Barluenga, S.; Mitchell, H. Natural product-like combinatorial libraries based on privileged structures. 1. General principles and solid-phase synthesis of benzopyrans. J. Am. Chem. Soc. 2000, 122, 9939-9953.

100. Nicolaou, K.; Pfefferkorn, J.; Mitchell, H.; Roecker, A.; Barluenga, S.; Cao, G.-Q.; Affleck, R.; Lillig, J. Natural product-like combinatorial libraries based on privileged structures. 2. Construction of a 10 000-membered benzopyran library by directed split-and-pool chemistry using NanoKans and optical encoding. J. Am. Chem. Soc. 2000, 122, 9954-9967.

101. Nicolaou, K.; Pfefferkorn, J.; Barluenga, S.; Mitchell, H.; Roecker, A.; Cao, G.-Q. Natural product-like combinatorial libraries based on privileged structures. 3. The “libraries from libraries” principle for diversity enhancement of benzopyran libraries. J. Am. Chem. Soc. 2000, 122, 9968-9976.

102. Mun, J.; Jabbar, A. A.; Devi, N. S.; Yin, S.; Wang, Y.; Tan, C.; Culver, D.; Snyder, J. P.; Van Meir, E. G.; Goodman, M. M. Design and in vitro activities of N-alkyl-N-[(8-R-2,2-dimethyl-2H-chromen-6-yl)methyl]heteroarylsulfonamides, novel, small-molecule hypoxia inducible factor-1 pathway inhibitors and anticancer agents. J. Med. Chem. 2012, 55, 6738-6750.

103. Tan, C.; de Noronha, R. G.; Devi, N. S.; Jabbar, A. A.; Kaluz, S.; Liu, Y.; Mooring, S. R.; Nicolaou, K. C.; Wang, B.; Van Meir, E. G. Sulfonamides as a new scaffold for hypoxia inducible factor pathway inhibitors. Bioorg. Med. Chem. Lett. 2011, 21, 5528-5532.

104. Edward H. K.; Li D.; Guy T. C. In Vitro Solubility Assays in Drug Discovery. *Cur. Drug Met.* **2008**, 9, 879-885

105. Adair, T. H.; Montani, J. P. Integrated Systems Physiology: from Molecule to Function to Disease. In Angiogenesis, Morgan & Claypool Life Sciences: San Rafael (CA), 2010.

106. Lim, J. MS Thesis, Seoul National University, 2012.

107. An, H. Doctoral Degree Thesis, Seoul National University, 2012.

VI. Appendix

▼ ^{1}H-NMR ($CDCl_3$, 500 MHz)

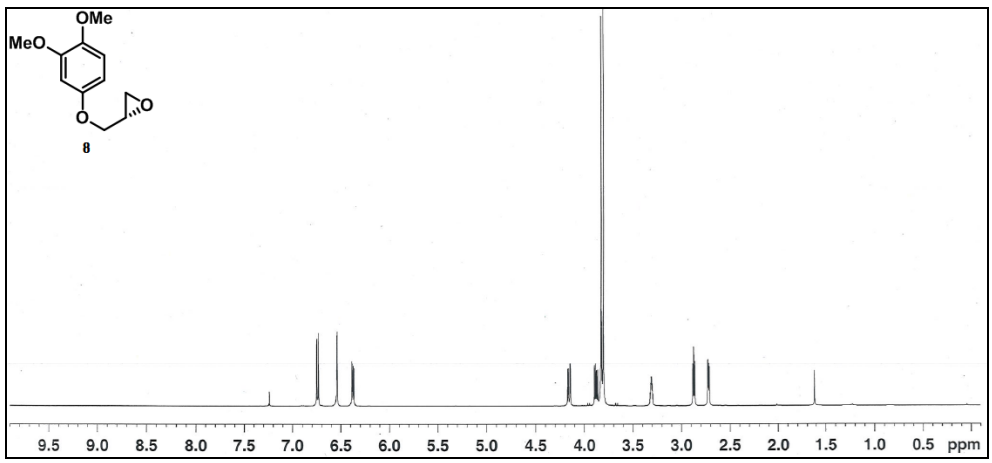

▼ ^{13}C-NMR ($CDCl_3$, 125 MHz)

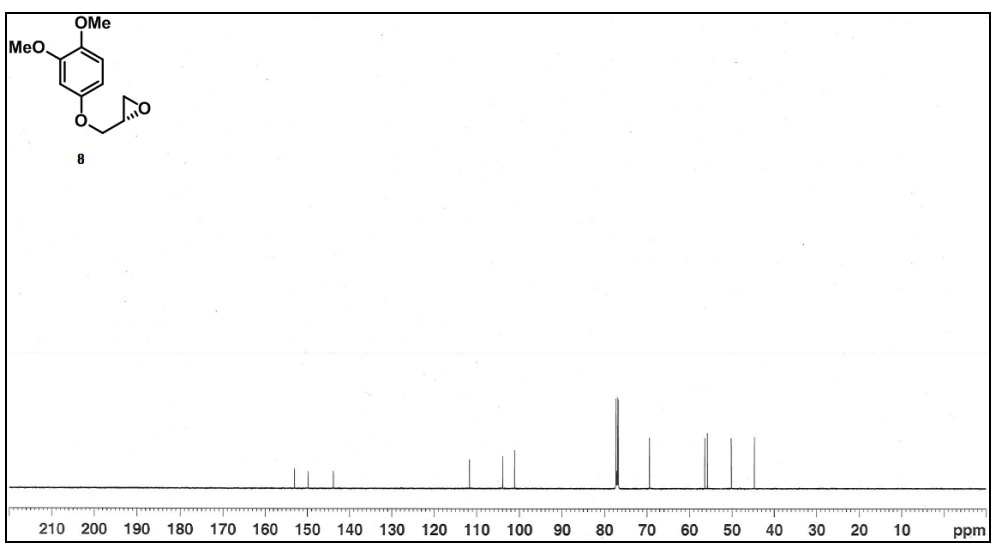

▼ ^{1}H-NMR ($CDCl_3$, 500 MHz)

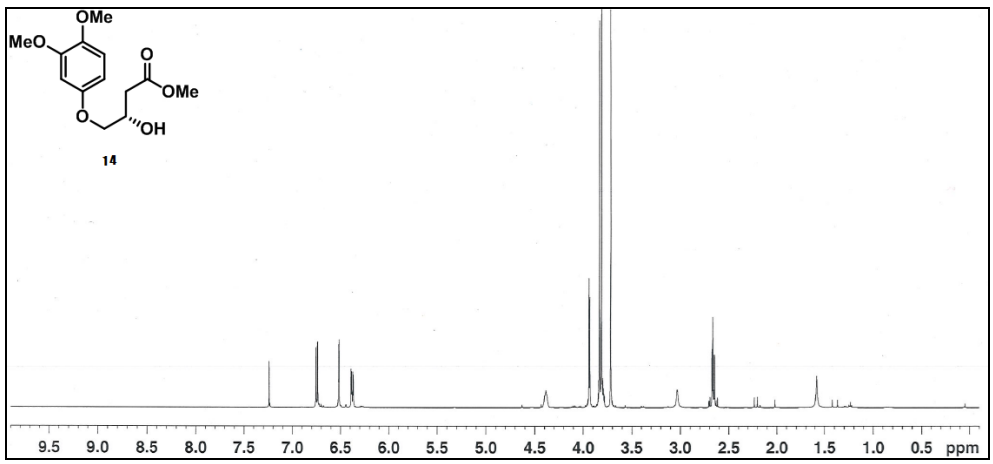

▼ ^{13}C-NMR ($CDCl_3$, 125 MHz)

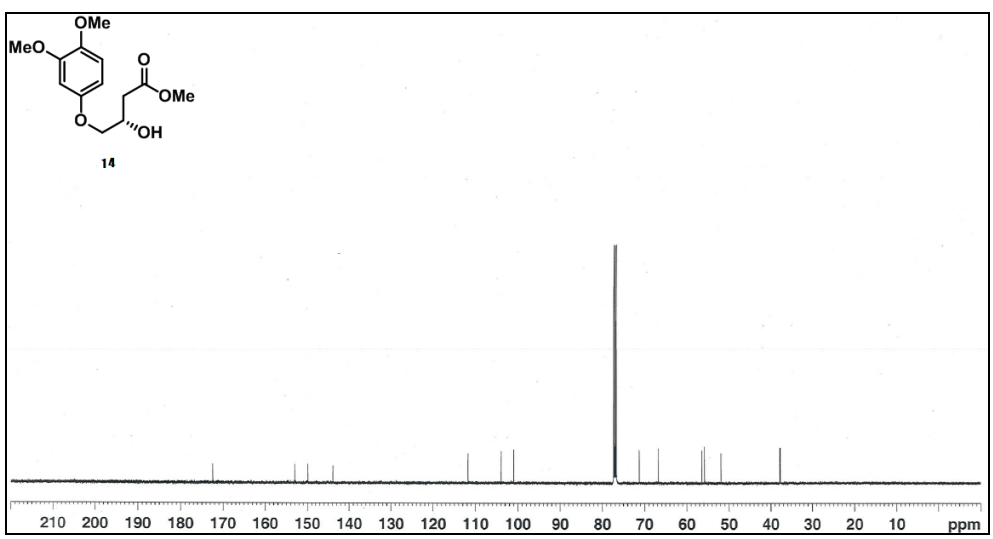

▼ ^{1}H-NMR ($CDCl_3$, 500 MHz)

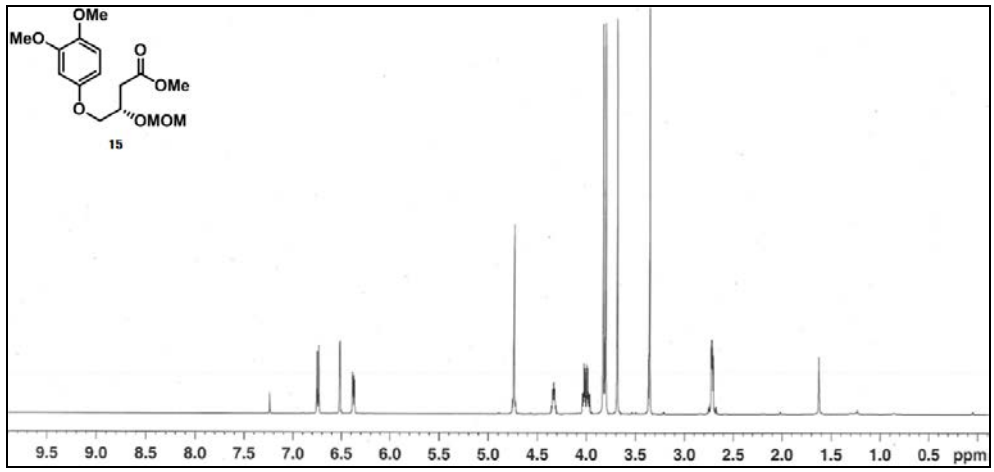

▼ ^{13}C-NMR ($CDCl_3$, 125 MHz)

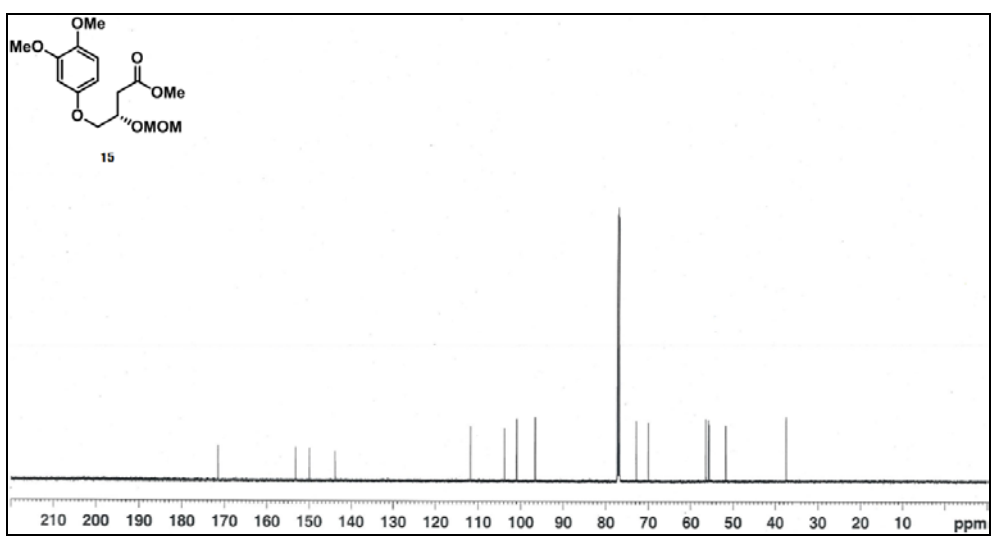

▼ ^{1}H-NMR ($CDCl_3$, 500 MHz)

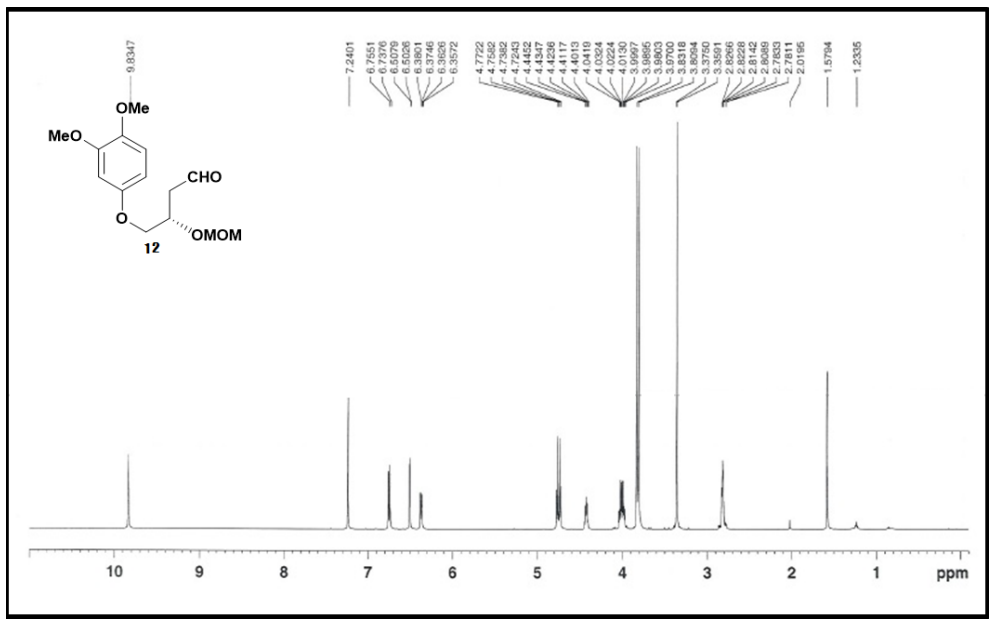

▼ ^{13}C-NMR ($CDCl_3$, 100 MHz)

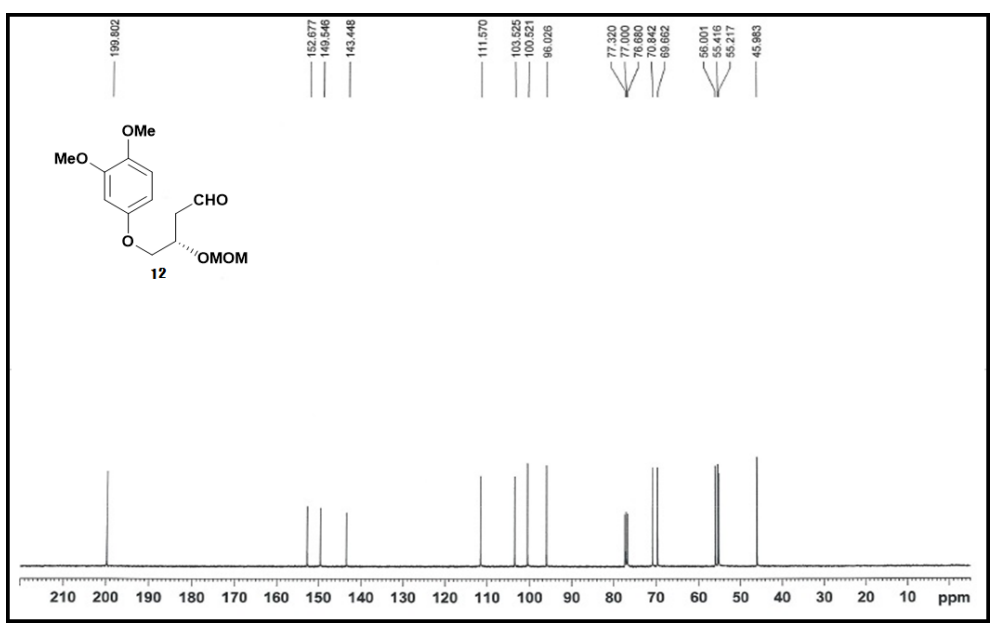

▼ ^{1}H-NMR ($CDCl_3$, 500 MHz)

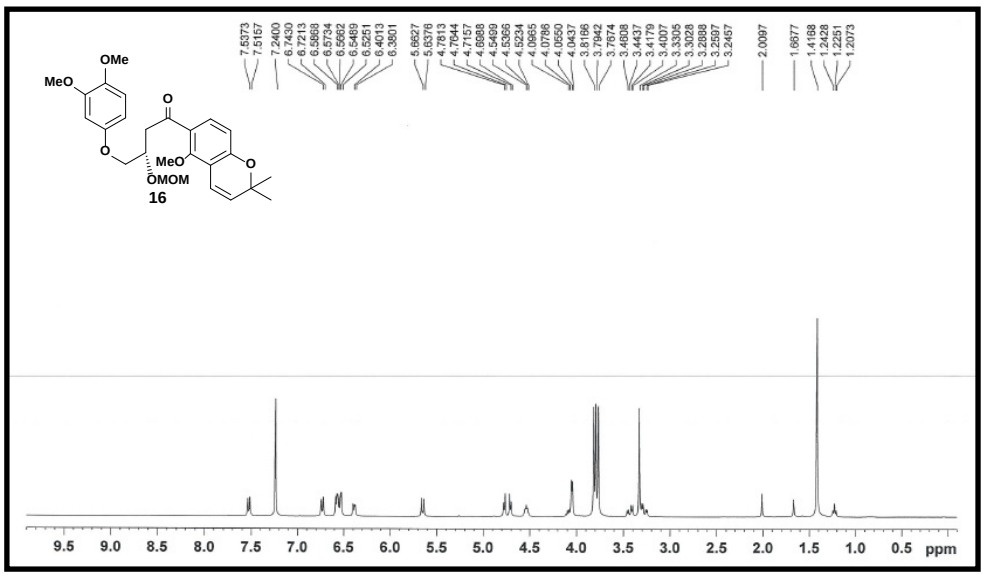

▼ ^{1}H-NMR ($CDCl_3$, 125 MHz)

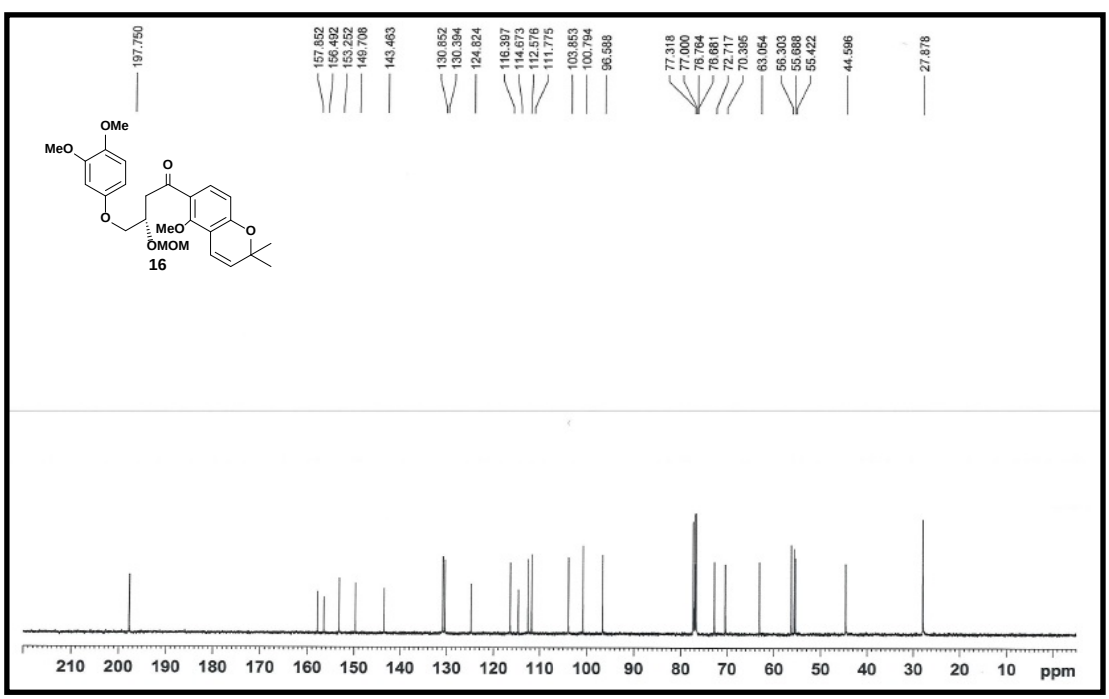

▼ ^{1}H-NMR ($CDCl_3$, 400 MHz)

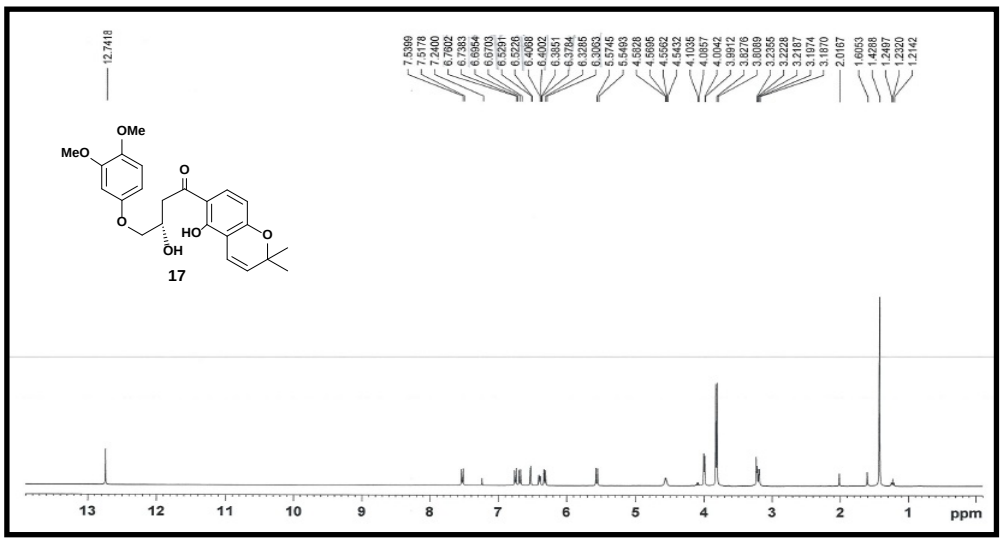

▼ ^{13}C-NMR ($CDCl_3$, 100 MHz)

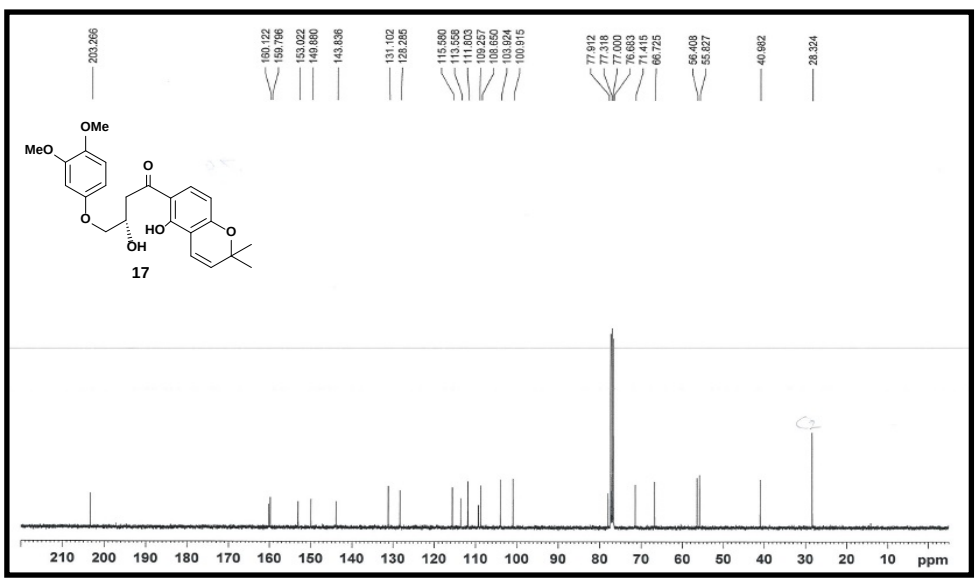

▼ ^{1}H-NMR ($CDCl_3$, 500 MHz)

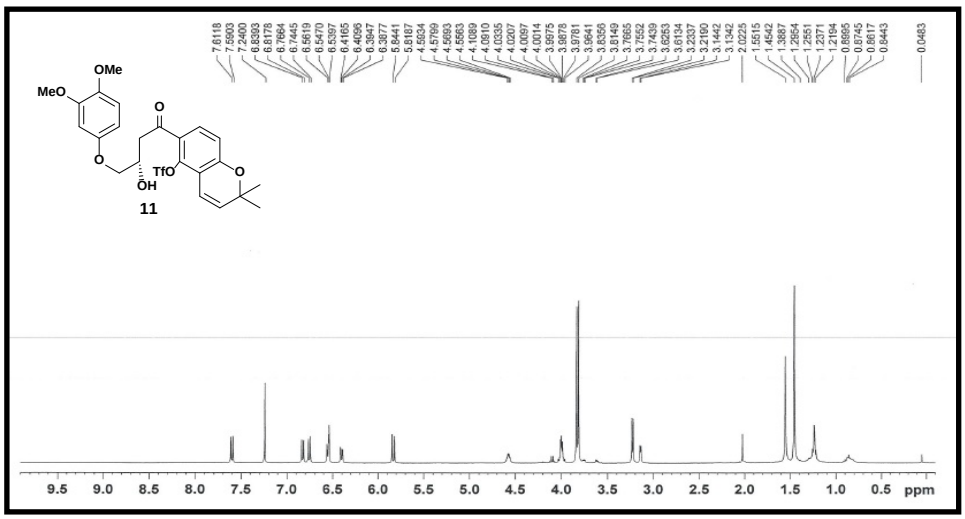

▼ ^{13}C-NMR ($CDCl_3$, 125 MHz)

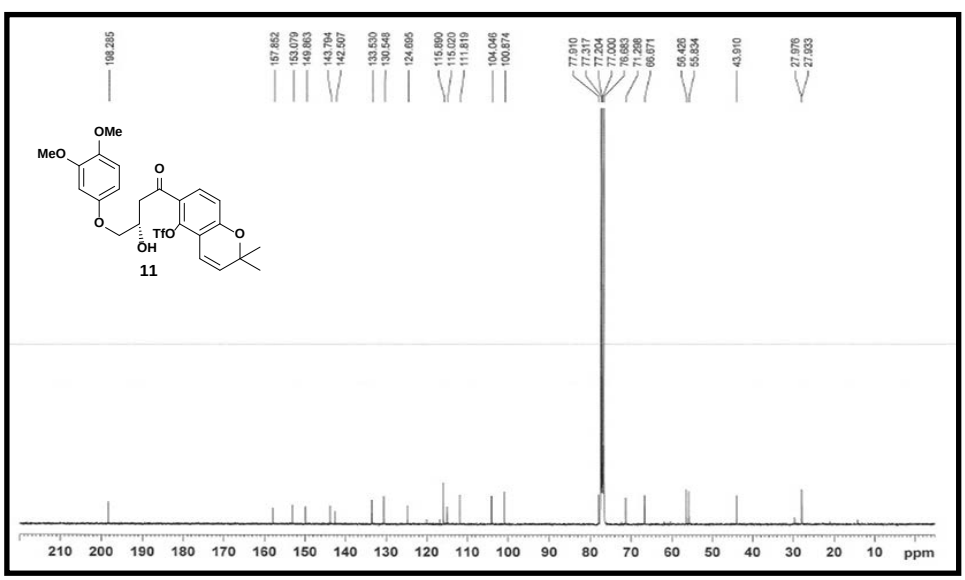

▼ ^{1}H-NMR ($CDCl_3$, 500 MHz)

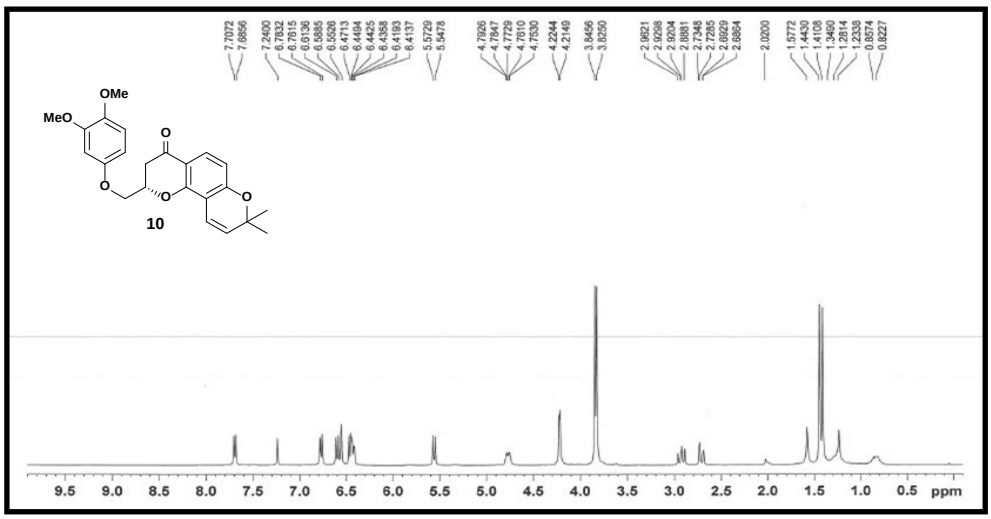

▼ ^{13}C-NMR ($CDCl_3$, 150 MHz)

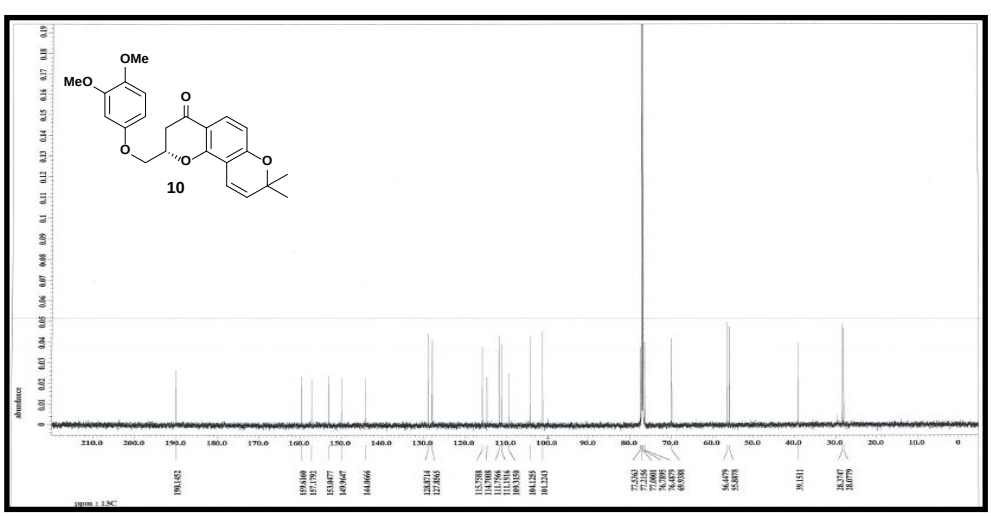

▼ ^{1}H-NMR ($CDCl_3$, 400 MHz)

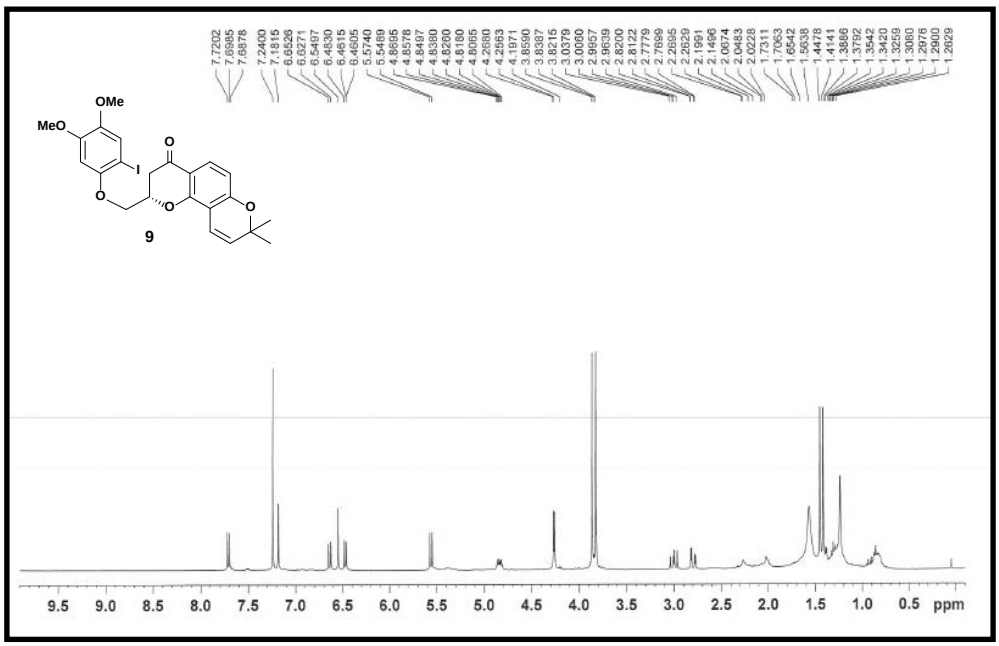

▼ ^{13}C-NMR ($CDCl_3$, 100 MHz)

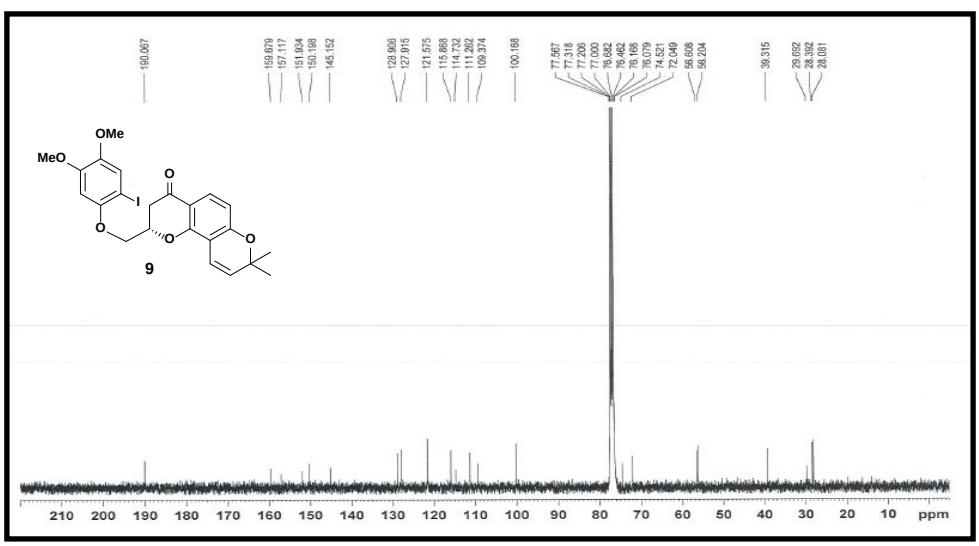

▼ ^{1}H-NMR ($CDCl_3$, 300 MHz)

▼ ^{13}C-NMR ($CDCl_3$, 100 MHz)

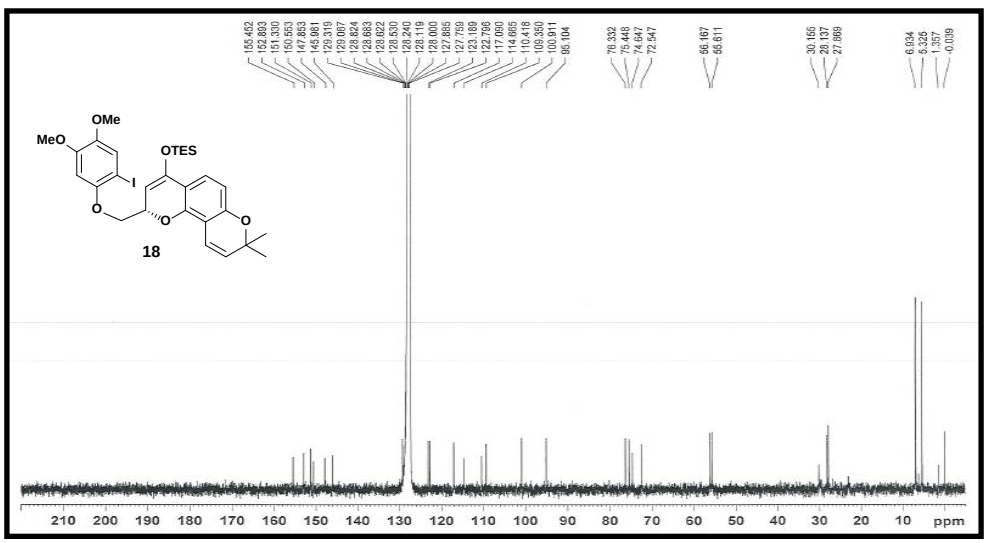

▼ ^{1}H-NMR ($CDCl_3$, 500 MHz)

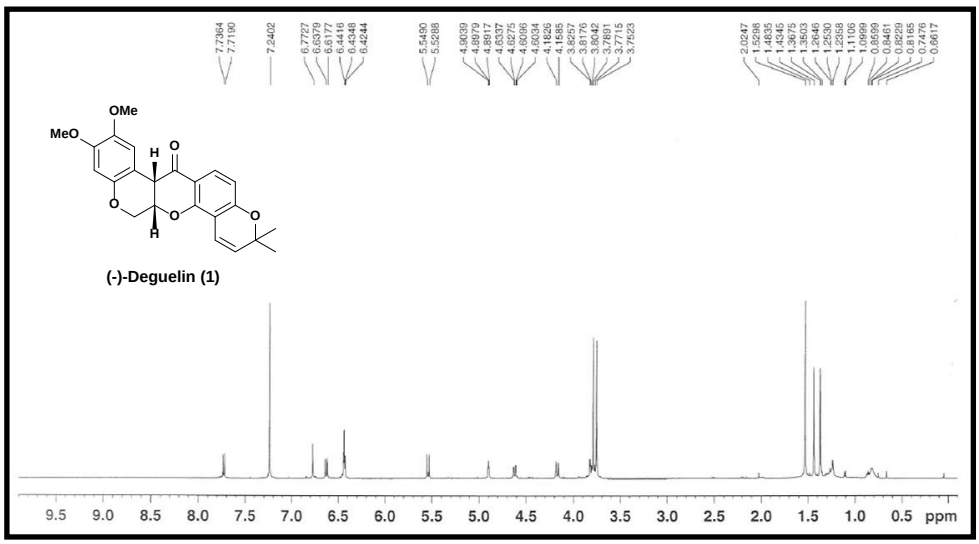

▼ ^{13}C-NMR ($CDCl_3$, 125 MHz)

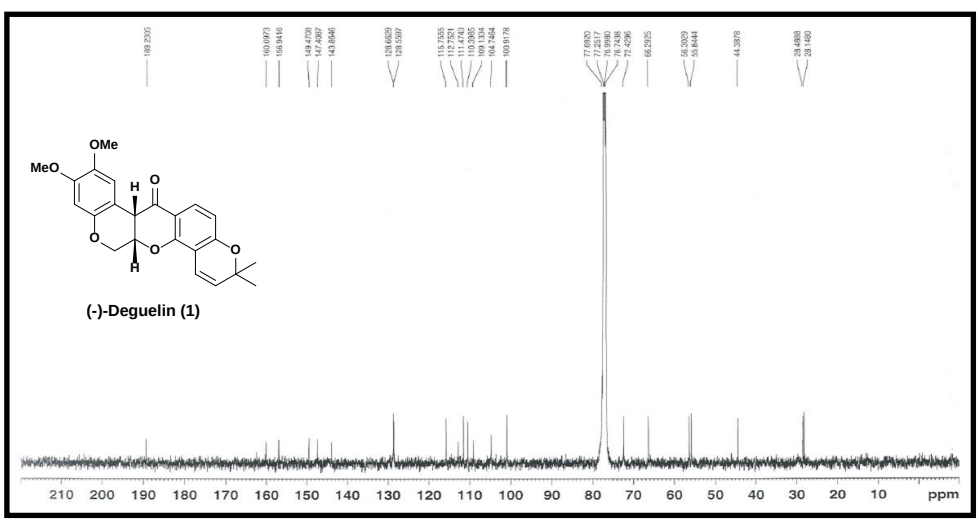

HPLC Analysis for Iodosilylenolether (18)

Column conditions: CHIRALPAK® AD-H, 0.8ml/min, 1:7 IPA:hexanes

(+)-18

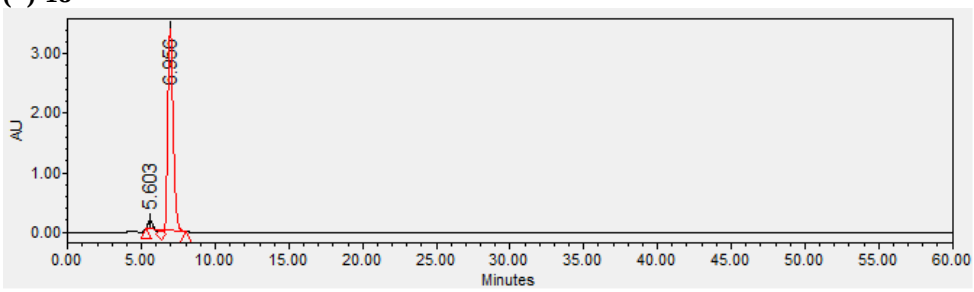

Retention Time (min)	Area (μV*sec)	% Area	Height (μV)
5.603	3424699	3.86	135104
6.956	85308291	96.14	3379976

(-)-18

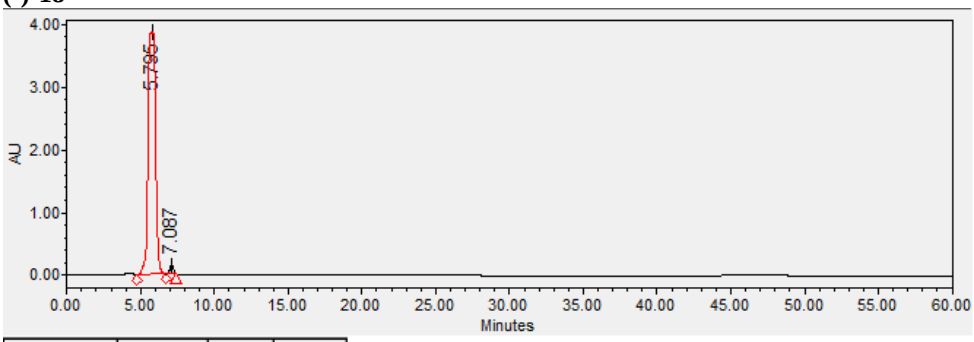

Retention Time (min)	Area (μV*sec)	% Area	Height (μV)
5.795	137326442	98.38	3848922
7.087	2266287	1.62	133025

HPLC Analysis for (-)-Deguelin (1)

(-)-Deguelin from (-)-18 (Table 2, entry 3)

Column conditions: CHIRALPAK® AD-H, 0.8ml/min, 1:4 IPA:hexanes

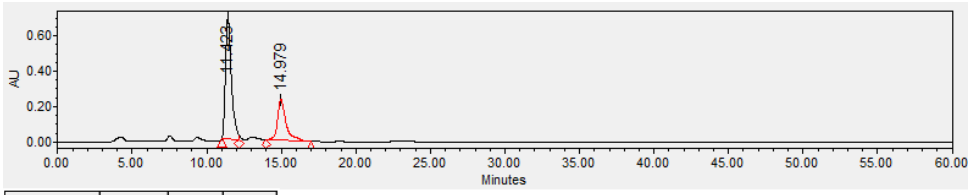

Retention Time (min)	Area (μV*sec)	% Area	Height (μV)
11.423	19264877	67.61	688737
14.979	9227953	32.39	233320

(-)-Deguelin from (-)-18 (Table 2, entry 7)

Column conditions: CHIRALPAK® AD-H, 0.8ml/min, 1:4 IPA:hexanes

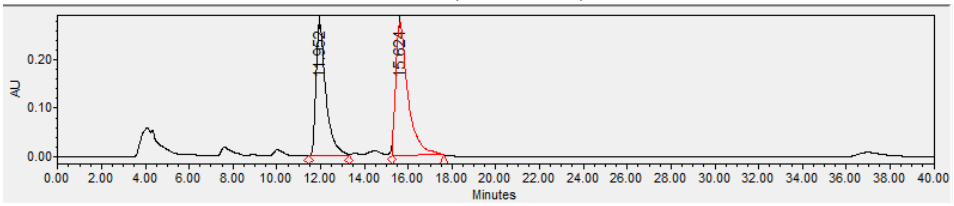

Retention Time (min)	Area (μV*sec)	% Area	Height (μV)
11.952	8644112	44.85	274322
15.624	10627136	55.15	274520

(-)-Deguelin from (-)-18 (Table 2, entry 8)

Column conditions: CHIRALPAK® AD-H, 0.8ml/min, 1:4 IPA:hexanes

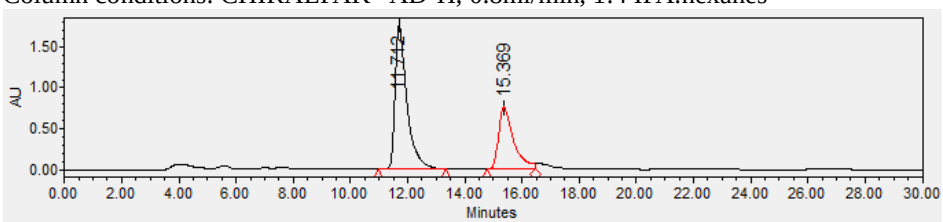

Retention Time (min)	Area (μV*sec)	% Area	Height (μV)
11.712	50734933	64.70	1757603
15.369	27683833	35.30	757745

(-)-Deguelin from (-)-18 (Table 2, entry 9)

Column conditions: CHIRALPAK® AD-H, 0.8ml/min, 1:4 IPA:hexanes

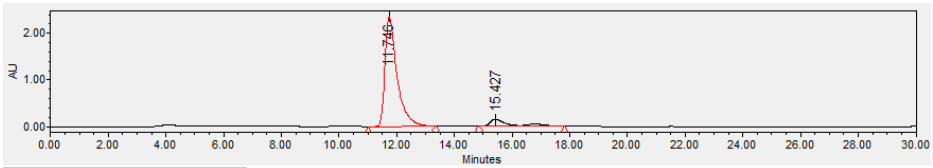

Retention Time (min)	Area (μV*sec)	% Area	Height (μV)
11.746	68627778	90.28	2361514
15.427	7390004	9.72	152073

(-)-Deguelin from (-)-18 (Table 2, entry 10)

Column conditions: CHIRALPAK® AD-H, 0.8ml/min, 1:4 IPA:hexanes

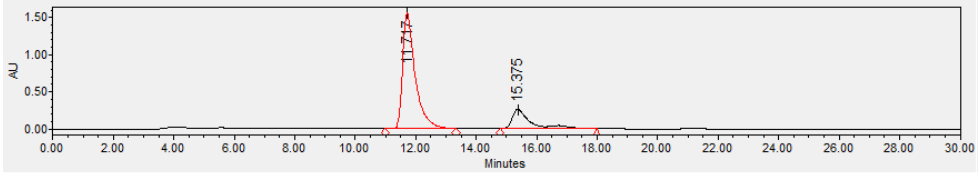

Retention Time (min)	Area (μV*sec)	% Area	Height (μV)
11.717	44962701	80.07	1558874
15.375	11189597	19.93	259686

▼ ^{1}H-NMR ($CDCl_3$, 400 MHz)

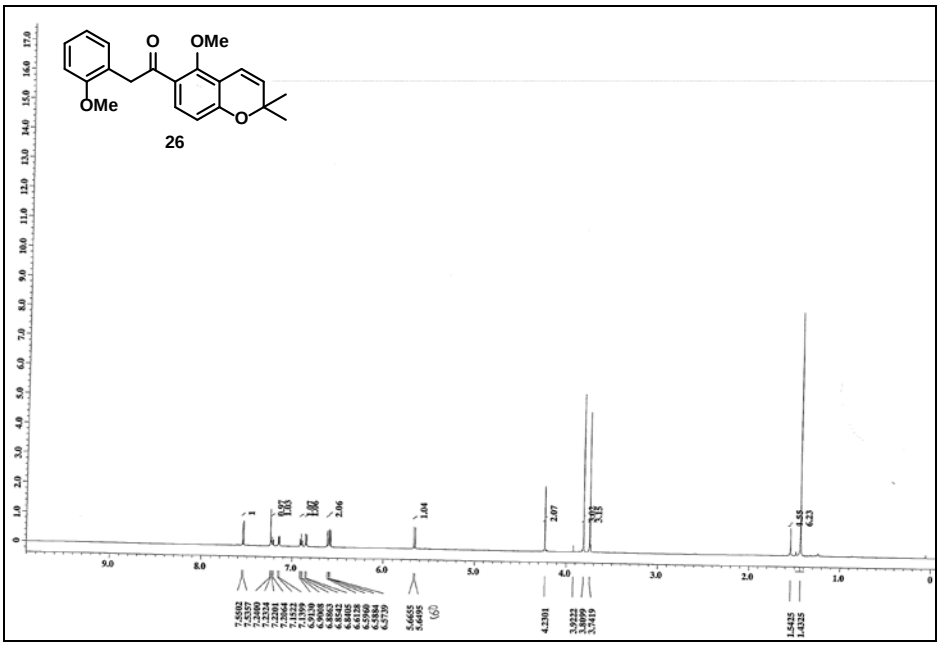

▼ ^{13}C-NMR ($CDCl_3$, 150 MHz)

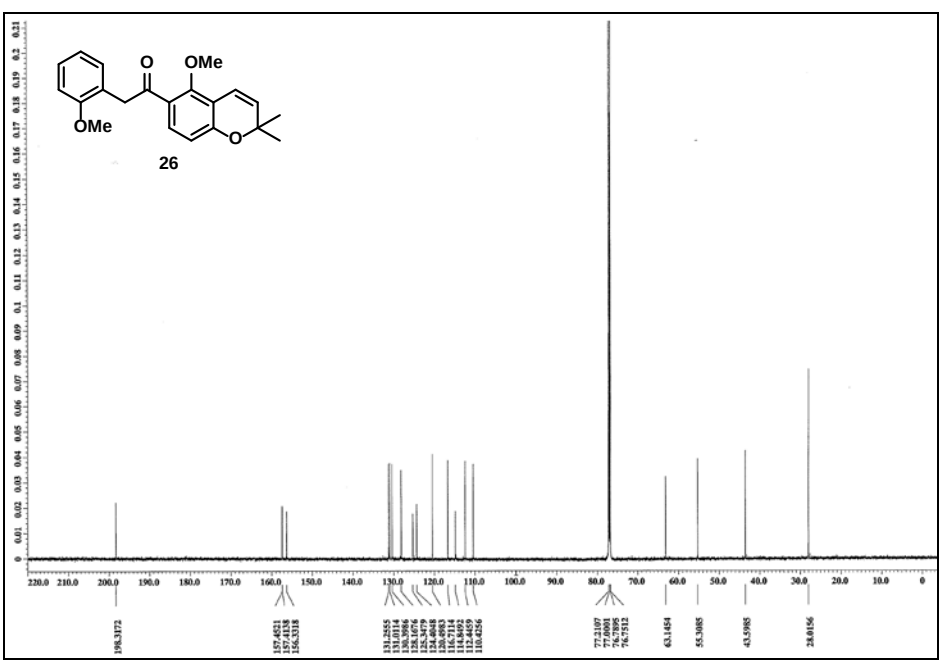

▼ ^{1}H-NMR ($CDCl_3$, 500 MHz) 28a

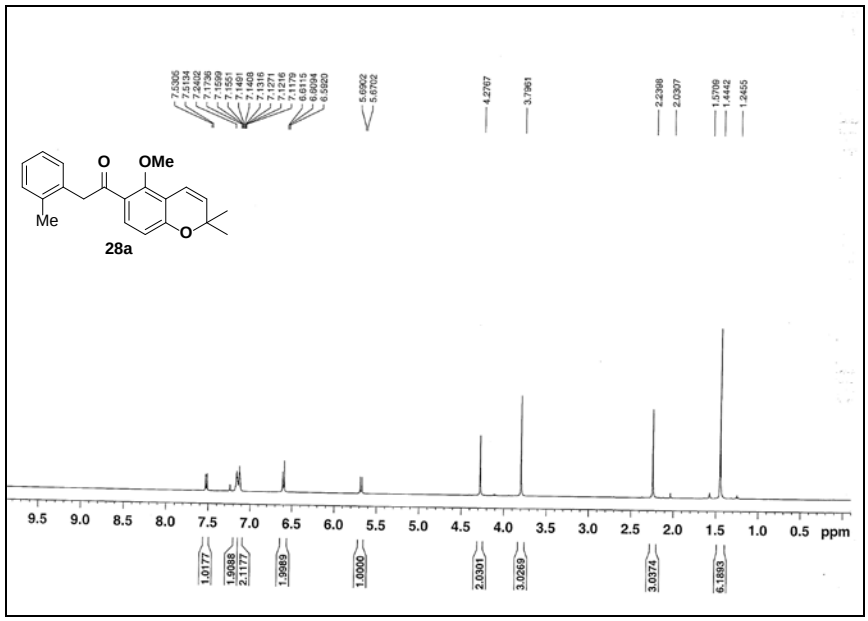

▼ ^{13}C-NMR ($CDCl_3$, 125 MHz)

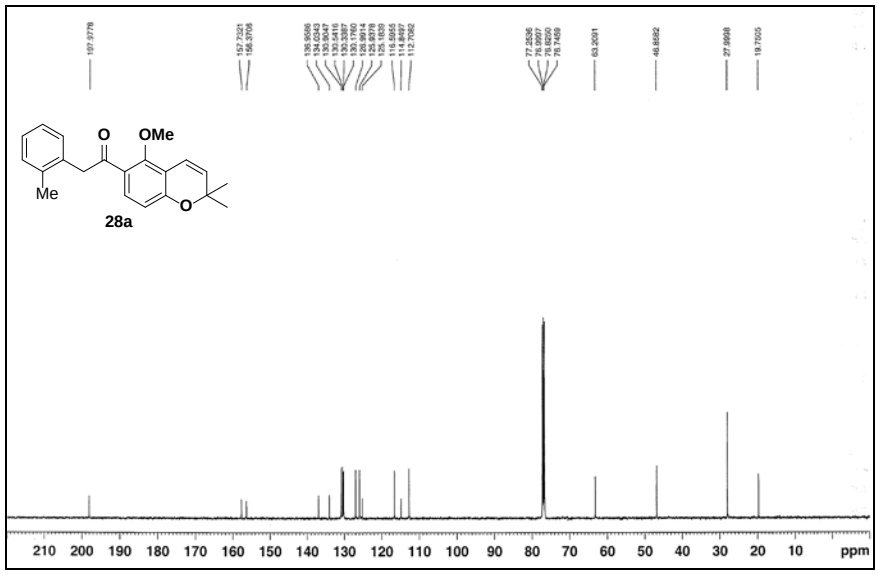

▼ ^{1}H-NMR ($CDCl_3$, 500 MHz)

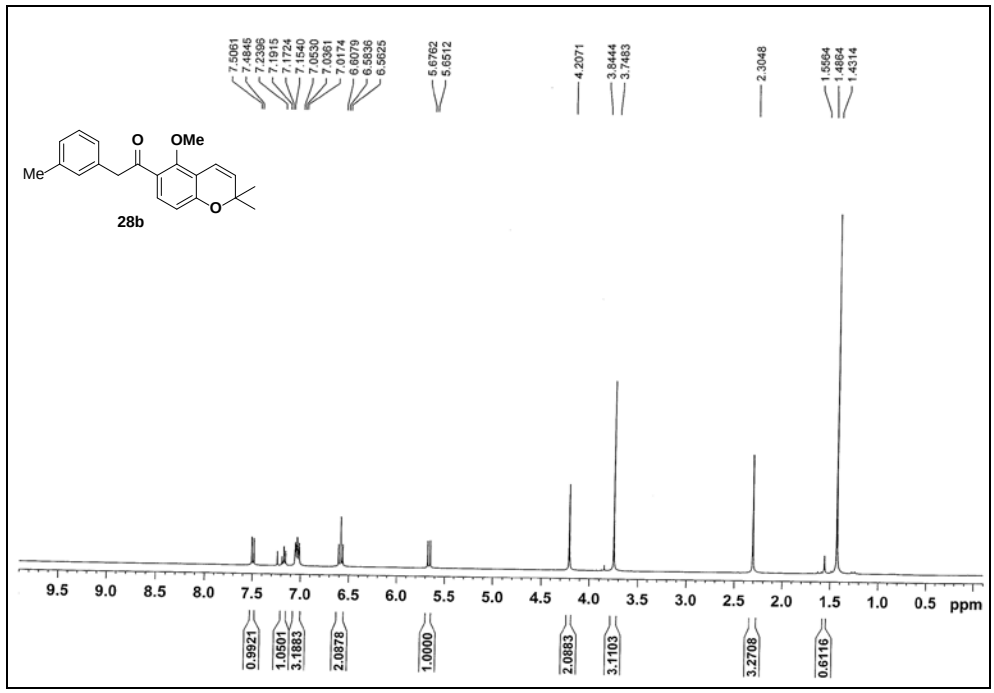

`

▼ ^{13}C-NMR ($CDCl_3$, 125 MHz)

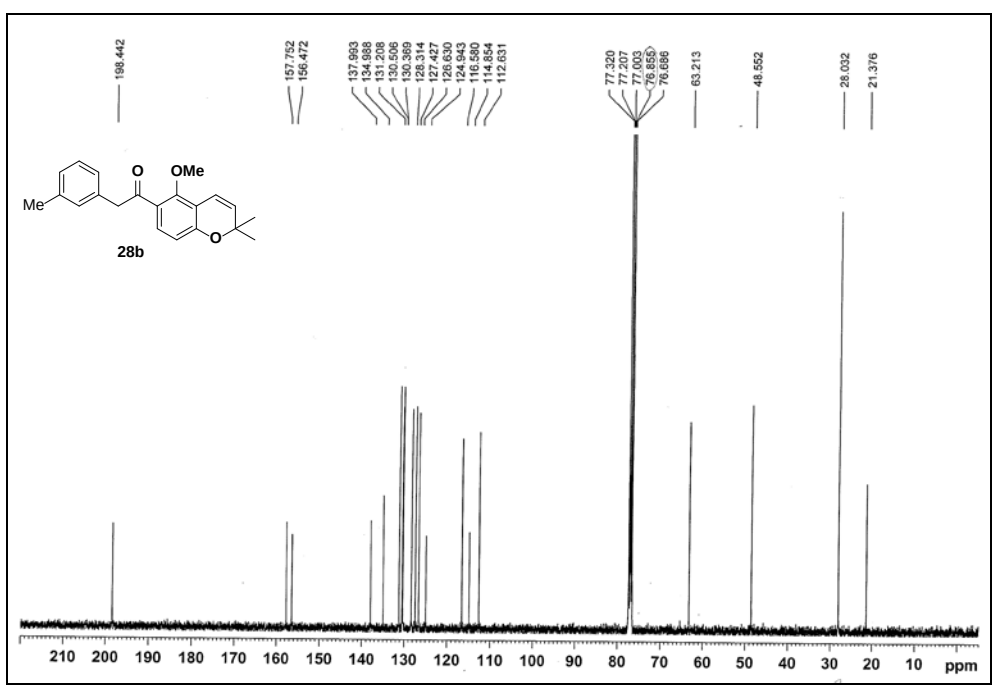

▼ ^{1}H-NMR ($CDCl_3$, 500 MHz)

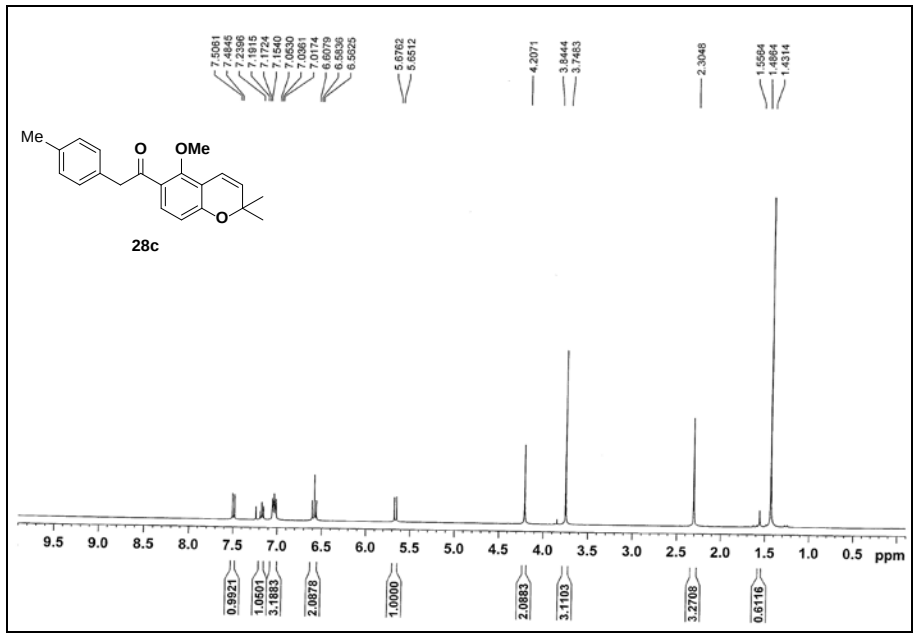

▼ ^{13}C-NMR ($CDCl_3$, 125 MHz)

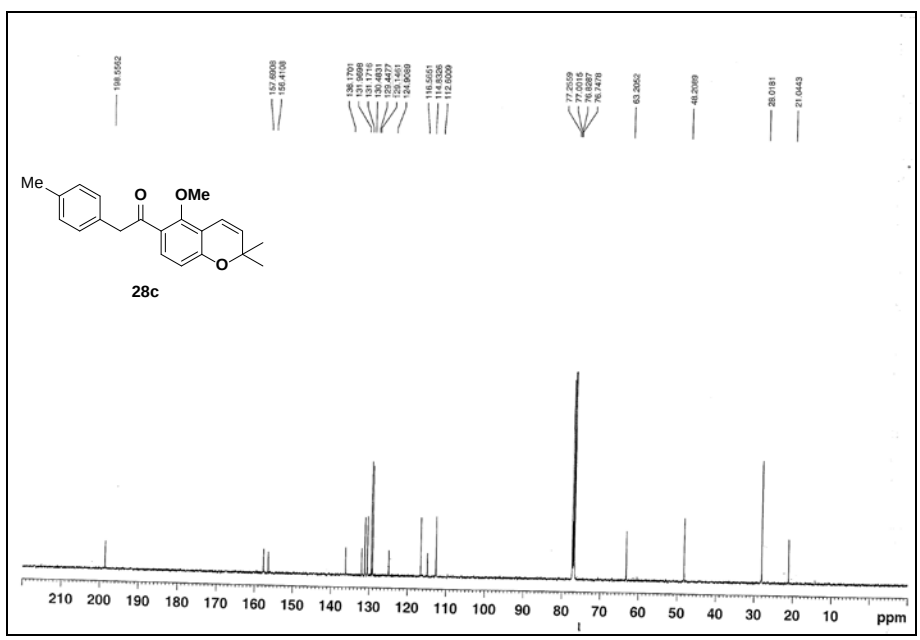

▼ ^{1}H-NMR ($CDCl_3$, 800 MHz)

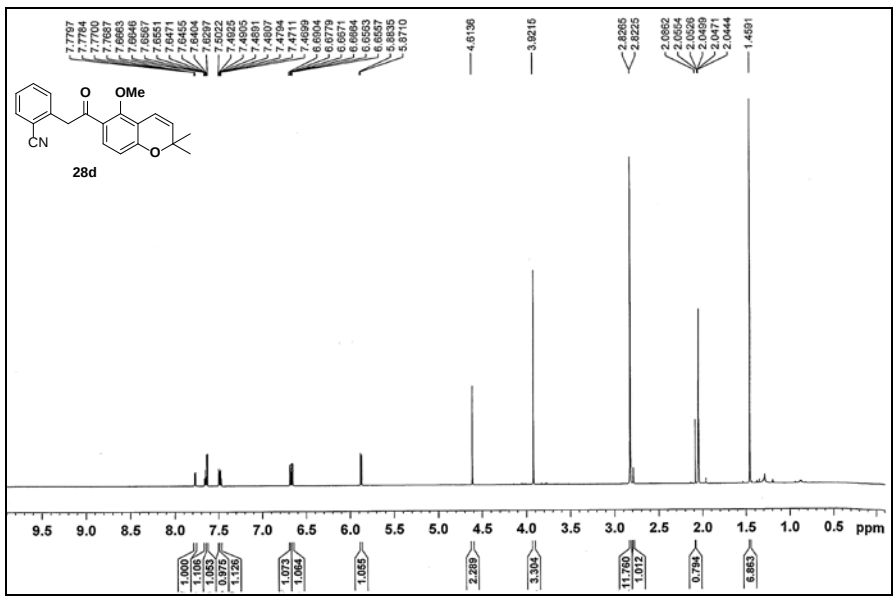

▼ ^{13}C-NMR ($CDCl_3$, 200 MHz)

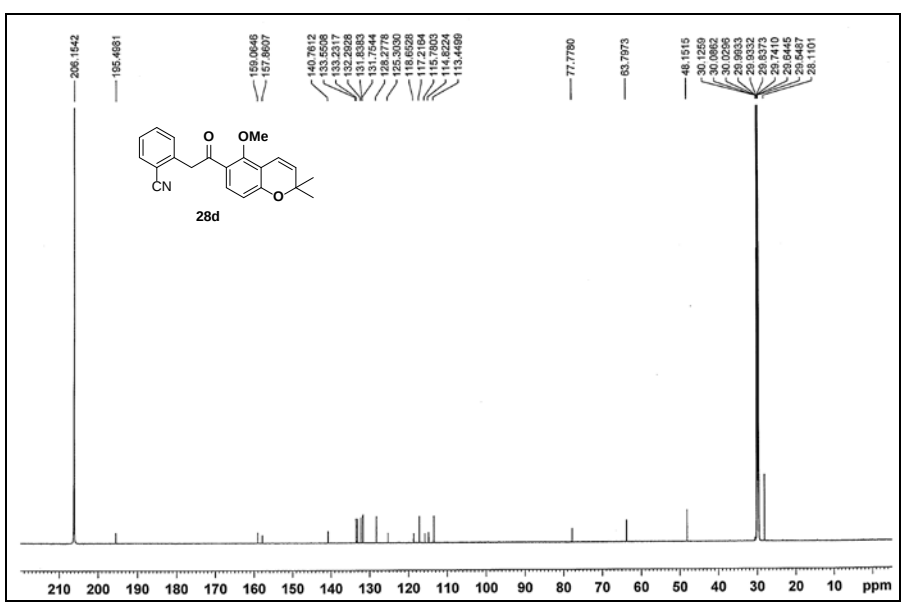

▼ ^{1}H-NMR ($CDCl_3$, 600 MHz)

▼ ^{13}C-NMR ($CDCl_3$, 150 MHz)

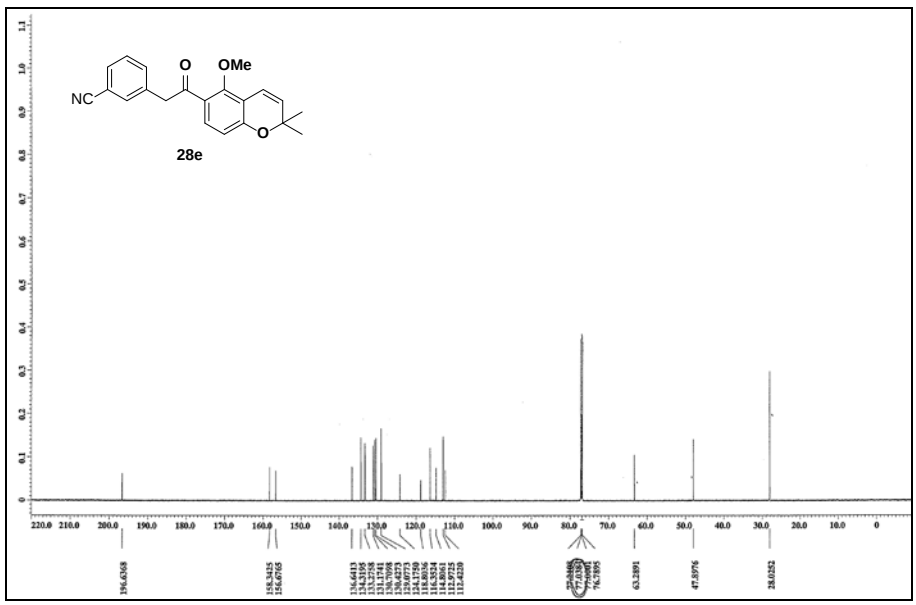

▼ ^{1}H-NMR ($CDCl_3$, 300 MHz) 28f

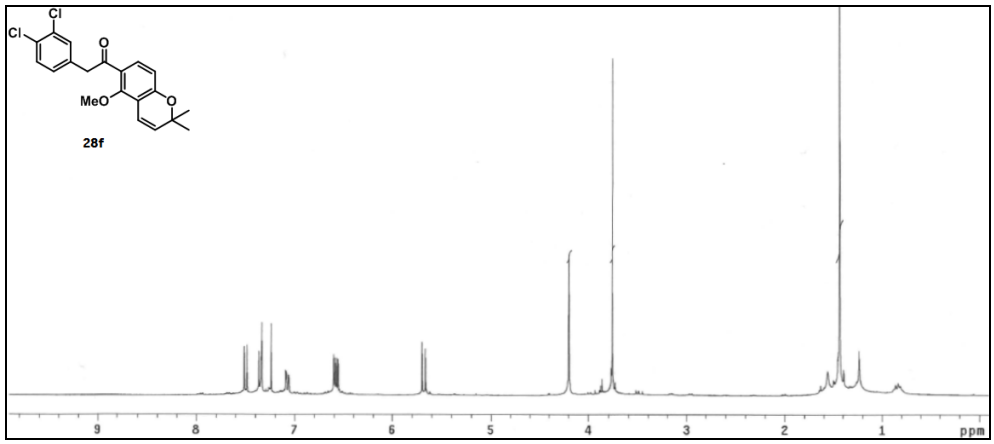

▼ ^{13}C-NMR ($CDCl_3$, 75 MHz)

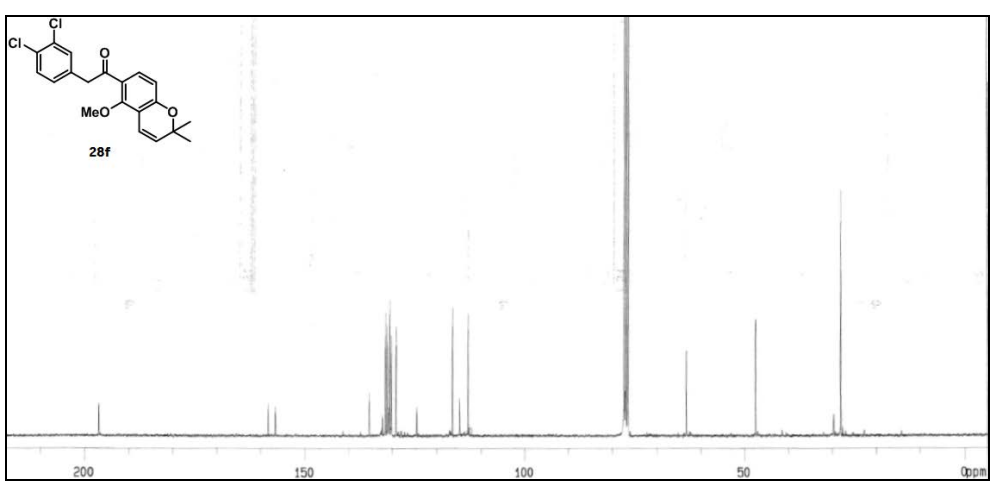

VII. 국문초록

천연물 데구엘린은 예로부터 쓰이던 몇몇 약용식물들에서 분리된 로테노이드 화합물이다. 데구엘린은 그 구조적 특이성과 강력한 항암 활성 때문에 많은 학자들에게 주목 받아왔다. HIF-1α를 안정화시키고 세포 핵내로 위치시킨다고 알려진 Hsp90의 ATP 결합부위에서 ATP의 결합을 방해함으로써 HIF-1α를 저해한다는 기전을 본 연구실에서 최근 보고한 바 있다. 본 연구에서는 먼저 상업적으로 구매가능한 3,4-dimethoxyphenol을 출발물질으로 한 12단계에 거친 천연물 데구엘린의 입체선택적인 전합성을 기술 하였다. 합성의 주요 특징으로는 두번의 Pd 촉매를 사용한 연속된 cis-융합 형태의 pyran 고리의 합성, 해당 촉매 반응을 위한 기질의 convergent chemistry를 이용한 효율적인 준비와 늦은 단계에서의 산촉매 하에 진행하는 선택적인 요오드화 반응을 들 수 있다. 한편 본 연구에는 천연물 데구엘린의 유도체인 **SH-42**의 구조-활성관계에 관한 연구를 통한 망막 신생혈관 질환 치료제의 개발도 기술 하였다. 안구내 신생혈관 질환은 시력손실 더 나아가 실명을 야기한다. 이러한 질환의 치료제로 현재 고가의 VEGF를 타겟으로 하는 항체시약이 유일한 치료제로 사용되고 있는 실정이며 VEGF를 직접 표적으로 하였을 때에 정상 신경 발달등에 악영향을 끼친다는 연구가 발표되어 새로운 표적의 망막 혈관질환 치료제가 필요한 실정이다. 따라서 본 연구실에서는 VEGF의 상위 기전인 HIF-1α를 표적으로 하는 망막혈관질환 치료제를 개발하고자 하였으며 이전 연구로 좋은 신생혈관 억제 활성의 감소된 독성을 보이는 **SH-42**를 도출해 낸 바 있다. 따라서 본 연구는 도출된 **SH-42**와 **SH-80**의 구조를 3개의 부분으로 나누어 각 부분이 바뀐 유도체들을 합성하였고 HIF-1α luciferase reporter assay를 통해 구조-활성 상관관계를 확립하였다. 그 과정에서 100 nM의 IC50 값을 가지는 강력한 활성의 HIF-1α 저해제인 **SH-199**를 도출하였으며 더 나아가 약리활성이 잘

알려진 chromene ring을 개열하여 신규성과 개선된 물성을 확보한 **SH-173**를 도출하였다. chromene ring이 없는 유도체 **SH-173**에서도 신생혈관 저해 효과와 동물 모델에서 평가하였고 각각 **SH-42**와 유사한 활성을 보인 다는 것을 확인하였다. 이를 통해 **SH-173**과 같이, chromene ring이 없는 특징적인 구조를 갖는 새로운 HIF-1α 저해제의 모핵을 도출하였다.

주요어 : 입체특이적 전합성, 데구엘린, Pd-catalyzed α-arylation, 저산소유도인자-1α, 망막혈관질환, 대량합성, 연속된 claisen 축합-탈탄산-알킬화 연계 반응

학번 : 2012-21609

이 승 범